Chapter 10: Global Climate Projections

Coordinating Lead Authors: Gerald A. Meehl, Thomas F. Stocker

Lead Authors: William Collins, Pierre Friedlingstein, Amadou Gaye, Jonathan Gregory, Akio Kitoh, Reto Knutti, James Murphy, Akira Noda, Sarah Raper, Ian Watterson, Andrew Weaver, Zong-Ci Zhao

Contributing Authors: J. Annan, J. Arblaster, C. Bitz, A. le Brocq, P. Brockmann, L. Buja, G. Clarke, M. Collins, E. Driesschaert, N.A. Diansky, K. Dixon, J.-L. Dufresne, M. Dyurgerov, M. Eby, N. Edwards, S. Emori, P. Forster, R. Furrer, J. Hansen, G. Hegerl, M. Holland, A. Hu, P. Huybrechts, F. Joos, J. Kettleborough, M. Kimoto, M. Krynytzky, M.-F. Loutre, J. Lowe, M. Meinshausen, S. Müller, S. Nawrath, J. Oerlemans, T. Palmer, A. Payne, G.-K. Plattner, J. Räisänen, G.L. Russell, A. Rinke , D. Salas y Melia, G. Schmidt, B. Schneider, A. Shepherd, D. Stainforth, C. Tebaldi, H. Teng, L. Terray, A. Sokolov, P. Stott, E. M. Volodin, B. Wang, T. M. L. Wigley, Y. Yu, S. Yukimoto

Review Editors: M. R. Allen, G. B. Pant

Date of Draft: 15 August 2005

Notes: This is the TSU compiled version

Table of Contents

Executive Summary

The future climate change results assessed in this chapter are based on a hierarchy of models, ranging from AOGCMs to EMICs to simple models. In general, we assess projections of future climate change on scales from global to hundreds of kilometers. Further assessments of regional and local climate changes are provided in Chapter 11.

Since the TAR, there have been climate change modeling studies using AOGCMs that rely not only on single realizations with single models, but on multi-member ensembles from single models and from multi-model ensembles. With regard to the latter, two significant AOGCM multi-model datasets have become available for analysis since the TAR. The first is the latest in the Coupled Model Intercomparison Project (CMIP), idealized 1% per year forcing series that extended the CMIP2 experiments for control and transient climate change to CMIP2+ where all fields from a multi-model dataset were collected by the Program for Climate Model Diagnosis and Intercomparison (PCMDI). This presented an opportunity for analysts to have access to all the data generated in these experiments, and enabled new and innovative analyses to be performed. The second is a multi-model dataset from the largest coordinated AOGCM climate change experiment and model analysis activity ever attempted, with PCMDI collecting and archiving a subset of the model data. For future climate change, three SRES scenario simulations (A1B, B1 and A2) were performed to the year 2100. Three different stabilization scenarios have been run, the first with all atmospheric constituents fixed at year 2000 values and the models run for an additional 100 years, and the second and third with constituents fixed at year 2100 values for A1B and B1, respectively, for another 100 to 200 years. Consequently, the concept of climate change commitment is addressed in much wider in scope and greater in detail than in any previous IPCC assessment.

A multi-model EMIC dataset complements these AOGCM experiments to extend the time horizon for several more centuries into the future, and to provide a greater range of model responses. Finally, a simple model calibrated to the AOGCMs is used to address uncertainties regarding carbon cycle feedbacks, and to explore the full range of the global mean climate response to all 31 SRES scenarios.

The following findings corroborate the results from the TAR:

- Geographical patterns of warming show greatest temperature increases at high northern latitudes and over land, with less warming over the southern oceans and North Atlantic. In spite of a slowdown of the meridional overturning circulation in most models, there is still warming over the North Atlantic and Europe due to the overwhelming effects of the increase of GHGs.
- Precipitation generally increases in the tropical precipitation maxima (such as the monsoon regimes) and over the tropical Pacific in particular, with general decreases in the subtropics and some midlatitude areas, and increases at high latitudes.
- Sea level pressure generally increases over the subtropics and midlatitudes, and decreases over high latitudes associated with an expansion of the Hadley Circulation and a poleward shift of the storm tracks.
- The pattern of zonal mean warming in the atmosphere, with a maximum in the upper tropical troposphere and cooling in the stratosphere, becomes established early in the 21st century, while zonal mean warming in the ocean is seen first near the surface and in the northern midlatitudes, with the warming gradually penetrating downward during the course of the 21st century, most evident at high latitudes where mixing is greatest.
- As the climate warms, snow cover and sea ice extent decrease; glaciers and ice caps lose mass and contribute to sea level rise.
- During the 21st century, global average sea level rises by 0.13–0.34 m due to thermal expansion. This range does not represent all modelling and scenario uncertainties.
- Globally averaged mean water vapour, evaporation and precipitation increase
- Intensity of rainfall events increases
- There is a tendency for summer drying of the mid-continental areas during summer, though there is variation across models concerning the areas where this occurs
- A majority of models show a mean El Niño-like response in the tropical Pacific, with the central and eastern equatorial Pacific sea surface temperatures warming more than the western equatorial Pacific, with a corresponding mean eastward shift of precipitation

- The multi-model ensemble signal to noise ratio is greater for surface air temperature than for precipitation
- In experiments where the atmospheric GHG concentration is stabilized, the MOC recovers from initial weakening within one to several centuries
- Precipitation extremes increase more than does the mean in most areas
- Sea ice reduces in the 21st century both in the Arctic and Antarctic with a rather large range of model responses. The reduction is accelerated in the Arctic where some models project sea ice cover to become seasonal in the second half of the 21st century.
- No coupled model simulation of the Atlantic MOC shows an increase of the MOC in response of global warming. Those models consistent with present day observations project a reduction of the Atlantic MOC ranging from 0 to 60% .
- Models which show a large reduction in MOC still show a warming in the Atlantic region and Western Europe due to the overwhelming effect of the radiative forcing.
- Although the MOC weakens in most models, the relative roles of surface heat and freshwater fluxes responsible for this weakening vary from model to model
- In the 21 AOGCMs run for the three SRES scenarios, none shows a collapse of the MOC by the year 2100 (though none have interactive ice sheets)
- Beyond 2100, the MOC could shut-down if the rate of change of radiative forcing was large enough and applied long enough, though such a large radiative forcing would produce such a large magnitude of warming that high latitudes would still warm even without the contributions from ocean heat transport associated with the MOC
- Future changes of ENSO interannual variability differ from model to model. Some models that show increases more successfully simulate present day characteristics of ENSO, though the large inter-model differences in future changes of El Niño amplitude, and the inherent century-timescale variability of El Niño in the models, preclude a definitive assessment of what the actual possible changes could be
- Cloud feedback remains the largest source of uncertainty in simulated global temperature changes.
- There is unanimous agreement amongst the models that future climate change will reduce the efficiency of the Earth system to absorb anthropogenic carbon dioxide. As a result, a larger fraction of anthropogenic CO_2 will stay airborne under a warmer climate.
- By 2100, atmospheric CO_2 varies between 730 and 1020 ppm for the climate-carbon cycle coupled models, to be compared with 830 ppm for the SRES-A2 concentration used by the standard IPCC-AR4 climate models
- As a result of a much larger CO_2 concentration by 2100 in the climate-carbon cycle coupled models, the upper estimate of the global warming by 2100 is 0.7°C higher for the climate-carbon cycle coupled models than for the SRES-A2 concentration standard simulations.

The following are new results since the TAR for projected future climate change:

- The close agreement of warming for the early 21st century in the three SRES scenarios run by the AOGCMs (with a range of only 0.06°C , from 0.64°C to 0.70°C) shows that no matter what scenario we follow, the warming is similar on the timescale of the next decade or two. This is corroborated by probabilistic projections from a hierarchy of models.
- Nearly half of the early 21st century climate change arises from warming we are already committed to (0.31°C for early century). By mid-century, in the AOGCMs the choice of scenario becomes more important for the magnitude of warming, with a range of 0.31°C from 1.30°C to 1.73°C, and with only about a quarter of that warming due to climate change we are already committed to (0.42°C). By late century, there are clear consequences for which scenario is followed, with a range of 1.27°C from 1.78°C to 3.05°C, with only about 15% of that warming coming from climate change we are already committed to (0.52°C). These results are also corroborated by a hierarchy of models and probabilistic projections.
- There is an expansion of the Hadley Circulation and a poleward shift of the storm tracks.
- In spite of a slowdown of the meridional overturning circulation across models, there is still warming over the North Atlantic and Europe due to the overwhelming effects of the increase of GHGs.

- Considering the mean of 11 AOGCM model tunings, the global mean temperature change between 1990 and 2100 spans a range of 2.4°C, from 1.9°C to 4.3°C, for all SRES scenarios. This is the uncertainty in temperatures resulting solely from the 'emissions uncertainty'.
- For the A2 scenario the 'response uncertainty' associated with model climate sensitivities in the range 1.7 to 4.2°C, is comparable in size to the 'emission uncertainty', when carbon cycle feedback uncertainties are included (2.6°C to 5.0°C). The response and its uncertainty are smaller for lower emissions scenarios, such as the B1 scenario (1.3°C to 2.9°C).
- Due to changes in wind, the length of day is projected to increase on the order of 1 microsecond per year.
- The current generation of AOGCMs covers a range of climate sensitivity from 2.1–4.4°C, similar to the TAR (2001), with a mean value of 3.2°C. The AOGCMs do not sample the full range of sensitivities constrained from observations, in particular not the high values.
- Though studies performed to date have not been able to strongly constrain climate sensitivity, confidence in the shape of the PDF and the lower bound has increased significantly. The PDF of climate sensitivity is very likely right-skewed, with maximum probabilities from individual studies between 1 and 4°C, on average around 3°C, and lower probabilities of higher values such that those higher climate sensitivities cannot be ruled out. The lower bound is well constrained, but a definitive quantification of the 95% bound is not possible at this stage.
- Based on a conservative estimate satisfying each of the individual observational studies, climate sensitivity is very unlikely to be below 1°C, and it is unlikely (<33%) to be above 6°C, given several independent lines of evidence from climate models and climate change in different periods. For an average of nine PDFs, climate sensitivity is very unlikely below 1.5°C (8% probability) and unlikely above 4.5°C (28% probability); best agreement with observations is found for a sensitivity of 3.0°C, with a median value of 3.4°C, similar to the centre of the TAR range and close to the AOGCM average.
- Many more studies on changes of extremes have been performed since the TAR, including many aspects of extremes not previously addressed, and a considerable number of these studies have been performed with multi-model ensembles. A number of models have calculated the ten Frich et al. (2002) extremes indices for temperature and precipitation.
- The result from the TAR of increased precipitation intensity and associated risk of flooding has been documented in the newer generation of models in the tropics and at mid and high latitudes, with associated longer dry periods between rainfall events mainly in the subtropics and lower midlatitudes. Increased precipitation intensity tends to increase more where mean precipitation increases at mid and high latitudes.
- The result from the TAR of a very likely risk of increased temperature extremes has been confirmed in the recent models. A new result is that heat waves are projected to be more intense, more frequent and longer lasting in a future warmer climate.
- Cold air outbreaks are projected to significantly decrease in a future warmer climate.
- Diurnal temperature range is projected to decrease almost everywhere in future climate.
- There are now a number of studies showing future decreases in frost days almost everywhere in the mid and high latitudes, and a comparable increase in growing season length.
- Previous results from the TAR from an embedded hurricane model in a global coupled model have been confirmed with that configuration for future increases in tropical cyclone (i.e., hurricane) intensity and precipitation, and this result has been replicated in global atmospheric models of about 1 degree resolution that can begin to resolve individual tropical cyclone characteristics.
- New results from global models of around 1 degree resolution, and a new global model with 20 km resolution, show a future global decrease of tropical cyclones of around 30% (but with regional increases in the North Atlantic), and an increase of precipitation in those storms.
- Results from global models with about 100km and 20km resolution show strongest tropical cyclones with extreme surface winds increase in number while weaker storms decrease, the tracks are not appreciably altered, and there is about a 10% increase in maximum wind speeds in future simulated tropical cyclones, with a globally averaged decrease in tropical cyclones but an increase in the Atlantic.
- More evidence has been presented to support the conclusion from the TAR that in the future there could be fewer midlatitude storms but more intense storms with associated damaging winds in some regions.

- New results have been presented that indicate there could be a poleward shift of midlatitude storms, with an associated increase in cyclonic circulation patterns over the high latitude Arctic and Antarctic regions.
- New results have shown that for most regions of the midlatitude oceans, there is a likely increase of extreme wave height in a future warmer climate. This is related to increased wind speed associated with stronger midlatitude storms, resulting in higher waves produced by these storms, and is consistent with other studies that show decreased numbers of total midlatitude storms but more intense storms.
- There is a positive trend of the NAM (or NAO) as well as the SAM index projected by many models, though the magnitude of that increase is generally greater for the SAM, though there is considerable spread among the models.
- Coupled model simulations show that 21st century warming may melt large portions of the Greenland ice sheet. This is caused by the dominance of summer melting over increased winter precipitation. Models suggest that sustained warming will lead to an irreversible meltdown later.
- Atlantic MOC projections are now based on coupled model simulations without flux corrections. In most simulations, the MOC reduction by the end of the 21st century is clearly distinguishable from natural fluctuations and reaches as much as 60%.
- Most model simulations agree that the warming causes a stratification of the Labrador Sea, and potentially other marginal seas, which reduces or suppresses the ventilation of the intermediate and deep ocean in the North Atlantic.
- All model simulations agree that the reduction of the MOC evolves on the time scale of the warming. No model simulations exhibit an abrupt shutdown of the MOC during the 21st century in response to the slow warming.
- While some models of reduced complexity suggest a complete, or even irreversible, shutdown of the MOC as a long term response to sufficiently strong warming, the few long term simulations using AOGCMs do not show complete shut down of the MOC.
- Increases in precipitation will offset 25–50% of the increased melting of glaciers and ice caps, slowing their retreat.
- During the 21st century, the net contribution of the Antarctic ice sheet to sea level change is likely to be negative. Recent accelerated discharge by some ice streams in West Antarctica is likely to have been caused by enhanced melting resulting from ocean warming. This process could therefore affect other areas; a quantitative projection of the consequences is not yet possible, but it is unlikely to outweigh increased precipitation. Current ice dynamic models project a contribution of no more than 2.5 mm yr^{-1} from retreat of the ice sheet resulting from ocean warming.
- It is likely that climate change commitment from emissions during the 21st century will produce sufficient warming to melt the Greenland ice sheet, if the warming is sustained. With an annual-average warming in Greenland of 8–10 °C, possible under high-CO_2 scenarios, the sea level contribution would be about 6 mm yr^{-1} for the first several centuries. Elimination of the ice sheet would add about 7 m to sea level but would take >1000 years. If the ice sheet were removed, there is medium likelihood that it could not be regenerated if the climate were subsequently returned to pre-industrial.
- Results from the AOGCM multi-model climate change commitment experiments (20th century commitment, and B1 and A1B commitment) indicate that at any given point in time we are committed to about another 0.5°C warming over the next 100 years after concentrations of GHGs are stabilized, with most of this warming occurring in the first several decades after stabilization.
- Globally averaged precipitation commitment 100 years after stabilizing GHG concentrations is roughly an additional 1 to 2%.
- We are committed to a few 0.1 m per century of additional sea level rise due to thermal expansion for the next several centuries, such that sea level rise commitment continues to occur long after surface air temperatures have levelled off.
- Climate models of intermediate complexity show that sea level continues to rise due to thermal expansion for up to 1000 years after stabilization, while temperature nearly levels off after a century.
- EMICs with coupled carbon cycle show that for a reduction to zero emissions at year 2100 the climate change commitment is of the order of a thousand years, and even then temperature and sea level do not return to pre-industrial values

- Results from the coupled climate carbon cycle models intercomparison project (C4MIP) show unanimous agreement amongst the models that future climate change will reduce the efficiency of the Earth system to absorb anthropogenic carbon dioxide. As a result, a larger fraction of anthropogenic CO_2 will stay airborne under a warmer climate. By the end of the 21st century, this additional CO_2 varies between 20 ppm and 200 ppm for the two extreme models, the majority of the models lying between 50 and 100 ppm. The positive feedback in the climate-carbon system leads to an additional atmospheric CO_2 and hence an additional warming ranging between 0.1 and 1.5°C.

10.1 Introduction

This chapter addresses various aspects regarding projections of future climate change. Similar chapters have appeared in every IPCC Assessment, so it will be useful at the outset to provide an indication concerning what is new in this chapter since the TAR.

The global coupled climate modeling community has undertaken the largest coordinated global coupled climate model experiment ever attempted to provide the most comprehensive multi-model perspective on climate change of any IPCC assessment. This open process involves experiments with idealized climate change scenarios (i.e., 1% per year CO_2 increase, also included in the newer Coupled Model Intercomparison Project phase 2 and phase 2+ (CMIP2 and CMIP2+) (e.g., Covey et al., 2003; Meehl et al., 2005c), equilibrium $2 \times CO_2$ experiments with atmospheric models coupled to non-dynamic slab oceans, and idealized stabilized climate change experiments at $2 \times CO_2$ and $4 \times CO_2$ in the 1% CO_2 increase simulations. Simulations of 20th century climate have been completed that include time-evolving natural and anthropogenic forcings. For future climate change, three SRES scenario simulations (A1B, B1 and A2) have been performed to the year 2100. Three different stabilization scenarios have been run, the first with all atmospheric constituents fixed at year 2000 values and the models run for an additional 100 years, and the second and third with constituents fixed at year 2100 values for A1B and B1, respectively, for another 100 to 200 years. Consequently, the concept of climate change commitment will be addressed in much wider scope and greater detail than in any previous IPCC assessment. Results based on this AOGCM multi-model data set will be featured in Section 10.3.

In addition to this coordinated international multi-model experiment, a number of entirely new types of experiments have been performed since the TAR to quantify uncertainty regarding climate model response to external forcings. The extent to which uncertainties in parameterizations translate into the uncertainty in climate change projection has been addressed in much greater detail. New calculations of future climate change from the larger suite of SRES scenarios with simple models and earth system models of intermediate complexity (EMICs) provide additional information regarding uncertainty related to the choice of scenario. Such models also provide estimates of long-term evolution of global mean temperature, ocean heat uptake, and sea level rise beyond the 21st century, and thus allow us to better constrain climate change commitments.

Climate sensitivity has always been a focus in the IPCC assessments, and here we obtain more quantitative estimates of equilibrium climate sensitivity and transient climate response (TCR) in terms of not only ranges but also probabilities within these ranges. Some of these probabilities are derived from ensemble simulations subject to various observational constraints, and no longer rely solely on expert judgement. This gives us a much more complete understanding of model response uncertainties from these sources than ever before. These are now standard benchmark calculations with the global coupled climate models, and are useful to assess model response in the subsequent time-evolving climate change scenario experiments.

With regard to these time-evolving experiments simulating 21st century climate, since the TAR we have seen increased computing capabilities that now allow routine performance of multi-member ensembles in climate change scenario experiments with global coupled climate models. This provides us with the capability to analyze more multi-model results and multi-member ensembles, and yields more probabilistic estimates of time-evolving climate change in the 21st century.

Finally, while future changes in some weather and climate extremes were addressed in the TAR, there were relatively few studies on this topic available for assessment at that time. Since then, more analyses have been performed regarding possible future changes in a variety of extremes. These new studies provide a more complete range of results for assessment regarding possible future changes in these important phenomena with their notable impacts on human societies and ecosystems. A synthesis of results from studies of extremes from observations and model is given in Chapter 11.

Uncertainty of climate change projections has always been a subject of previous IPCC assessments, and there has been considerable new work done on this topic that will be assessed in this chapter. In particular, it is important to keep in mind the sources and propagation of uncertainty in climate model projections (Figure 10.1.1). First, there are multiple emission scenarios for the 21st century, and even at this first stage there is uncertainty with regards to what will be the future time-evolution of emissions of various forcing agents such as greenhouse gases (GHGs) (box at left in Figure 10.1.1). Then these emissions must be converted to concentrations of constituents in the atmosphere. Gas cycle models must be employed, and these models include their own set of parameterisations, assumptions and caveats. Then the concentrations in the atmospheric models produce radiative forcing that acts on the climate system within the atmospheric model components, each with their own radiation schemes and other formulations that affect radiative forcing. Finally, the modelled coupled climate system takes those radiative forcings and produces a future simulated climate. The components of the atmosphere, ocean, sea ice and land surface in each model interact with their sets of strengths and weaknesses to produce a spread of outcomes for future climate. Thus at every step in this process, there are uncertainties and assumptions that must be made to get from emissions to concentrations to radiative forcing to simulated climate changes.

This apparent bewildering array of uncertainty suggests that it is difficult to be able to come to any conclusions regarding possible future climate change. However, the use of multi-model ensembles has been shown in other modelling applications to produce simulated climate features that are improved over single models alone (see discussion of Chapters 8 and 9). The expanded use of multi-model ensembles for future climate change provides higher quality and more quantitative climate change information compared to the TAR. The use of large (order 20) global coupled climate multi-model ensembles provides the ability to better quantify differences of model response. A hierarchy of models ranging from simple to intermediate to complex allows better quantification of the consequences of various parameterisations and formulations. Very large ensembles (order hundreds) with single models provides the means to quantify parameterisation uncertainty. Finally, being able to constrain future climate model projections with information from climate characteristics we have already observed, helps us better quantify possible future climate changes.

[INSERT FIGURE 10.1.1 HERE]

10.2 Projected Radiative Forcing

10.2.1 Forcings of Multi-Model Global Climate Projections

10.2.1.1 Projections for radiatively active species

Evidence from recent economic activity suggests that emissions of CO_2, CH_4, BC, and SO_2 from China decreased from 1996 (the peak year) to 2000 (Streets et al*.,* 2001). SO_2 is one of the primary chemical precursors of anthropogenic sulphate (SO_4) aerosol. The amount of CO_2 emitted from all sources fell from 3470 Tg/yr to 3220 Tg/yr during that period, a 7.3% decline. Decreases of 32% in BC emissions and 21% in SO_2 have been qualitatively confirmed by aerosol measurements in the Asian outflow from Midway Island (Prospero et al*.,* 2003). In situ data on sulfate and nitrate from Midway show that concentrations nearly doubled from 1981 to roughly 1995, then began to decline. An economic recession in 1997–1998 contributed to a decline in emissions from many countries in east and southeast Asia (Carmichael et al*.,* 2002). In addition, China took several steps to reduce air pollution, including closure of some high-sulfur coal mines, closure of inefficient industrial plants, and the institution of a SO_2 reduction program for environmentally sensitive regions. A global model calculation (Jacobson*,* 2001) of the effect of the emission reductions finds that the global mean surface temperature for the 21st century increases by (+0.012 ± 0.02) °C due primarily to the reduced cooling by sulfate aerosols.

Streets et al. (2001) suggest that anthropogenic emissions from China will rebound from the economic downturn and imposition of emission controls of the late 1990s, but that the emissions growth would probably grow much less rapidly than previous projections. Carmichael et al (2002) estimate that Asian emissions SO_2 will grow from 34.4 Tg yr^{-1} in 2000 to perhaps 40–45 Tg yr^{-1} in 2020, a value considerably lower than previous estimates as high as 80–110 Tg yr^{-1} (Foell et al*.,* 1995). The new estimates are consistent with the SRES B1 scenario (Nakicenovic and Swart*,* 2000) but are markedly lower than the A1B and A2 scenarios. Since the Asian emissions are the dominant contribution to the total annual flux of SO_2, these results strongly suggest that the emissions in the A1B and A2 scenarios are unrealistically large. Nonetheless, these scenarios form the basis for two of the standard projection experiments considered in this chapter. The overestimation of SO_2 in all the SRES scenarios is already evident at the starting point of the scenario time series in 2000 (Smith et al*.,* 2001). Several simulations with AOGCMs of the transition from the 20th century to the SRES scenarios have used the modern SO_2 emissions data sets and have therefore had to introduce a transition to the higher SRES time series at the year 2000.

Estimation of ozone forcing for the 21st century is complicated by the short chemical lifetime of ozone compared to atmospheric transport timescales and by the sensitivity of the radiative forcing to the vertical distribution of ozone. Gauss et al. (2003) have calculated the forcing by anthropogenic increases tropospheric ozone through 2100 from eleven different chemical transport models integrated with the SRES A2p scenario. Since the emissions of CH_4, CO, NO_x, and VOCs, which strongly affect the formation of ozone, are maximized in the A2p scenario, the modelled forcings should represent an upper bound for the forcing produced under more constrained emissions scenarios. The eleven models simulate an increase in tropospheric ozone of 11.4 to 20.5 DU by 2100 corresponding to a range of radiative forcing from 0.40 to 0.78 W m^{-2}. Under this scenario, stratospheric ozone increases by between 7.5 to 9.3 DU, which raises the radiative forcing by an additional 0.15 to 0.17 W m^{-2}.

10.2.1.2 Relationship of fluxes, instantaneous forcing, and adjusted forcing

The differences in radiative forcing computed with and without fixed dynamical heating (FDH) are particularly large for ozone (Ramanathan and Dickinson*,* 1979). Evidence from transient coupled integrations, however, suggests that the differences may be roughly 10% (relative). Johns et al. (2003) computed ozone radiative forcing for HadCM3 using instantaneous state information from the transient integrations and using FDH methods applied to a control integration. Under the more emissions-intensive A1FI and A2 scenarios, the FDH forcing is larger than the instantaneous forcing by less than 0.1 W m^{-2}, while under the less emissions-intensive scenarios B1 and B2, and the FDH forcing is smaller than the instaneous forcing by less than 0.8 W m^{-2}. Compared to the radiative forcing of 4.0 to 7.8 W m^{-2}, these differences are not significant.

10.2.1.2.1 Comparison of modelled forcings to estimates in Chapter 2

The forcings used to generate climate projections for the standard SRES scenarios are not necessarily uniform across the multi-model ensemble. Differences among models may be caused by different projections for radiatively active species (Section 10.2.1.1) and by differences in the formulation of radiative transfer (Section 10.2.1.2.2). The AOGCMs in the ensemble include many species which are not specified or constrained by the SRES scenarios, including ozone, tropospheric non-sulphate aerosols, and stratospheric volcanic aerosols. Other types of forcing which vary across the ensemble include solar variability, the indirect effects of aerosols on clouds, and the effects of land-use change on land-surface albedo and other land-surface properties. While the time series of well-mixed greenhouse gases for the future scenarios are identical across the ensemble, the concentrations of these gases in the 19th and early 20th centuries are left to the discretion of individual modelling groups. The differences in radiatively active species and the formulation of radiative transfer affect both the simulations of the 19th and 20th centuries and the scenario integrations initiated from these historical simulations. The resulting differences in the forcing complicate the separation of forcing and response across the multi-model ensemble. These differences can be quantified by comparing the range of forcings across the multi-model ensemble against standard estimates of radiative forcing over the historical record.

The longwave radiative forcings for the SRES A1B scenario from fourteen climate model simulations are compared against estimates using the IPCC formulae (Chapter 2) in Figure 10.2.1. The graph also shows the IPCC estimate for the forcing between 1850 to 2000 and the model forcings between the start of the model integrations and 2000. The forcings from the models are diagnosed from changes in top-of-atmosphere fluxes and the forcing for doubling carbon dioxide (Forster*,* 2005). The IPCC and median model estimates of the longwave forcing are in very good agreement over the 21st century, with differences ranging from –0.27 to 0 W m^{-2}. However, the range of the models for the period 2080–2099 is nearly 4 W m^{-2}, or approximately 60% of the median longwave forcing for that time period. For the year 2000, the IPCC and median model values differ by only –0.06 W m^{-2}.

[INSERT FIGURE 10.2.1 HERE]

The corresponding time series of shortwave forcings for the SRES A1B scenario are plotted in Figure 10.2.2. It is evident that the differences among the models and between the models and the IPCC estimates are larger for the shortwave band. The IPCC value is larger than the median model forcing by 0.2 to 0.5 W m^{-2} for individual 20-year segments of the integrations. For the year 2000, the IPCC estimate is larger by 0.44 W m^{-2}. In addition, the range of modelled forcings is sufficiently large that it includes positive and negative values for every 20-year period. For the year 2000, the shortwave forcing from individual AOGCMs ranges from approximately –1.5 W m^{-2} to +1.5 W m^{-2}. The reasons for this large range include the variety of the aerosol treatments and parameterizations for the indirect effects of aerosols in the multi-model ensemble.

[INSERT FIGURE 10.2.2 HERE]

Since the large range in both longwave and shortwave forcings may be caused by a variety of factors, it is useful to determine the range caused just by differences in model formulation for a given (identical) change in radiatively active species. A standard metric is the global-mean, annually-averaged all-sky forcing at the tropopause for doubling carbon dioxide. Estimates of this forcing for nine of the models in the ensemble are given in Table 10.2.1. The range in the longwave forcing is 1.24 W m^{-2} and the coefficient of variation, or ratio of the standard deviation to mean forcing, is 0.13. These results suggest that up to 30% of the range in longwave forcing in the ensemble for the period 2080–2099 is due to the spread in forcing from the increase in CO_2. Although the shortwave forcing has a coefficient of variation in excess of 2, the range across the ensemble explains less than 13% of the range in shortwave forcing at the end of the 21st-century simulations. This suggests that the large variation among modelled shortwave forcings is caused by species and forcing agents other than carbon dioxide.

Table10.2.1. All-sky adjusted forcing for doubling carbon dioxide

Group	Model	Longwave (W m^{-2})	Shortwave (W m^{-2})
CCCma	CGCM 3.1	3.39	–0.07
GISS	GISS-ER	4.21	–0.15
IPSL	IPSL-CM4	3.50	–0.02
CCSR	MIROC 3.2-hires	3.06	0.08
CCSR	MIROC 3.2-medres	2.99	0.11
MPI	ECHAM5/MPI-OM	3.98	0.03
NCAR	CCSM3	4.23	–0.28
UKMO	UKMO-HadCM3	4.03	–0.17
UKMO	UKMO-HadGEM1	4.02	–0.19
Mean ± RMS		3.71 ± 0.48	–0.07 ± 0.13

10.2.1.2.2 Results from RTMIP: implications for fidelity of forcing projections

To help understand the response of the ensemble of coupled climate models to the various emissions scenarios, the AOGCM modelling community has engaged in a radiative-transfer model intercomparison, or RTMIP (Collins et al., 2005b). The primary objective is to determine the differences in forcing caused by the use of different radiation codes in the AOGCMs used for climate change simulations in the IPCC AR4. The basis of RTMIP is an evaluation of the forcings computed by AOGCMs using benchmark line-by-line (LBL) radiative transfer codes. The comparison is focused on forcing by the well-mixed greenhouse gases (WMGHGs) CO_2, CH_4, N_2O, CFC-11, CFC-12, and the increased H_2O expected in warmer climates. The data requested for RTMIP is the instantaneous changes in clear-sky fluxes and heating rates. While the relevant quantity for climate change is all-sky forcing, the introduction of clouds would greatly complicate the intercomparison exercise. In addition, the calculations omit the effects of stratospheric thermal adjustment to forcing using fixed dynamical heating. This omission facilitates comparison of fluxes from LBL codes and AOGCM parameterizations. The results below include numerical results from fourteen AOGCM groups representing twenty of the models in the multi-model ensemble. The benchmark calculations represent a synthesis of five different LBL codes. All the calculations are for mid-latitude summer.

The sets of calculations in RTMIP cover several forcing configurations:

1. Forcing for CO_2 change;
    a. Present – preindustrial (2000 AD–1860 AD)
    b. $2 \times CO_2 - 1 \times CO_2$ (relative to 1860 AD)
2. Forcing for changes in major well-mixed GHGs (present – preindustrial); and
3. The effect of water vapor changes on the forcing by CO_2.

The concentrations of the WMGHGs and water vapor in the calculations for RTMIP are shown in Table 10.2.2. Differences among these experiments yield the forcing by various combinations of WMGHGs and H_2O. The total (longwave plus shortwave) forcings at 200mb, a surrogate for the tropopause, are shown in Table 10.2.3. For example, the differences between the fluxes calculated for 3b and 3a represent the instantaneous clear-sky radiative forcing from changes in WMGHGs between 1860 and 2000 under mid-latitude conditions.

Table 10.2.2. Concentrations of H_2O and WMGHGs in RTMIP

Experiment	H_2O	CO_2	CH_4	N_2O	CFC-11	CFC-12
Units	%	ppmv	ppbv	ppbv	pptv	pptv
1a	100%	287	0	0	0	0
2a	100%	369	0	0	0	0
2b	100%	574	0	0	0	0
3a	100%	287	806	275	0	0
3b	100%	369	1760	316	267	535
3c	100%	369	1760	275	0	0
3d	100%	369	806	316	0	0
4a	120%	574	0	0	0	0

The basic finding of RTMIP is that there are no sign inconsistencies in the mean forcings averaged across the AOGCM ensemble relative to the LBL models. The AOGCM calculation for the mid-latitude summer forcing by WMGHGs between 1860 and 2000 is 2.68 ± 0.30 W m^{-2}, an estimate in good agreement with the LBL value of 2.58 ± 0.11 W m^{-2} (Table 10.2.3). Based upon the student t-test, none of the differences in mean forcings shown in Table 10.2.3 are statistically significant at the 0.01 level. This indicates that the ensemble-mean forcings are in reasonable agreement with the LBL codes. However, the forcings from individual models, for example from doubling CO_2, span a range at least 10 times larger than that exhibited by the LBL models.

Table 10.2.3. Total Instantaneous Forcing at 200 mb (W m^{-2}) from AOGCMs and LBL codes in RTMIP

Experiments	2a–1a	2b–1a	3a–1a	3b–3a	3b–3c	3b–3d	4a–2b
Gases	CO_2	CO_2	CH_4+ N_2O	All	N_2O+ CFCs	CH_4+ CFCs	H_2O
Forcing*	20th-19th	2×–1×	1860–0×	2000–1860	2000-1860	2000–1860	1.2×–1×
<AOGCM>	1.56	4.28	3.37	2.68	0.47	0.95	4.82
σ(AOGCM)	0.23	0.66	0.73	0.30	0.15	0.30	0.34
<LBL>	1.69	4.75	3.12	2.58	0.38	0.73	5.08
σ(LBL)	0.02	0.04	0.05	0.11	0.12	0.12	0.16

Notes:
*<M> and σ(M) are the mean and standard deviation of forcings computed from model type M.

The forcings from doubling CO_2 from its concentration at 1860 AD are shown in Figure 10.2.3 at the top of the model (TOM), 200 mb, and the surface. The AOGCMs tend to underestimate the longwave forcing at these three levels. The relative differences in the mean forcings are less than 8% for the pseudo-tropopause at 200 mb but increase to approximately 13% at the TOM and to 33% at the surface. The small errors at 200 mb may reflect earlier efforts to improve the accuracy of AOGCM calculations near the tropopause in order to produce reasonable estimates of radiative forcing. In general, the mean shortwave forcings from the LBL and AOGCM codes are in good agreement at all three surfaces. However, the range in shortwave forcing at the surface from individual AOGCMs is quite large. The coefficient of variation (the ratio of the standard deviation to the mean) for the surface shortwave forcing from AOGCMs is 0.95. The forcing from the feedback from water vapour in response to doubling CO_2 is illustrated in Figure 10.2.4. The mean longwave forcing from increasing H_2O is quite well simulated with the AOGCM codes. In the shortwave, the only significant difference between the AOGCM and LBL calculations occurs at the surface, where the AOGCMs tend to underestimate the magnitude of the reduction in insolation.

[INSERT FIGURE 10.2.3 HERE]

[INSERT FIGURE 10.2.4 HERE]

Other calculations show that a few of the participating AOGCMs do not include the effects of CFCs on the longwave fluxes. In addition, all AOGCMs omit the effects of CH_4 and N_2O on the shortwave fluxes despite the large magnitude of the surface forcings by these gases. While the omission of N_2O does not introduce a large absolute error in the forcings, the omission of CH_4 introduces an error in the net surface shortwave forcing of 0.5 W m^{-2} relative to the LBL calculations. The biases in the AOGCM forcings are generally largest at the surface level. For five out of seven surface shortwave forcings and four out of seven surface forcings examined in the intercomparison, the probability that the mean AOGCM and LBL values agree is less than 0.01. The largest biases in the shortwave and longwave forcings from all seven experiments occur at the surface layer.

10.2.1.2.3 Magnitude of aerosol indirect effects

There is some evidence that the first indirect (Twomey) effect saturates under the more emissions intensive scenarios considered in the IPCC TAR and AR4. Johns et al. (2003)parameterize the first indirect effect of anthropogenic emissions as perturbations to the effective radii of cloud drops in simulations of the B1, B2, A2, and A1FI scenarios using HadCM3. At 2100, the first indirect forcings range from –0.50 to –0.79 W m^{-2}. The normalized indirect forcing decreases by a factor of 4 from approximately –7 W/mg[S] in 1860 to between –1 to –2 W/mg[S] by the year 2100. Johns et al. (2003) attribute the decline to the decreased sensitivity of clouds to greater sulfate concentrations at sufficiently large aerosol burdens.

10.2.2 Assessment of Recent Developments in Forcing Projections for the 21st Century

10.2.2.1 Developments in projections for radiative species: extensions beyond SRES

One aspect of future direct aerosol radiative forcing omitted from all but 2 (the NASA GISS-EH and –ER models) of the 23 AOGCMS analyzed in IPCC AR4 is the role of nitrate aerosols. Rapid increases in emissions of NO_x could produce enough nitrate aerosol to offset the expected decline in sulfate forcing by 2100. Adams et al. (2001) have computed the radiative forcing by sulfate and nitrate accounting for the interactions among sulfate, nitrate, and ammonia. For 2000, the sulfate and nitrate forcing are –0.95 and –0.19 W m^{-2}, respectively. Under the SRES A2 scenario, by 2100 declining SO_2 emissions cause the sulfate forcing to drop to –0.85 W m^{-2}, while the nitrate forcing rises to –1.28 W m^{-2}. Hence the total sulfate-nitrate forcing increases from –1.14 W m^{-2} to –2.13 W m^{-2} rather than declining as models that omit nitrates would suggest.

Recent field programs focused on Asian aerosols have demonstrated the importance of BC and OC for regional climate, including potentially significant perturbations to the surface energy budget and hydrological cycle (Ramanathan et al., 2001). The SRES scenarios include time series for chemical precursors of sulfate aerosols, but the SRES scenarios do not prescribe future concentrations of BC and OC. As a result, modelling groups have developed a multiplicity of projections for the concentrations of these aerosol species. For example, Takemura et al. (2001) use data sets for BC released by fossil fuel and biomass burning (Cooke and Wilson, 1996) under current conditions and scale them by the ratio of future to present-day CO_2. The emissions of OC are derived using OC:BC ratios estimated for each source and fuel type. Koch (2001) also employs scaling of present-day emissions inventories by the ratio of future to present-day CO_2. There are still very large uncertainties in current inventories of BC and OC (Bond et al., 2004), the ad hoc scaling methods used to produce future emissions, and the enormous disparity among various treatments of the optical properties of carbonaceous species. Given these uncertainties, future projections of forcing by BC and OC should be quite model dependent, even for a particular SRES emissions scenario.

The SRES scenarios did not explicitly consider changes in composition of the upper troposphere and lower stratosphere. Recent evidence suggests that there are detectable anthropogenic increases in stratospheric sulfate (e.g., Myhre et al., 2004), water vapour (e.g., Forster and Shine, 2002), and condensed water in the form of aircraft contrails. However, extant modelling studies suggest that these forcings are relatively minor compared to the major WMGHGs and aerosol species. Marquart et al. (2003) estimate that the radiative forcing by controls will increase from 0.035 W m^{-2} in 1992 to 0.094 W m^{-2} in 2015 and to 0.148 W m^{-2} in 2050. The rise in forcing is due to an increase in subsonic aircraft traffic following estimates of future fuel consumption (Penner et al., 1999). These estimates are still subject to considerable uncertainties related to poor constraints on the microphysical properties, optical depths, and diurnal cycle of contrails (Myhre and Stordal, 2001; 2002; Marquart et al., 2003). Pitari et al. (2002) examine the effect of future emissions under the A2 scenario on stratospheric concentrations of sulfate aerosol and ozone. By 2030, the mass of stratospheric sulfate increases by approximately 1/3, with the majority of the increase contributed by enhanced upward fluxes of anthropogenic SO_2 through the tropopause. The increase in aerosol forcing from 2000 to 2030 in the A2 scenario is –0.06 W m^{-2}.

Some recent studies have suggested that the global atmospheric burden of soil dust aerosols could decrease by between 20 and 60% due to reductions in desert area associated with climate change (Mahowald and Luo, 2003). Tegen et al. (2004) compared simulations of ECHAM4 and HadCM3 including the effects of climate-induced changes in meteorology and vegetation cover and the effects of increased CO_2 concentrations on vegetation density. In every simulation, the net changes in global atmospheric dust loading have opposite sign, These simulations are forced with identical (IS92a) time series for well-mixed greenhouse gases. Tegen et al. (2005) findings suggest that future projections of changes in dust loading are quite model dependent. They also conclude that dust from agriculturally disturbed soils is less than 10% of the current burden, and that climate-induced changes in dust concentrations would dominate land-use changes under both minimum and maximum estimates of increased agricultural area by 2050.

10.3 Projected Changes in the Physical Climate System

The context for the climate change results presented here has been set in Chapter 8 (evaluation of simulation skill of the control runs and inherent natural variability of the global coupled climate models), and in Chapter 9 (evaluation of the simulations of 20th century climate using the global coupled climate models). A table describing the characteristics of the models was given in Chapter 8, and Table 10.3.1 summarizes the climate change experiments that have been performed with the AOGCMs and other models that will be assessed in this chapter.

The TAR showed multi-model results for future climate change from simple 1% per year CO_2 increase experiments, and from several scenarios including the older IS92a, and, new to the TAR, two SRES scenarios (A2 and B2). For the latter, results from nine models were shown for global averaged temperature change and regional changes. Since the TAR, an unprecedented internationally coordinated climate change experiment has been performed by 21 models from around the world as noted in Table 10.3.1. This larger number of models running the same experiments allows us to better quantify the multi-model signal as well as uncertainty regarding spread across the models (in this section), and also point the way to probabilistic estimates of future climate change (Section 10.5). The scenarios considered here include one of the SRES scenarios from the TAR, A2, along with two additional scenarios, A1B and B1 (see Section 10.2 for details regarding the scenarios). Additionally, three climate change commitment experiments were performed, one where concentrations of GHGs were held fixed at year 2000 values and the models were run to 2100 (termed 20th century stabilization here), and two where concentrations were held fixed at year 2100 values for A1B and B1, and the models were run for an additional 100 to 200 years (see Section 10.7).

[INSERT TABLE 10.3.1 HERE]

This section considers the basic changes in climate over the next hundred years simulated by current climate models under plausible anthropogenic forcing scenarios. While we assess all studies in this field, the presentation will focus on results derived from the new data set for the three SRES scenarios considered in 10.2. Following TAR, we use means across the multi-model ensemble to illustrate representative changes. Studies such as Phillips and Gleckler (2005) have shown that such means are able to simulate the contemporary climate more accurately that individual models, and it is anticipated that this is true for climate changes also. While we indicate the range of results here, the consideration of uncertainty resulting from this range is addressed more completely in Section 10.5.

Standard metrics for response of global coupled models are the equilibrium climate sensitivity, defined as the globally averaged surface air temperature change for a doubling of CO_2 for the atmosphere coupled to a non-dynamic slab ocean, and the transient climate response (TCR), defined as the globally averaged surface air temperature change at the time of CO_2 doubling in the 1% per year transient CO_2 increase experiment. The

TAR showed results for these 1% simulations, and we discuss equilibrium climate sensitivity, TCR and other aspects of response in 10.5.2. Chapter 8 includes processes and feedbacks involved with these metrics.

The following subsections begin with the basic global warming signal relative to the contemporary climate period considered in Chapter 8. We then address patterns of change in warming, precipitation and quantities of particular relevance to impacts. Later subsections consider other important aspects of the climate system, with more reliance on published studies of the multi-model data set and similar results.

10.3.1 Time-Evolving Global Change

The globally averaged surface warming time series from each model in the multi-model data set is shown in Figure 10.3.1, either as a single member (if that was all that was available) or a multi-member ensemble mean, for each scenario in turn. The multi-model ensemble mean warming is also plotted for each case. The surface air temperature is used, averaged over each year, shown as an anomaly relative to the 1980–1999, and offset by any drift in the corresponding control runs. The base period is chosen to match the contemporary climate simulation that is the focus of previous chapters. Similar results have been shown in studies of these models (e.g., Meehl et al., 2005e; Xu et al., 2005; Yukimoto et al., 2005). Interannual variability is evident for each single-model series, but little remains in the ensemble mean. This is because most of this is unforced and is a result of internal variability, as has been presented in detail in Section 9.2.2 of TAR. Clearly, there is a range of model results at each year, although as warming grows this becomes relatively small. The range is somewhat smaller than the range of warming at 2100 for the A2 scenario in the comparable Figure 9.6 of TAR, despite the larger number of models here. Consistent with the range of forcing presented in 10.2, the warming by 2100 is largest in the high GHG growth scenario A2, intermediate in the moderate growth A1B, and lowest in the low growth B1. Naturally, models with high sensitivity tend to have above average warming in each scenario. Global mean precipitation increases in all scenarios (Figure 10.3.1, right column), indicating an acceleration of the hydrological cycle. The multi-model mean varies approximately in proportion to the mean warming.

[INSERT FIGURE 10.3.1 HERE]

The trends of the multi-model mean temperature vary somewhat over the century because of the varying forcings, in particular aerosol (see 10.2). This is illustrated more clearly in Figure 10.3.2, which shows the mean warming series for each scenario as an extension of the 20th century simulations, assessed in Chapter 9. The time series beyond 2100 are derived from the extensions of the simulations (those available) under the idealised constant-forcing scenarios considered further in 10.7.1.

[INSERT FIGURE 10.3.2 HERE]

In order to focus on the forced response of the models at the regional scale, we reduce the internal variability further by averaging over 20-year time periods. This span is shorter than the traditional 30-year climatological period, in recognition of the transience of the simulations, and of the larger size of the ensemble. We focus on three periods over the coming century: a near future period 2011–2030, a mid-century period 20462065, and the late-century period 2080–2099. Again, we consider changes of temperature, and other quantities that follow, relative to the 1980–1999 means. The multi-model ensemble mean warming for the three future periods in the different experiments are given in Table 10.3.2, among other results. The close agreement of warming for early century (with a range of only 0.06°C, from 0.64°C to 0.70°C) shows that no matter which scenario is followed, the warming is similar on the timescale of the next decade or two. It is also worth noting that nearly half of the early century climate change arises from warming we are already committed to (0.31°C for early century). By mid-century, the choice of scenario becomes more important for the magnitude of warming, with a range of 0.31°C from 1.30°C to 1.73°C, and with only about a quarter of that warming due to climate change we are already committed to (0.42°C). By the late century, there are clear consequences for which scenario is followed, with a range of 1.27°C from 1.78°C to 3.05°C, with only about 15% of that warming coming from climate change we are already committed to (0.52°C).

Table 10.3.2. Global mean warming (annual mean surface air temperature, in °C) for several time periods relative to 1980-1999 for the four scenarios simulated by the multi-model ensemble mean. Shown in italics

are metrics related to the geographic patterns of warming (see Figure 10.3.5), first the M values for agreement of the normalized fields of warming, with the A1B 2080–2099 case, and second 100 times the mae (global mean absolute 'error' –difference, in °C) between the fields. Here $M=(200/\pi) \arcsin[1 - mse / (V_X+V_Y + (G_X - G_Y)^2)]$, with mse the mean square error between the two fields X and Y, and V and G are variance and global mean of the fields (as subscripted). Values of 100 for M and 0 for mae indicate perfect agreement with the pattern of warming in A1B at the end of the 21st century.

	2011–2030	2046–2065	2080–2099	2180–2199
A2	0.64, *84, 7*	1.61, *91, 4*	3.05, *93, 3*	
A1B	0.69, *87, 5*	1.73, *93, 3*	2.59, *100, 0*	3.30, *88, 5*
B1	0.70, *84, 7*	1.30, *87, 5*	1.78, *90, 4*	2.11, *85, 7*
Commit	0.31, *67, 15*	0.42, *61, 15*	0.52, *64, 15*	

10.3.2 Patterns of Change in the 21st Century

10.3.2.1 Warming

It was noted in the TAR that much of the regional variation of the annual mean warming in the multi-model means is associated with high to low latitude contrast. We can better quantify this from the new multi-model mean in terms of zonal averages. A further contrast is provided by partitioning the land and ocean values (e.g., Watterson, 2003), based on model data interpolated to a standard grid. Figure 10.3.3 illustrates the late-century A2 case, with all values shown relative to (or 'normalized' by) the global mean warming. Warming over land is greater than the mean except in the southern midlatitudes, where the warming over ocean is a minimum. Warming over ocean is smaller than the mean except at high latitudes. There is some contrast in ratio with the Commitment case to be considered in 10.7.1. At nearly all latitudes the A1B and B1 warming ratios lie between A2 and Commitment, with A1B particularly close to the A2 results. Warming is relatively smaller in low latitudes for B1 (and larger at high latitudes), but by differences of 10% at most. (These values and results for other periods can be seen in supplementary material[1]). Aside from the Commitment case, the ratios for the other time periods are also quite similar to those for A2. We consider regional patterns shortly.

[INSERT FIGURE 10.3.3 HERE]

Zonal means also depict much of the atmospheric and oceanic variation of warming, and it is instructive to illustrate these features of the coupled system together. Figure 10.3.4 shows the warming for the A1B scenario at each latitude from the bottom of the ocean, to the top of the atmosphere for the three 21st century periods used in Table 10.3.2. To produce this ensemble mean, we first interpolated the model data to standard ocean depths and atmospheric pressures. Consistent with the global transfer of excess heat from the atmosphere to the ocean, and the difference between warming over land and ocean, there is some discontinuity between the plotted means of the lower atmosphere and the upper ocean. The relatively uniform warming of the troposphere and cooling of the stratospheric in this multi-model mean is consistent with that shown in Figure 9.8 of TAR, but now additionally given its evolution during the 21st century. Upper tropospheric warming reaches a maximum in the tropics and is seen even in the early century time period.. The pattern is very similar over the three periods, consistent with the rapid adjustment of the atmosphere to the forcing. These changes are simulated with good consistency among the models (the larger values of both signs are stippled, indicating that the ensemble mean is larger in magnitude than the inter-model standard deviation).

The ocean warming evolves more slowly. There is initially little warming below the mixed layer, except at some high latitudes. Even as a ratio with mean surface warming, later in the century the temperature increases more rapidly in the deep ocean, consistent with results from individual models (e.g., Watterson, 2003). This rapid warming of the atmosphere, and the slow penetration of the warming into the ocean has implications for the timescales of climate change commitment discussed in Section 10.7. It has been noted in a 5 member multi-model ensemble analysis that, associated with the changes in temperature of the upper ocean in Figure 10.3.4, the tropical Pacific ocean heat transport remains nearly constant with increasing GHGs due to the compensation of the subtropical cells (STCs) and the horizontal gyre variations, even as the

[1] Supplementary material is available to reviewers at the same web site as used for the chapter drafts.

STCs change in response to changes in the trade winds (Hazeleger, 2005). Additionally, a southward shift of the Antarctic Circumpolar Current is projected to occur in a 15 member multi-model ensemble due to changes of surface winds in a future warmer climate (Fyfe and Saenko, 2005). This is associated with a poleward shift of the westerlies at the surface (see Section 10.3.6), in the upper troposphere (particularly notable in the Southern Hemisphere) (Stone and Fyfe, 2005), and increased relative angular momentum from stronger westerlies (Räisänen, 2003) and westerly momentum flux in the lower stratosphere particularly in the tropics and southern midlatitudes (Watanabe et al., 2005). The surface wind changes are associated with corresponding changes in wind stress curl and horizontal mass transport in the ocean (Saenko et al., 2005).

[INSERT FIGURE 10.3.4 HERE]

We turn to the regional warmings for each scenario and time period, shown as maps in Figure 10.3.5. In each case greater warming over most land is evident (e.g., Kunkel and Liang, 2005). Over ocean warming is relatively large in the Arctic, and particularly pronounced along the equator in the Pacific, with less warming to the north and south (Liu et al., 2005), and little warming over the North Atlantic and the southern oceans (e.g., Xu et al., 2005). It is clear that the pattern of change is very similar among the late century cases, with the pattern correlation coefficient as high as 0.994 between A2 and A1B. As for the zonal means, the fields normalized by the mean warming are very similar. The agreement between the A1B case, as a standard, and the others is quantified in Table 10.3.2, by the absolute measure M (Watterson, 1996), with 100 meaning identical fields and zero meaning no similarity. Values of M become progressively larger later in the 21st century, with values of 90 or larger for the late 21st century, thus confirming the high similarity of the patterns of warming in the late century cases. The deviation from 100 is approximately proportional to the mean absolute difference also given. The earlier warming patterns are also similar to the standard case, particularly for the same scenario A1B. Furthermore, the zonal means over land and ocean considered above are representative of much of the small differences in warming ratio. While there is some influence of differences in forcing patterns among the scenarios, and of effects of oceanic uptake and heat transport in modifying the patterns over time, there is also support for the role of atmospheric heat transport in offsetting such influences (e.g., Boer and Yu, 2003b; Watterson and Dix, 2005). Dufresne et al. (2005) show that aerosol provides modest cooling of northern hemisphere up to mid 21st century in the A2 scenario.

[INSERT FIGURE 10.3.5 HERE]

Such similarities in patterns of change have been described recently by Mitchell (2003) and Harvey (2004). They aid the efficient presentation of the broad scale multi-model results, as patterns depicted for the standard A1B 2080–2099 case are usually typical of other cases. As can be seen in the supplementary material[1], to a large extent this applies to other seasons and also other variables under consideration here, with significant exceptions to be noted. Where there is similarity of normalized changes, values for other cases can be estimated by scaling by the appropriate ratio of global means from Table 10.3.2.

The surface warming fields for the extratropical winter and summer seasons, December-February (DJF) and June-August (JJA), are shown for the standard case in Figure 10.3.6. The high latitude warming is rather seasonal, being larger in winter as a result of sea ice and snow as noted in Chapter 9 of the TAR. However the relatively low warming in southern South America is more extensive in southern winter. Similar patterns of change in earlier model simulations are described by Giorgi et al. (2001).

[INSERT FIGURE 10.3.6 HERE]

The patterns of warming are similar to Figure 10.3.5, with consistency among models almost everywhere (almost the entire area of the globe is stippled). Such warming has many consequences, one of which could be the disappearance of certain climate regimes and appearance of others (Williams et al., 2005a). That study used a 9 member multi-model ensemble to show that roughly 5% to 35% of the earth's terrestrial surface may experience both novel and disappearing climates by the end of the 21st century in the A2 scenario.

10.3.2.2 Cloud and diurnal cycle

In addition to being an important link to humidity and precipitation, cloud cover plays an important role in the sensitivity of the GCMs (e.g., Soden and Held, 2005) and to the diurnal temperature range (DTR) over land (e.g., Dai and Trenberth, 2004) so we consider the projection of these variables by multi-model ensemble. This was not shown in the TAR, and is aided here by the new multi-model data set. Cloud radiative feedbacks to GHG forcing are sensitive to the elevation, latitude and hence temperature of the clouds (Chapter 8). Current GCMs simulate clouds through various complex parameterizations (Chapter 8), to produce cloud quantified by an area fraction within each grid square, and each atmospheric layer. Taking zonal means of this quantity, averaged over the present and future periods produces a relative change that is indicative of the latitude-height structure of the cloud changes. Averaging across the multi-model ensemble (from available data), using results interpolated to standard pressure levels and latitudes, produces the changes depicted in Figure 10.3.7a. At all latitudes there are increases in the upper troposphere, and mostly decreases below, indicating an increase in the altitude of clouds overall. This shift occurs consistently across models. There are increases in near-surface amounts at some latitudes. There is considerable variation across the ensemble in these changes, as indicated by the small ratio of mean to SD, with few areas stippled in the figure. It is worth noting that the stippled part in this figure and others under-represents mean changes that are formally statistically significant, if the individual model results were to be considered a sample (of size 16 or more).

The total cloud area fraction from an individual model represents the net coverage over all the layers, after allowance for the overlap of clouds, and is an output included in the data set. The change in the ensemble mean of this field is shown in Figure 10.3.7b. Much of the low and middle latitudes experience a small decrease in cloud cover. There are a few low latitude regions of increase, as well as substantial increases at high latitudes. Naturally, these larger changes relate well to changes in precipitation depicted earlier. Moderate spatial correlation between cloud cover and precipitation holds for seasonal means of both the present climate and changes.

[INSERT FIGURE 10.3.7 HERE]

Clouds act to cool the climate system by reflecting shortwave radiation, and also warm it by trapping long wave radiation (e.g., Stowasser and Hamilton, 2005; Williams et al., 2005c). The radiative effect of clouds is represented by the cloud radiative forcing diagnostic (see earlier chapters). This can be evaluated from radiative fluxes at the top-of-atmosphere calculated with or without the presence of clouds, which are output by the GCMs. The global and annual mean averaged over the models, for 1980–1999, is –22.3 W m^{-2}. Change in cloud radiative forcing, indicative of the sign of cloud feedback in global coupled models, has been shown to have different signs in a limited number of previous modelling studies (Meehl et al., 2004b; Tsushima et al., 2005b). Figure 10.3.7b shows globally averaged cloud radiative forcing changes for the end of the A1B scenario for the last 20 years of the 21st century compared to the last 20 years of the 20th century for individual models of the data set. These current models show a variety of different magnitudes and even signs. The ensemble mean change is –0.6 W $m^{-2.}$ This range indicates that cloud feedback is still an uncertain feature of the global coupled models as related to climate sensitivity.

Mean change in diurnal range of surface air temperature (DTR) has been shown to be decreasing in several land areas of the globe in observations of the 20th century (Chapter 3), together with increasing cloud cover. In the multi-model mean of present climate DTR over land is indeed closely anti-correlated, spatially, to the total cloud cover field, because of the diurnal surface radiative effect of cloud (e.g., Dai and Trenberth, 2004). This is true also of the 21st century changes in the fields, under A1B, as can be seen by comparing the change in DTR, shown as Figure 10.3.8b, with Figure 10.3.7b. Changes reach magnitude 0.5°C in some regions, with some consistency over the models. Smaller widespread decreases are likely due to the radiative effect of the enhanced greenhouse gases including water vapour (see also Stone and Weaver, 2002). Further consideration of DTR is given in Section 10.3.7.2.

In addition to the diurnal temperature range, Kitoh and Arakawa (2005) document changes in the regional patterns of diurnal precipitation over the Maritime Continent, and show that over ocean nighttime precipitation decreases and daytime precipitation increases, while over land the opposite is the case, thus producing a decrease in the diurnal precipitation amplitude over land and ocean. They attribute these changes to a larger nighttime temperature increase over land due to increased GHGs.

[INSERT FIGURE 10.3.8 HERE]

10.3.2.3 Precipitation and surface water

Models simulate that global mean precipitation increases with global warming. However, there are substantial spatial and seasonal variations in this field even in the multi-model means depicted in Figure 10.3.6. There are fewer areas stippled for precipitation than for the warming, indicating more variation among the ensemble of models. Increases of precipitation at high latitudes in both seasons are very consistent across models. The increases of precipitation over the tropical oceans and in some of the monsoon regimes (e.g., South Asian monsoon in JJA, Australian monsoon in DJF) are notable but are not all consistent. There are smaller amplitude decreases of midlatitude summer precipitation. Decreases in precipitation over many subtropical areas are evident in the multi-model ensemble mean, but again are less consistent than the increases at high latitudes. For example, Liu et al. (2003) show, for a 5 member multi-member ensemble, a northward shift of the Sahara as it becomes hotter and drier. Further discussion of changes in the regional monsoon regimes is presented in Chapter 11.

With annual mean precipitation being of particular importance, the global map of the A1B 2080–2099 change is shown in Figure 10.3.9, along with some other hydrological quantities from the multi-model ensemble. Emori and Brown (2005) show percentage changes of annual precipitation from the ensemble. Increases of over 20% occur in most high latitudes, as well as eastern Africa, central Asia and the equatorial Pacific Ocean. The change over ocean between 10°S and 10°N accounts for about half the increase in the global mean seen in Figure 10.3.1. Substantial decreases, reaching 20%, occur in the Mediterranean region, the Caribbean region, and the subtropical western coasts of each continent. Overall, changes over land account for 24% of the global mean increase in precipitation, a little less than the proportion of land by area (29%), but with local values of both signs. These patterns of change occur in the other cases, although with agreement (by *M*) a little lower than for the warming.

[INSERT FIGURE 10.3.9 HERE]

Wetherald and Manabe (2002) provide a good description of the mechanism of hydrological change simulated by GCMs. In GCMs the global mean evaporation changes closely balance the precipitation change, but not locally because of changes in the atmospheric transport of water vapour. Annual average evaporation (Figure 10.3.9) increases over much of the ocean, with spatial variations tending to relate to those in the surface warming (Figure 10.3.5). As found by Kutzbach et al. (2005) and Bosilovich et al. (2005), atmospheric moisture convergence increases over the equatorial oceans and over high latitudes. In the tropics, the increases in precipitation are associated with a slight weakening of the tropical atmospheric circulation due to the compensating effects of increased SSTs and evaporation working to increase precipitation, and the reduction of radiative cooling in the lower troposphere that tends to stabilize the atmosphere (Sugi and Yoshimura, 2004). However, a complete deforestation of the tropics had little effect on the hydroclimate in the midlatitudes in one modelling study, suggesting that the extratropical response to the forcings included in the present models would not appreciably be changed by future land cover changes in the tropics (Findell and Knutson, 2005).

Over land, rainfall changes tend to be balanced by both evaporation and runoff. Runoff is notably reduced in southern Europe and increased in south-east Asia. Nohara et al. (2005) and Milly et al. (2005) assess the impacts of these changes in terms of river flow, finding that discharges from high latitude rivers increase, while those from major rivers in the Middle East, Europe and central America tend to decrease. In the annual mean, soil moisture (Figure 10.3.9) declines predominate, particularly over subtropical lands. There are increases in equatorial lands and northern Europe. Hydrological impacts are considered in Chapter 11.

10.3.2.4 Sea-level pressure and atmospheric circulation

As a basic component of the mean atmospheric circulations and weather patterns, we consider projections of the mean sea-level pressure. Seasonal mean changes for DJF and JJA are shown in Figure 10.3.6. Sea level pressure differences show decreases at high latitudes in both seasons in both hemispheres, although the magnitudes of the changes vary (with no areas stippled). The compensating increases are predominantly over the midlatitude and subtropical ocean regions, extending across South America, Australia and southern Asia in JJA, and the Mediterranean in DJF. Many of these increases are consistent across the models. This pattern of change has been linked to an expansion of the Hadley Circulation and a poleward shift of the midlatitude storm tracks (Yin, 2005). This helps explain, in part, the increases of precipitation at high latitudes and decreases in the subtropics and parts of the midlatitudes. Further analysis of the regional details of these changes is given in Chapter 11. The pattern of pressure change implies increased westerly flows across the western parts of the continents. These contribute to increases of mean precipitation (Figure 10.3.6) and increased precipitation intensity (Meehl et al., 2005a).

The zonal mean temperature change shown in Figure 10.3.4 gives us an insight into the change in atmospheric circulation in a warmer climate. A large temperature increase is found in the tropical upper troposphere. This warming enhances both the meridional temperature gradient and the static stability. Rind et al. (2005b) finds that forcings such as SST, CO_2, O_3, aerosols etc., which increase the meridional temperature gradient in the upper troposphere and/or in the lower stratosphere, produce a positive AO/NAO and AAO-like change. Such a change is also found in the sea-level pressure field in Figure 10.3.6. On the other hand, the increased static stability reduces overturning circulations (Knutson and Manabe, 1995; Sugi et al., 2002). A weakening in the Hadley, Walker and monsoon overturning circulations by 2100 simulated by the AR4 GCMs was found by Tanaka et al. (2005). The El Niño-like change discussed in the TAR models is consistent with the general reduction of tropical circulations in a warmer climate. Thus the current models suggest that a positive AO/NAO and AAO-like change and an El Niño-like change are basic response patterns in middle to high latitudes and in low latitudes, respectively, in a warmer climate. However, these two patterns have opposite pressure anomalies over the North Pacific so that the local response is sensitive to the magnitudes of the patterns. Yamaguchi and Noda (2005) found that the current models are not deterministic yet. This is related to the lack of consistency (and stippling) over the North Pacific in the sea-level pressure change field in Figure 10.3.6.

10.3.3 Changes in Ocean/Ice and High Latitude Climate

10.3.3.1 Changes in sea ice cover

Models of the 21st century project that future warming is amplified at high latitudes resulting from positive feedbacks involving snow and sea ice. The warming is particularly large in fall and early winter (Manabe and Stouffer, 1980; Holland and Bitz, 2003) when sea ice is thinnest and the snow depth is insufficient to blur the relationship between surface air temperature and sea ice thickness (Maykut and Untersteiner, 1971). As shown by Zhang and Walsh (2005), the coupled models show a range of responses in northern hemisphere sea ice areal extent ranging from very little change to a dramatic, and accelerating reduction over the 21st century (Figure 10.3.10a).

[INSERT FIGURE 10.3.10 HERE]

An important characteristic of the projected change is for summertime ice area to decline far more rapidly than wintertime ice area (Gordon and O'Farrell, 1997), and hence sea ice rapidly approaches a seasonal ice cover in both hemispheres (Figures 10.3.10b, 10.3.11). Seasonal ice cover is, however, rather robust and persists to some extent throughout the 21st century in most (if not all) models. Bitz and Roe (2004) noted that future projections show Arctic sea ice thins fastest where it is initially thickest (Figure 10.3.12), a characteristic that future climate projections share with sea ice thinning observed in the late 20th century (Rothrock et al., 1999). Consistent with these results, a projection by Gregory et al., (2002b) showed Arctic sea ice volume decreases more quickly than sea ice area (because trends in winter ice area are low) in the 21st century.

In 20th and 21st century simulations, Antarctic sea ice cover decreases more slowly than in the Arctic (see Figure 10.3.11), particularly in the vicinity of the Ross Sea where most models predict a local minimum in surface warming. This is commensurate with the region with the greatest increase in ocean heat uptake, which results from reduced vertical mixing in the ocean (Gregory, 2000). The ocean stores much of its increased heat below 1 km depth in the Southern Ocean. In contrast, horizontal heat transport poleward of about 60N increases in many models (Holland and Bitz, 2003), but much of this heat remains in the upper 1 km of the northern subpolar seas and Arctic Ocean (Gregory, 2000; Bitz et al., 2005). Bitz et al. (2005) argue that these differences in the depth where heat is accumulating in the high latitude oceans has consequences for the relative rates of sea ice decay in the Arctic and Antarctic.

While most climate models share these common characteristics (peak surface warming in fall and early winter, sea ice rapidly becomes seasonal, Arctic ice decays faster than Antarctic ice, and northward ocean heat transport increases into the northern high latitudes), models have poor agreement on the amount of thinning of sea ice (Flato and Participating CMIP modeling groups, 2004; Arzel et al., 2005) and the overall climate change in the polar regions (IPCC TAR) (Holland and Bitz, 2003). Flato (2004) showed that the basic state of the sea ice and the reduction in thickness and/or extent have little to do with model physics among CMIP2 models. At the same time, Holland and Bitz (2003) and Arzel et al. (2005) found serious biases in the basic state of simulated sea ice thickness and extent. Further, Rind et al. (1995), Holland and Bitz (2003), and Flato (2004) showed that the basic state of the sea ice had a significant influence on the change in sea ice thickness in the Arctic and extent in the Antarctic.

[INSERT FIGURE 10.3.11 HERE]

[INSERT FIGURE 10.3.12 HERE]

10.3.3.2 Other high latitude changes

Snow cover is an integrated response to both temperature and precipitation and exhibits strong negative correlation with air temperature in most areas with a seasonal snow cover. Because of this temperature association, the simulations project widespread reductions in snow cover over the 21st century (Figure 10.3.13). For the Arctic Climate Impact Assessment (ACIA) model mean, at the end of the 21st century the projected reduction in the annual mean Northern Hemisphere snow coverage is –13% under the B2 scenario (ACIA, 2004). The individual model projections range from –9% to –17%. The actual reductions are greatest in spring and late autumn/early winter indicating a shortened snow cover season (ACIA, 2004). The beginning of the snow accumulating season (the end of the snow melting season) is projected to be later (earlier), and the fractional snow coverage is projected to decrease during the snow season (Hosaka et al., 2005).

Regionally, the changes are a response to both increased temperature and increased precipitation (changes in circulation patterns) and are complicated by the competing effects of warming and increased snowfall in those regions that remain below freezing. Therefore, in contrast to the general Northern Hemisphere decrease of snow amount (SWE) and snow coverage, some areas are projected to increase over parts of high-latitude northern regions during the cold seasons (Figure 10.3.13), and this is attributed to the increase of precipitation (snowfall) from autumn to winter (Hosaka et al., 2005; Kattsov et al., 2005). However, the projected snow coverage changes by the end of the 21st century are small (ACIA, 2004; Hosaka et al., 2005) and of comparable or smaller order than the present-day AR4 model bias (Hosaka et al., 2005; Roesch, 2005) (see Chapter 8.3.4 for evaluation of present-day snow cover simulation by AR4 models). Further discussion of regional changes can be found in Section 11.3.8.

[INSERT FIGURE 10.3.13 HERE]

10.3.3.3 Changes in Greenland ice sheet mass balance

As noted in Section 10.6, modelling studies (e.g., Hanna et al., 2002; Kiilsholm et al., 2003; Wild et al., 2003) as well as satellite observations and airborne altimeter surveys (Krabill et al., 2000; Paterson and Reeh, 2001; Mote, 2003) suggest a slightly negative Greenland ice sheet mass balance associated with the thinning of ice sheet margins. A consistent feature of all climate models is the projection of 21st century warming which is amplified in northern latitudes. This suggests a continuation of melting of the Greenland ice sheet, since increased summer melting dominates over increased winter precipitation in model projections of future climate. Ridley et al. (2005) coupled HadCM3 to an ice sheet model to explore the melting of the Greenland ice sheet under elevated (four times preindustrial) levels of atmospheric CO_2. While the entire Greenland Ice sheet eventually completely ablated (after 3000 years), the peak rate of melting was only 0.1 Sv and its effect on the North Atlantic meridional overturning was minimal. Toniazzo et al. (2004) also showed that in HadCM3, the complete melting of the Greenland Ice sheet was an irreversible process at preindustrial levels of atmospheric CO_2. Dethloff et al. (2004) went on to further show that Greenland's deglaciation had a profound influence on Arctic winter circulation with much less effect in the summer (consistent with Toniazzo et al., 2004).

10.3.4 Changes in the Meridional Overturning Circulation

A feature common to all climate model projections is the increase of high latitude temperature as well as an increase of high latitude precipitation. This was already reported in the IPCC TAR and is confirmed by the projections using the latest versions of comprehensive climate models (Section 10.3.2). Both of these effects tend to make the high latitude surface waters lighter and hence increase their stability. As more coupled models have become available since the TAR, the evolution of the Atlantic meridional overturning circulation (MOC) can be more thoroughly assessed. Figure 10.3.14 shows simulations from 15 coupled models integrated from 1850 to 2100 under emissions scenario SRES A1B up to year 2100, and constant thereafter. Many of the models are run without flux adjustments (see Chapter 8). The MOC is influenced by the density structure of the Atlantic Ocean, small-scale mixing and the surface momentum and buoyancy fluxes. It is evident from Figure 10.3.14 that some models give a MOC strength that is inconsistent with present-day estimates (Smethie and Fine, 2001; Ganachaud, 2003; Lumpkin and Speer, 2003; Talley, 2003). The MOC for these models is shown for completeness but cannot be used in assessing potential future changes in the MOC in response to various emissions scenarios.

Generally, the simulated late 20th century Atlantic MOC shows a spread ranging from a weak MOC of about 12 Sv (1 Sv = $10^6\ m^3 s^{-1}$) to over 20 Sv (Figure 10.3.14). When forced with the SRES A1B scenario, the models show a reduction of the MOC, but in one model, the changes are not distinguishable from the simulated natural variability. The reduction of the MOC proceeds on the time scale of the simulated warming, because it is a direct response to the decrease in buoyancy at the ocean surface. A positive NAO trend might delay, but not prevent, this response by a few decades (Delworth and Dixon, 2000). Such a weakening of the MOC in future climate is associated with SST and salinity changes in the region of the Gulf Stream and North Atlantic Current (Dai et al., 2005). South of 60°N this can produce a decrease in northward heat transport south of 60N, but increased northward heat transport north of 60°N (Hu et al., 2004a). No model shows an increase of the MOC in response to the increase in greenhouse gases, and no model simulates an abrupt reduction of the MOC within the 21st century. One study has suggested that inherent low frequency variability of the MOC (Atlantic Multidecadal Oscillation or AMO) may produce a natural weakening over the next few decades that could further accentuate the decrease due to anthropogenic climate change (Knight et al., 2005).

In some of the older models (e.g., Dixon et al., 1999), increased high latitude precipitation dominates over increased high latitude warming in causing the weakening, while in others (e.g., Mikolajewicz and Voss, 2000), the opposite dominance is found. In a recent model intercomparison, Gregory et al. (2005b) found that for all eleven models analysed, the MOC reduction was caused more by changes in surface heat flux than changes in surface freshwater flux. In addition, simulations using models of varying complexity (Stocker et al., 1992b; Weaver et al., 2003). Saenko et al. (2003) have shown that freshening or warming in the Southern Ocean acts to increase or stabilize the MOC. This is a consequence of the fundamental coupling of Southern Ocean Processes with North Atlantic Deep Water production.

A few simulations using coupled models are available which permit the assessment of the long-term stability of the MOC (Stouffer and Manabe, 1999; Voss and Mikolajewicz, 2001; Stouffer and Manabe, 2003; Bryan et al., 2005; Nakashiki et al., 2005). Most of these simulations assume an increase of CO_2 by 1%/year to various levels ranging from 2 to 4 times preindustrial levels. One study also considers slower increases (Stouffer and Manabe, 1999), or a reduction of CO_2 (Stouffer and Manabe, 2003). The more recent models are not flux adjusted and have high resolution (T85) (Bryan et al., 2005; Nakashiki et al., 2005). A common feature of all simulations is a reduction of the MOC in response to the warming and a stabilization or recovery of the MOC when the concentration is kept constant after achieving a level of 2 to 4 times the preindustrial atmospheric CO_2 concentration. None of these models shows a spin-down of the MOC which continues after the forcing is kept constant. But such a long-term shut-down cannot be excluded if the amount of warming and its rate exceed certain thresholds as shown using a model of intermediate complexity (Stocker and Schmittner, 1997). Complete shut-downs, although not permanent, were also simulated by a flux adjusted coupled model (Manabe and Stouffer, 1994; Stouffer and Manabe, 2003). Since in none of these simulations the thresholds determined by the model of intermediate complexity were passed, the long-term stability of the MOC found in the present simulations is consistent with the results from simpler models.

[INSERT FIGURE 10.3.14 HERE]

The reduction in MOC strength associated with increasing greenhouse gases represents a negative feedback for the warming in and around the North Atlantic. That is, through reducing the transport of heat from low to high latitudes, SSTs are cooler than they would otherwise be if the MOC was left unchanged. As such, warming is reduced over and downstream of the North Atlantic. It is important to note that in models where the MOC weakens, warming still occurs downstream over Europe due to the dominating role of the radiative forcing associated with increasing greenhouse gases. In different models, this MOC-SST feedback is fundamentally determined by the competing effects of interhemispheric differential heat and freshwater flux forcing. Many future projections show that once the radiative forcing is held fixed, reestablishment of the MOC occurs to a state similar to that for the present day (Gregory et al., 2005b). During this slow reestablishment phase, the MOC acts as a positive feedback to warming in and around the North Atlantic and, at equilibrium, there is close to zero net feedback. While the oceanic meridional heat flux at low latitude reduced upon a slowdown of the MOC, many simulations show increasing meridional heat flux into the Arctic which contributes to accelerated warming and sea ice melting there. This is due both to the advection of warmer water, as well as an intensification of the influx of North Atlantic water into the Arctic (Hu et al., 2004a).

Climate models for which a complete shutdown of the MOC has been found in response to sustained warming were flux adjusted coupled GCMs or intermediate complexity models. A robust result from such simulations is that the spin-down of the MOC takes several centuries after the forcing is kept fixed (e.g., at 4 $\times$ CO_2). None of the current state-of-the art models has been integrated long enough to determine whether the MOC spins down, settles at a reduced level, or recovers under any perturbation. Besides the forcing amplitude and rate (Stocker and Schmittner, 1997), the amount of mixing in the ocean also appears to determine the stability of the MOC: increased vertical and horizontal mixing trends to stabilize the MOC and eliminate the possibility of a second equilibrium state (Manabe and Stouffer, 1999; Longworth et al., 2005).

The MOC is not necessarily a comprehensive indicator of ocean circulation changes in response to global warming. In a transient 2 $\times$ CO_2 experiment using a coupled AOGCM, the MOC changes were small, but convection in the Labrador Sea stopped due to warmer, and hence lighter waters that inflow from the Greenland-Iceland-Norwegian Sea (GIN Sea) (Wood et al., 1999). Similar results were found by Hu et al. (2004a), who also report an increase in convection in the GIN Sea due to the influx of more saline waters from the North Atlantic. Various simulations using coupled models of different complexity find significant reductions in convection in the GIN Sea in response to warming (Schaeffer et al., 2004; Bryan et al., 2005). Presumably, a delicate balance exists in the GIN Sea between the circum-Arctic river runoff (Kattsov et al., 2005), sea ice production, and advection of saline waters from the North Atlantic, and on a longer time scale, the inflow of fresh water through Bering Strait. The projected increases in circum-Arctic river runoff may enhance the tendency toward a reduction in GIN Sea convection (Stocker and Raible, 2005; Wu et al., 2005). Cessation of convection in the Labrador Sea in the next few decades is also simulated in a high-resolution model of the Atlantic Ocean driven by surface fluxes from two AOGCMs (Schweckendiek and Willebrand, 2005). The large-scale responses of the high-resolution ocean model (e.g., MOC, Labrador Seas) agree with those from the AOGCMs. The grid resolution of the ocean components in the coupled AOGCMs has significantly increased since the TAR, and some consistent patterns of changes in convection and water mass properties in the Atlantic Ocean emerge in response to the warming, but models still show a variety of responses in detail.

One of the most misunderstood issues concerning the future of the MOC under anthropogenic climate change is its often cited potential to cause the onset of the next ice age. A relatively solid understanding of glacial inception exists wherein a change in seasonal incoming solar radiation (warmer winters and colder summers) associated with changes in the Earth’s axial tilt, longitude of perihelion and the precession of its elliptical orbit around the sun is required (Crucifix and Loutre, 2002; Yoshimori et al., 2002). This small change must then be amplified by albedo feedbacks associated with enhanced snow/ice cover, vegetation feedbacks owing to the expansion of tundra, and greenhouse gas feedbacks associated with the uptake (not release) of carbon dioxide and reduced release or increased destruction rate of methane. As discussed by Berger and Loutre (2002) and Weaver and Hillaire Marcel (2004b), it is not possible for global warming to cause an ice age.

The best estimate of sea level change over the 20th century (IPCC TAR) associated with the slight net negative mass balance from Greenland is 0.0-0.1 mm/yr. This converts to only about 0.0–0.001 Sv (1 Sv $\equiv$ 10^6 m^3s^{-1}) of freshwater forcing over the total ocean. Such an amount even when added directly and exclusively to the North Atlantic has been suggested to be too small to affect the North Atlantic MOC (see

Weaver and Hillaire-Marcel, 2004a), although one model exhibits a MOC response in the later part of the 21st century (Fichefet et al., 2003). As noted in Section 10.3.3.3, Ridley et al. (2005) found the peak rate of Greenland Ice Sheet melting was 0.1 Sv when they instantaneously elevated Greenhouse gas levels in HadCM3. They further noted that this had little effect on the North Atlantic meridional overturning, although 0.1 Sv is sufficiently large to cause more dramatic transient changes in the strength of the MOC in other models (Stouffer et al., 2005).

Taken together, it is likely that the MOC will reduce, perhaps associated with a significant reduction in LSW formation, but very unlikely that the MOC will undergo an abrupt transition during the course of the 21st century. At this stage it is too early to assess the likelihood of an abrupt change of the MOC beyond the end of the 21st century. The few available simulations with models of different complexity rather suggest a centennial slow-down. Recovery of the MOC is likely if the radiative forcing is stabilised but would take several centuries.

10.3.5 Changes in Variability

10.3.5.1 ENSO changes in the tropics

Enhanced GHG concentrations result in a general increase in sea surface temperatures (SST). These SST increases will not be spatially uniform. A majority of recent models have projected that the background tropical Pacific SST change from global warming (upon which individual El Niño/Southern Oscillation (ENSO) events occur) will be an El Niño-like pattern (Collins and The CMIP Modelling Groups, 2005; Yamaguchi and Noda, 2005). This is also particularly evident late in the 21st century in the A1B and A2 scenarios for the multi-model mean in Figure 10.3.5. That is, the amount of SST rises over the eastern tropical Pacific is larger than that over the western tropical Pacific, together with an eastward shift of the tropical Pacific rainfall distribution. CMIP2 models showed that the most likely scenario is for no trend towards either mean El Niño-like or La Niña-like conditions, while there remains a small probability (16%) for a change to El Niño-like conditions (Collins and The CMIP Modelling Groups, 2005) (Figure 10.3.15). Based on the spatial anomaly pattern of SST, SLP and precipitation, Yamaguchi and Noda (2005) show that the CO_2-induced response pattern is closely related to the model natural variability, and in the tropical Pacific, an ENSO-like global warming pattern is simulated by many models with mostly an El Niño-like change. They also discussed the model response of ENSO versus AO, and find that many models project a positive AO-like change. In the Northern Pacific in high latitudes, the SLP anomalies are incompatible between the El Niño-like change and the positive AO-like change, because models that project an El Niño-like change over the Pacific give a non-AO-like pattern in the polar region. Different behaviors of coupling/decoupling between them lead to very different warming patterns on regional scales over the North Pacific. In the models with the El Niño-like response, the positive feedback between SST, convection and atmospheric circulation (Bjerknes feedback) overwhelmed the negative cloud-radiation feedback (Jin et al., 2001; Yu and Boer, 2002). Boer et al. (2004) further suggested that the La Niña-like SST pattern reconstructed at the Last Glacial Maximum when the sign of radiative forcing was opposite to the future warming supports an El Niño-like SST response in the future global warming.

[INSERT FIGURE 10.3.15 HERE]

The projected change of the amplitude, frequency, and spatial pattern of El Niño itself is addressed next. The mean state change, through change in the sensitivity of SST variability to surface wind stress, plays a key role in determining the ENSO variance characteristics (Hu et al., 2004b; Zelle et al., 2005). For example, a more stable ENSO system is less sensitive to changes in the background state than one that is closer to instability (Zelle et al., 2005). Thus GCMs with an improper simulation of present-day climate mean state and air-sea coupling strength are not suitable for ENSO amplitude projections. Van Oldenborgh et al. (2005) categorized 19 models with their skill in the present-day ENSO simulations. In the most realistic six out of 19 models, they find no statistically significant changes in amplitude of ENSO variability in the future. Large uncertainties in the skewness of the variability limits the assessment of the future relative strength of El Niño and La Niña events. Even with the larger warming scenario under $4 \times CO_2$ climate, Yeh and Kirtman (2005) find that despite the large changes in the tropical Pacific mean state, the changes in ENSO amplitude are highly model dependent. Meehl et al. (2005b) analysed two AOGCMs with increased GHGs and found that the decrease of El Niño amplitude in those two models was related to warming below the thermocline that weakened the stratification. On the other hand, Guilyardi (2005) assessed mean state, coupling strength and modes (SST mode or thermocline mode), using the pre-industrial control, stabilized 2 × CO_2 and 4 × CO_2 simulations in a multi-model ensemble. The models that exhibit the largest El Niño amplitude change in scenario experiments are those that shift towards a thermocline mode. The observed 1976 climate shift in the tropical Pacific actually involved such a mode shift (Fedorov and Philander, 2001). Those models that best simulate the tropical Pacific climatology in terms of mean state, seasonal cycle and coupling strength show the above mode change, implying an increasing likelihood of increased El Niño amplitude in a warmer climate. Merryfield (2005) also analysed a multi-model ensemble and found a wide range of behaviour for future El Niño amplitude, ranging from little change to larger El Niño events to smaller El Niño events, though several models that simulated some observed aspects of present-day El Niño events showed future increases in El Niño amplitude.

For the change of ENSO frequency, Saenko (2005) showed a decrease in the time scale for large-scale dynamic oceanic adjustment based on increases in the first baroclinic Rossby radius of deformation due to oceanic stratification in warmer climate. These oceanic stratification changes and calculated increasing oceanic internal wave speeds are seen in most of the AOGCMs. A shorter ENSO period is also shown by the ensemble simulations of the CCSM (Zelle et al., 2005). However, multi-model analyses by Guilyardi (2005) find no clear indication of ENSO frequency change in a warmer climate.

The tropospheric biennial oscillation (TBO) has been suggested as a fundamental set of coupled interactions in the Indo-Pacific region that encompass ENSO and the Asian-Australian monsoon, and the TBO has been shown to be simulated in current AOGCMs (Chapter 8). Nanjundiah et al. (2005) analyse a multi-model dataset to show that, for models that successfully simulate the TBO for present-day climate, the TBO becomes more prominent in a future warmer climate due to changes in the base state climate, though, as with ENSO, there is considerable inherent decadal variability regarding the relative dominance of TBO and ENSO with time.

In summary, the mean tropical Pacific state tends to shift towards mean El Niño-like conditions with the eastern Pacific warming more than the western Pacific in a future warmer climate. There is a wide range of behaviour among the current models with no clear indication regarding possible changes of future El Niño amplitude or period.

10.3.5.2 ENSO-monsoon relationship

ENSO affects interannual variability in the whole tropics through changes in the Walker circulation. It has been known that there is a significant correlation between ENSO and tropical circulation/precipitation from the analysis of observational data. There is a tendency for less Indian summer monsoon rainfall in El Niño years, and above normal rainfall in La Niña years. Recent analyses have revealed that the amplitude of this correlation has a decadal fluctuation (see Chapter 3). Variability of the relationship between the East Asian summer monsoon and ENSO has also been reported (Wang, 2002). Moreover, since the correlation between ENSO and the Indian summer monsoon has decreased recently, many hypotheses have been raised concerning the reason, including decadal variability (Kripalani and Kulkarni, 1997), change in seasonality of ENSO cycle (Kawamura et al., 2003), Indian Ocean Dipole mode (Ashok et al., 2001), Atlantic Oscillation (Chang et al., 2001) and global warming. With respect to global warming, one hypothesis is that the Walker circulation accompanying ENSO shifted south-eastward, reducing downward motion in the Indian monsoon region, which originally suppressed precipitation in that region at the time of El Niño, but now produces normal precipitation as a result (Krishna Kumar et al., 1999). Another explanation is that as the ground temperature of the Eurasian continent has risen in the winter-spring season due to global warming,, the temperature difference between the continent and the ocean has become large, thereby causing more precipitation, and the Indian monsoon is normal in spite of the occurrence of El Niño (Ashrit et al., 2001).

It is reported that the MPI model (Ashrit et al., 2001) and the CNRM model (Ashrit et al., 2003) showed no global warming-related change in the ENSO-monsoon relationship, although a decadal-scale fluctuation is seen, suggesting a weakening of the relationship might be part of the natural variability. However, Ashrit et al. (2001) showed that while the impact of La Niña does not change, the influence of El Niño on the monsoon becomes small, suggesting the possibility of asymmetric behavior of the changes in the ENSO-monsoon relationship. The ARPEGE-OPA model also showed no significant change of this ENSO-monsoon relationship due to global warming (Camberlin et al., 2004). On the other hand, the MRI-CGCM2 indicates a strong weakening of the correlation into the 21st century particularly after 2050 (Ashrit et al., 2005). The

MRI-CGCM2 model results support the above hypothesis that the Walker circulation no longer influences India at the time of El Niño after global warming, because it is shifted eastward. This eastward shift is the expected response of an El Niño-like climate change (see Section 10.3.5.1). Camberlin et al. (2004) extended their analysis to other ENSO-affected regions and found decadal fluctuations in ENSO's effect on regional precipitation. In most cases, these fluctuations may reflect natural variability of the ENSO teleconnection, and long-term correlation trends may be comparatively weaker. One possible reason is that the ARPEGE-OPA model simulated very regular ENSOs through the 21st century with little change in either the mean annual cycle or the monthly standard deviation (Camberlin et al., 2004).

Recent research has shown that Sahelian rainfall variability is a response of the African monsoon to oceanic forcing. The semi-arid Sahel emerges as a region highly sensitive to SST variability in all tropical basins, remote (Pacific) and local (Atlantic and Indian) (Janicot et al., 2001; Giannini et al., 2003; Moron et al., 2003; Haarsma et al., 2005). The ENSO influence is confined to the interannual timescale (Janicot et al., 1998; Chiang and Sobel, 2002). Gianini et al. (2003) support the hypothesis that the oceanic warming around Africa may have weakened the land-ocean temperature contrast and consequently the monsoon. This induces the migration of deep atmospheric convection over the ocean causing widespread drought over land.

In summary, the ENSO-monsoon relationship can vary from decade to decade purely due to internal variability of the climate system. However it seems that the African monsoon is affected at the interannual timescale by SST variability including ENSO. In spite of the issues related to natural variability, there is some evidence of a future weakening of the ENSO-monsoon relationship in a future warmer climate.

10.3.5.3 Annular modes and mid-latitude circulation changes

Since the TAR, there have been a number of modeling studies that have investigated responses of extratropical climate variability to various anthropogenic and natural forcings with more comprehensive experiments including a larger size of ensemble simulations. Additionally, the analyses have incorporated model intercomparisons and model ensembles to reduce the uncertainties.

10.3.5.3.1 NAM (or AO) and NAO

Many simulations project some decrease of the Arctic surface pressure in the twenty-first century, as seen in the multi-model average (see Figure 10.3.6), which contributes to an increase of the Northern Annular Mode (NAM) or the Arctic Oscillation (AO) and North Atlantic Oscillation (NAO) index, at least to some extent. From the recent multi-model analyses (Osborn, 2004; Rauthe et al., 2004a; Kuzmina et al., 2005; Miller et al., 2005), more than half of the models exhibit a positive trend of the NAM (or NAO). Although the strength shows a large variation among different models, only one study (McHugh and Rogers, 2005) suggests a weakened NAO circulation from increased GHGs from a 10 member multi-model ensemble. However, the multi-model average from the larger number of models (21) shown in Figure 10.3.6 indicates that it is likely that the NAM would not significantly decrease in a future warmer climate. The average of IPCC-AR4 simulations from thirteen models suggests the response becomes statistically significant early in the twenty-first century (Figure 10.3.16) (Miller et al., 2005).

[INSERT FIGURE 10.3.16 HERE]

Generally, models simulate a much smaller trend of NAM (or NAO) than that observed in the last half of twentieth century (apparent in Figure 10.3.16) (Gillett et al., 2002; Osborn, 2004), however the observed trend may contain considerable internal decadal variability (Yukimoto and Kodera, 2005) as implied from a notable decline of the index after the 1990s (Chapter 3).

Geographical patterns of the simulated change are not consistent among different models, in spite of close correlations of the models' inter-annual (or internal) variability with the observations (Osborn, 2004; Miller et al., 2005). However at the hemispheric scale of surface pressure change, besides the lowering in the Arctic, an increase over the Mediterranean Sea (Figure 10.3.6) (Osborn, 2004) is significant with the multi-model statistics, which suggests an association with northeastward shift of the NAO's center of action (Hu and Wu, 2004). The diversity of the patterns seems to reflect different responses in the Aleutian Low (Rauthe et al., 2004b) that may be associated with delicate balance between the 'AO-like' response and the 'El Niño-like' response of the tropical Pacific (Yamaguchi and Noda, 2005). Rauthe et al. (2004b) suggest that the effects of sulfate aerosols contribute to a deepening of the Aleutian Low resulting in a slower or smaller increase of the AO.

Models with their upper boundaries extending farther into the stratosphere exhibit a relatively larger increase of the NAM and respond consistently to the volcanic forcing as observed (Figure 10.3.16) (Miller et al., 2005), implying the importance of the connection between the troposphere and the stratosphere (Shindell et al., 2001). However a few models with a lower top are also capable of simulating a relatively large NAM increase (Gillett et al., 2003; Miller et al., 2005).

A plausible explanation for the cause of the upward NAM trend in the models is an intensification of the polar vortex resulting from both tropospheric warming and stratospheric cooling mainly due to the increase of GHGs (Shindell et al., 2001; Sigmond et al., 2004; Rind et al., 2005a). The response may not be linear with the magnitude of radiative forcing (Gillett et al., 2002) since the polar vortex response is attributable to an equatorward refraction of planetary waves (Eichelberger and Holton, 2002) rather than radiative forcing itself. Since the long-term variation of the NAO is closely related with SST variations (Rodwell et al., 1999), it is considered to be essential that the projection of the changes in the tropical SST (Hoerling et al., 2004; Hurrell et al., 2004) and/or meridional gradient of the SST change (Rind et al., 2005b) should also be reliable. Rind et al. (2005b) suggested that it is likely that the current tendency for an increased positive phase of the AO/NAO will continue if there is significant tropical and high latitude warming. A related effect to changes in winds is the length of day, which, in a multi-model ensemble from CMIP2, is projected to increase on the order of 1 microsecond per year (de Viron et al., 2002).

10.3.5.3.2 SAM (or AAO)

The future trend of the Southern Annular Mode (SAM) or the Antarctic Oscillation (AAO) has been projected in a number of model simulations (Gillett and Thompson, 2003; Shindell and Schmidt, 2004; Arblaster and Meehl, 2005; Miller et al., 2005). According to the latest multi-model analysis (Miller et al., 2005), most models indicate a positive trend in the SAM, which implies a higher likelihood than for the future NAM trend. A larger positive trend on average is projected by models that include stratospheric ozone changes than those that do not (Figure 10.3.17), though there is a large amplitude range among the individual models. The cause of the positive SAM trend in the second half of the twentieth century is mainly attributed to the stratospheric ozone depletion, evidenced by the fact that the signal is largest in the lower stratosphere in austral spring through summer (Thompson and Solomon, 2002; Arblaster and Meehl, 2005). However, increases of GHGs are also important factors (Shindell and Schmidt, 2004; Arblaster and Meehl, 2005). During the twenty-first century, although the ozone amount is expected to stabilize or recover, the polar vortex intensification is likely to continue due to the increases of GHGs.

[INSERT FIGURE 10.3.17 HERE]

10.3.6 Future Changes in Weather and Climate Extremes from Global Coupled Climate Models

10.3.6.1 Droughts and floods

A long-standing result from global coupled models noted in the TAR was an increased chance of summer drying in the midlatitudes in a future warmer climate, and this has been documented in the more recent generation of models (Burke and Brown, 2005; Meehl et al., 2005e; Rowell and Jones, 2005). For example, Wang (2005) analyzed 15 recent AOGCMs to show that in a future warmer climate, the models simulate summer dryness and winter wetness in most parts of northern middle and high latitudes, but there is a large range in the amplitude of summer dryness across models.

Going along with the risk of drying is also an increased chance of intense precipitation and flooding. Though somewhat counter-intuitive, this is because precipitation is concentrated into more intense events, with longer periods of little precipitation in between. Therefore, intense and heavy episodic rainfall events are interspersed with longer relatively dry periods (Frei et al., 1998; Allen and Ingram, 2002; Palmer and Räisänen, 2002; Christensen and Christensen, 2003; Beniston, 2004; Christensen and Christensen, 2004; Pal et al., 2004). Another aspect of these changes has been related to the mean changes of precipitation, with wet extremes becoming more severe in many areas where mean precipitation increases, and dry extremes where the mean precipitation decreases (Räisänen, 2005a). Using an 8 member multi-model ensemble, Meehl et al.

(2005a) show a similar result, with increases of precipitation intensity occurring in areas where mean precipitation increases as noted by Räisänen (2005a). These areas include high latitude regions and many tropical areas, with the former being related to changes in atmospheric circulation.

Climate models continue to confirm the earlier results that in a future climate warmed by increasing GHGs, precipitation intensity increases over most regions (Wilby and Wigley, 2002). This increase of precipitation intensity in various regions has been attributed to contributions from both dynamic and thermodynamic processes associated with global warming (Daikaru and Emori, 2005; Emori et al., 2005). Recent studies have used more sophisticated statistical analyses involving extreme value theory that better quantify this result using a gamma distribution to study precipitation extremes. Watterson and Dix (2003) showed that an increase in the scale parameter from the gamma distribution represents an increase in precipitation intensity from a five member ensemble of an A2 simulation in a global coupled model, and various regions such as the Northern Hemisphere land areas in winter showed particularly high values of increased scale parameter. This result was also seen in the study by Semenov and Bengtsson (2002). Time slice simulations with a higher resolution model (roughly 1 degree) show similar results using changes in the gamma distribution, namely increased extremes of the hydrological cycle (Voss et al., 2002). However, there can also be some regional decreases, such as over the subtropical oceans (Semenov and Bengtsson, 2002).

Going along with the results above for increased extremes of intense precipitation in many models, Watterson (2005) showed for the A2 scenario in the CSIRO model that though the storms in future climate in that model did not change much in intensity, there was an increase in extreme rainfall intensity with the extra-tropical surface lows, particularly over Northern Hemisphere land. This implies an increase of flooding. In a multi-model analysis of the CMIP models, Palmer and Räisänen (2002) showed that there was a three to five time increase in the likelihood of very wet winters over much of central and northern Europe due to an increase of intense precipitation associated with midlatitude storms suggesting increasing floods over Europe. They found similar results for summer precipitation with implications for more flooding in the Asian monsoon region in a future warmer climate. Similarly, Milly et al. (2002), Arora and Boer (2001) and Voss et al. (2002) related the increased risk of floods in a number of major river basins in a future warmer climate to an increase in river discharge. Christensen and Christensen (2003) concluded there could be an increased risk of summertime flooding in Europe. McCabe et al. (2001) examined changes in Northern Hemisphere surface cyclones and came to similar conclusions regarding an enhanced risk for future intense storm-related precipitation events and flooding.

Global averaged time series of the Frich et al. (2002) indices from 8 models calculated by Tebaldi et al. (2005b) show simulated increases in precipitation intensity during the 20th century continuing through the 21st century, along with a somewhat weaker and less consistent trend for increasing dry periods between rainfall events for all scenarios (Figure 10.3.18). Part of the reason for these results is shown in the geographic maps for these quantities, where precipitation intensity increases almost everywhere, but particularly at mid and high latitudes where mean precipitation increases (Meehl et al., 2005a), (compare Figure 10.3.19 top to Figure 10.3.6). However, in Figure 10.3.19 bottom, there are regions of increased runs of dry days between precipitation events in the subtropics and lower midlatitudes, but decreased runs of dry days at higher midlatitudes and high latitudes where mean precipitation increases (compare Figure 10.3.6 with Figure 10.3.19 bottom). Since there are areas of both increases and decreases of consecutive dry days between precipitation events in the multi-model average in Figure 10.3.6, the global mean trends are smaller and less consistent across models as shown in Figure 10.3.18 bottom.

[INSERT FIGURE 10.3.18 HERE]

[INSERT FIGURE 10.3.19 HERE]

10.3.6.2 Temperature extremes

The TAR concluded there was a very likely risk of increased temperature extremes, with more extreme heat episodes in a future climate. This result has been confirmed in subsequent studies (Yonetani and Gordon, 2001). For example, Kharin and Zwiers (2005) show in a single model that future increases in temperature extremes follow increases in mean temperature over most of the world except where surface properties change (melting snow, drying soil). Furthermore, that study showed that warm extremes correspond to increases in daily maximum temperature, but cold extremes warm up faster than daily minimum temperatures. Weisheimer and Palmer (2005) examined changes in extreme seasonal (DJF and JJA) temperatures (exceeding the 95th percentile) in 14 models for 3 scenarios. They showed that by the end of 21st century; the probability of extreme warm seasons rises above 90% in many tropical areas, and around 40% elsewhere.

The TAR said nothing about possible changes in future cold air outbreaks. Vavrus et al. (2005) have analysed 7 AOGCMs run with the A1B scenario, and defined cold air outbreak as 2 or more consecutive days when the daily temperatures were at least 2 standard deviations below the winter-time mean. For a future warmer climate, they documented a decline in frequency of 50 to 100% in NH winter in most areas, with the smallest reductions occurring in western N. America, the North Atlantic, and southern Europe and Asia due to atmospheric circulation changes associated with the increase of GHGs.

There were no studies at the time of the TAR that specifically documented changes in heat waves. Several recent studies have addressed possible future changes in heat waves explicitly, and found that in a future climate there is an increased risk of more intense, longer-lasting and more frequent heat waves (Meehl and Tebaldi, 2004; Schär et al., 2004; Clark et al., 2005; Uchiyama et al., 2005). Meehl and Tebaldi (2004) showed that the pattern of future changes of heat waves, with greatest increases of intensity over western Europe and the Mediterranean, the southeast and western U.S., was related to base state circulation changes due to the increase in GHGs. Schär et al. (2004), Stott et al. (2004) and Beniston (2004) used the European 2003 heat wave as an example of the types of heat waves that are likely to become more common in a future warmer climate. Based on an 8 member multi-model ensemble heat waves are simulated to have been increasing for the latter part of the 20th century, and are projected to increase globally (Figure 10.3.20), and over most regions (Figure 10.3.21).

[INSERT FIGURE 10.3.20 HERE]

[INSERT FIGURE 10.3.21 HERE]

A decrease in diurnal temperature range in most regions in a future warmer climate was reported in the TAR. This has been re-confirmed by more recent studies from a variety of models (e.g., Stone and Weaver, 2002). This feature is shown for global averages in Figure 10.3.20 for an 8 member multi-model ensemble, with simulated decreases in diurnal temperature range in the 20th century in the models continuing into the 21st century for all three scenarios and in almost all regions (Figure 10.3.21).

It was concluded in the TAR that it would be likely that a future warmer climate would also be characterized by a decrease in frost days, though there were no studies at that time from global coupled climate models that addressed this issue explicitly. Since then it has been shown that there would indeed be decreases in frost days in a future climate in the extratropics (Meehl et al., 2004a; Uchiyama et al., 2005), with the pattern of the decreases dictated by the changes in atmospheric circulation from the increase in GHGs (Meehl et al., 2004a). Results from an 8 member multi-model ensemble show simulated decreases in frost days for the 20th century continuing into the 21st century globally (Figure 10.3.20) and in most regions (Figure 10.3.21). A quantity related to frost days is growing season length as defined by Frich et al. (2002), and this has been projected to increase in future climate (Uchiyama et al., 2005). This result is also shown in an 8 member multi-model ensemble where the simulated increase in growing season length in the 20th century continues into the 21st century globally (Figure 10.3.20) and in most regions (Figure 10.3.21).

10.3.6.3 Tropical cyclones

Earlier studies assessed in the TAR showed that future tropical cyclones would likely become more severe with greater wind speeds and more intense precipitation. More recent modelling experiments have confirmed that earlier result with a high resolution hurricane model embedded in a global coupled climate model (Knutson and Tuleya, 2004). That study also provided more details regarding how the choice of convective scheme can affect the quantitative nature of the results, though the main conclusions remain the same as in the earlier studies.

Recently there have been a number of climate change experiments with global models that can begin to simulate some characteristics of individual tropical cyclones. A study with a roughly 100 km resolution model (T106) showed a decrease in tropical cyclones globally but a regional increase over the North Atlantic and no significant changes in intensity (Sugi et al., 2002). Another study with that same resolution model indicated global decreases in tropical cyclone frequency and intensity in the tropical north Pacific but more mean and extreme precipitation from the tropical cyclones simulated in the future in that region (Hasegawa and Emori, 2005). Yoshimura and Sugi (2005) demonstrated in a sensitivity experiment with a T106 model that the decrease in tropical cyclone numbers was mainly due to the increase of CO_2, and not the increase of associated SST. Yoshimura et al. (2005) further documented these decreases regionally and showed they occurred even with two different convection schemes in their model, with increased precipitation near the storm centers in the future.

In another global modelling study with roughly a 100 km resolution, there was a 6% decrease in tropical storms globally and a slight increase in intensity, with both increases and decreases regionally related to the El Niño-like base state response in the tropical Pacific to increased GHGs (McDonald et al., 2005). A time slice experiment with a T106 global model has shown a global decrease in tropical cyclone frequency, mainly concentrated in the tropical north Pacific, but with a regional increase in the tropical North Atlantic mainly associated with the change in pattern of SSTs in a future warmer climate. However, in that experiment there was little change in intensity, though precipitation amounts in those storms were greater (Hasegawa and Emori, 2005) confirming the earlier embedded model results.

Recently a global 20km grid model has been run in time slice experiments for a present-day 10 year period and a 10 year period at the end of the 21st century for the A1B scenario to examine changes in tropical cyclones where, at that resolution, tropical cyclone characteristics, numbers, and tracks are relatively well-simulated for present-day climate (Oouchi et al., 2005). In that study, tropical cyclones decreased 30% globally (but increased in the North Atlantic). The strongest tropical cyclones with extreme surface winds increased in number while weaker storms decreased. The tracks were not appreciably altered, and there was about a 10% increase in maximum wind speeds in future simulated tropical cyclones in that model.

10.3.6.4 Extratropical storms and ocean wave height

It was noted in the TAR that there could be a future tendency for more intense extratropical storms, though the numbers could be less. This has been addressed by more recent studies. Watterson (2005) analyzed two global coupled models and found little change in either frequency or intensity of extratropical cyclones. But a tendency towards more intense systems was noted particularly in the A2 scenario in another global coupled climate model analysis (Leckebusch and Ulbrich, 2004), with a tendency towards more extreme wind events in association with those deepened cyclones for several regions of Western Europe, with similar changes in the B2 simulation though less pronounced in amplitude. Several studies have shown a possible reduction of midlatitude storms in the Northern Hemisphere but an increase in intense storms (Lambert and Fyfe, 2005) (for a 15 member multi-model ensemble) and for the Southern Hemisphere (Fyfe, 2003) (with a possible 30% reduction in sub-Antarctic cyclones).

Geng and Sugi (Geng and Sugi) used a higher resolution AGCM (T106 JMA AGCM) with time-slice experiments and obtained a decrease of cyclone density in both hemispheres, and in both the DJF and JJA seasons, associated with the changes in the baroclinicity in the lower troposphere, in general agreement with coarser GCM results (e.g., Dai et al., 2001a). Geng and Sugi (2003) further showed that the density of strong cyclones increases while the density of weak and medium-strength cyclones decreases. Regionally, there is a poleward shift of cyclone density, with a decrease in DJF extratropical cyclone density in East Asia around Japan (south of 50°N) and an increase north of that latitude. More regional aspects of these changes were addressed for the Northern Hemisphere in a single model study by Inatsu and Kimoto (2005) who showed a more active storm track in the western Pacific in the future but weaker elsewhere. Ulbrich et al. (2005) showed, for a 5 member multi-model ensemble, increased storm track activity over the North Atlantic and North Pacific, and lowered over Canada and poleward of 70N.

By analyzing stratosphere-troposphere exchanges using time-slice experiments with the middle atmosphere version of ECHAM4, Land and Feichter (2003) suggested that upper tropospheric (300 hPa) cyclonic activity becomes weaker poleward of 30°N in a warmer climate, while cyclonic activity becomes stronger in the Southern Hemisphere. The atmospheric circulation variability on the interdecadal time scales may also change by increasing GHG and aerosols. One model result (Hu et al., 2001) showed that interdecadal variability of the SLP and 500 hPa height fields increased over the tropics and decreased in high latitudes by global warming.

Two studies have documented a poleward shift in midlatitude storm tracks, one in a single model (Bengtsson et al., 2005) and one in a 15 member multi-model ensemble (Yin, 2005). Consistent with these shifts in storm track activity, Cassano et al. (2005), using a 10 member multi-model ensemble, showed a future change to a more cyclonically-dominated circulation pattern in winter and summer over the Arctic, and increasing cyclonicity and stronger westerlies in a 10 member multi-model ensemble for the Antarctic (Lynch et al., 2005).

A new feature that has been studied related to extreme conditions over the oceans is wave height. Studies by Wang et al. (2004), Wang and Swail (2004), and Wang and Swail (2005) have shown that for most regions of the midlatitude oceans, an increase of extreme wave height is likely to occur in a future warmer climate. This is related to increased wind speed associated with midlatitude storms, resulting in higher waves produced by these storms, and is consistent with the studies noted above that showed decreased numbers of midlatitude storms but more intense storms.

10.4 Carbon Cycle/Vegetation Feedbacks and Chemistry

10.4.1 Carbon Cycle/Vegetation Feedbacks

As a parallel activity to the standard IPCC AR4 climate projection simulations described in this chapter, the Coupled Climate Carbon Cycle Models Intercomparison Project (C4MIP) supported by WCRP and IGBP was initiated. Ten climate models with a representation of the land and ocean carbon cycle (see Chapter 7) performed simulations where the model is driven by anthropogenic CO_2 emissions scenario for the 1860-2100 time period (instead of atmospheric CO_2 concentration scenario in the standard IPCC AR4 simulations). Each C4MIP model performed two simulations, a “coupled” simulation where the growth of atmospheric CO_2 induces a climate change which impacts on the carbon cycle, and an “uncoupled” simulation, where atmospheric CO_2 is radiatively inactive in order to estimate the atmospheric CO_2 growth rate one would get if the carbon cycle was unperturbed by the climate. Emissions were taken from the observation for the historical period (Houghton and Hackler, 2000; Marland et al., 2005) and from the IPCC SRES A2 scenario for the future (Leemans et al., 1998).

Chapter 7 describes the major results of the C4MIP models in terms of climate impact on the carbon cycle. Here we start from these impacts to infer the feedback on atmospheric CO_2 and therefore on the climate system. There is unanimous agreement amongst the models that future climate change will reduce the efficiency of the Earth system to absorb anthropogenic carbon dioxide owing to the reduced CO_2 solubility when SSTs increase. As a result, a larger fraction of anthropogenic CO_2 will stay airborne under a warmer climate. By the end of the 21st century, this additional CO_2 varies between 20 ppm and 200 ppm for the two extreme models, the majority of the models lying between 50 and 100 ppm (Friedlingstein et al., 2005). The positive feedback in the climate-carbon system leads to additional atmospheric CO_2 and hence an additional warming ranging between 0.1 and 1.5°C.

The comparison of the C4MIP models with the standard IPCC models is not straightforward. Indeed, in terms of atmospheric CO_2 evolution, the majority of the C4MIP models simulate a higher atmospheric CO_2 growth rate than the one taken as a forcing for the standard coupled models of the IPCC AR4 exercise (e.g., Meehl et al., 2005c). By 2100, atmospheric CO_2 varies between 730 and 1020 ppm for the C4MIP models, compared with 830 ppm for the SRES-A2 concentration used by the standard IPCC-AR4 climate models (Figure 10.4.1). The CO_2 concentration envelope of the C4MIP uncoupled simulations is centred on the standard SRES-A2 concentration value, the range reflecting the uncertainty in the carbon cycle. However, it could be argued that the uncertainty range is too narrow because C4MIP did not fully account for non-climate feedback uncertainties. The effects of climate feedback uncertainties on the carbon cycle have been considered probabilistically by Wigley and Raper (2001) who accounted for both climate and non-climate feedbacks based on literature available at the time. A later paper (Wigley, 2004) considered individual emissions scenarios, accounting for carbon cycle feedbacks in the same way as Wigley and Raper (2001). The results of these studies are consistent with the more recent C4MIP results. For the A2 scenario considered in C4MIP, the CO_2 concentration range in 2100 using the Wigley and Raper model is 769–1088 ppm, compared with 730–1020 ppm in the C4MIP study (which ignored the additional warming effect due to non-CO_2 gases). Further uncertainties regarding carbon uptake were addressed in a 14 member multi-model ensemble using the CMIP2 models to quantify contributions to uncertainty with regards to inter-model variability versus internal variability (Berthelot et al., 2002). They found that the AOGCMs with the largest climate sensitivity also had the largest drying of soils in the tropics and thus the largest reduction of carbon uptake.

The envelope of the simulated climate change in the coupled C4MIP simulation is not higher than the one of the IPCC-AR4 climate models (Figure 10.4.2). The change in global mean temperature over the 21st century ranges between 1.3 and 3.6°C for the C4MIP coupled simulation, compared with 2.6 to 4.1°C for the SRES-A2 concentration simulations of the standard IPCC-AR4 climate models. The apparent contradiction between higher CO_2 for the C4MIP models but lower warming is due to the absence of non-CO_2 greenhouse gases and aerosols in the C4MIP simulation. CH_4, N_2O, CFCs and aerosols are kept at their pre-industrial value in the C4MIP models; CO_2 is the only greenhouse gas accounted for.

The SRES-A2 radiative forcings of CO_2 alone and total forcing (CO_2 plus non-CO_2 greenhouse gases and aerosols) are given in Appendix II of the TAR. Using these numbers, we can calculate the warming of the C4MIP models if they had included the non-CO_2 greenhouse gases and aerosols. As a first approximation, by 2100, an additional warming of 1.2°C should be added on the C4MIP models for comparison with the SRES-A2 standard simulations. Doing so, the C4MIP range of global temperature increase over the 21st century would be 2.4 to 4.8°C, compared with 2.6 to 4.1°C for standard IPCC-AR4 climate models (Figure 10.4.3). As a result of a much larger CO_2 concentration by 2100 in the C4MIP models, the upper estimate of the global warming by 2100 is 0.7°C higher than for the SRES-A2 concentration standard simulations.

The C4MIP results highlight the importance of coupling the climate system and the carbon cycle in order to simulate, for a given scenario of CO_2 emission, a climate change that takes into account the dynamic evolution of the Earth's capacity to absorb the CO_2 perturbation.

Both the standard IPCC-AR4 and the C4MIP models make the assumption that land cover change does not play any role in the climate system. However, as described in Chapters 2 and 7 past and future changes in land cover may affect the climate through several processes. First, they may change surface characteristics such as albedo. Second, they may affect the latent vs. sensible heat ratio and therefore impact on surface temperature. Third, they may induce atmospheric CO_2 emissions, and fourth, they can affect the capacity of the land to take up atmospheric CO_2. So far, no comprehensive coupled OAGCM has addressed these four components all together. Using AGCMs, Defries et al. (2004) studied the impact of future land cover change on the climate, while Maynard and Royer (2002) did a similar experiment on Africa only. Defries et al., (2002) forced the Colorado State University GCM (Randall et al., 1996) with AMIP climatological sea surface temperatures and with either the present-day vegetation cover or a 2050 vegetation map adapted from a low growth scenario of the IMAGE-2 model (Leemans et al., 1998). The study found that in the tropics and subtropics, replacement of forests by grassland or cropland leads to a reduction of carbon assimilation, and therefore of latent heat flux. This latter reduction leads to a surface warming of up to 1.5°C in deforested tropical regions. Using the ARPEGE-Climat AGCM (2004) with a high resolution over Africa, Maynard et al., (Déqué et al., 1994) performed two experiments, one simulation with 2 × CO_2 SSTs taken from a previous ARPEGE transient SRES-B2 simulation and present-day vegetation, and one with the same SSTs but the vegetation taken from a SRES-B2 simulation of the IMAGE-2 model (Leemans et al., 1998). Similarly to Defries et al., (2002), they found that future deforestation in tropical Africa leads to a redistribution of latent and sensible heat that leads to a warming of the surface. However, this warming is relatively small (0.4°C) and represents about 20% of the warming due to the atmospheric CO_2 doubling.

[INSERT FIGURE 10.4.1. HERE]

[INSERT FIGURE 10.4.2. HERE]

[INSERT FIGURE 10.4.3. HERE]

10.4.2 Simulations of Future Evolution of Methane, Ozone, and Oxidants

Simulations using coupled chemistry-climate models indicate that the trend in upper stratospheric ozone changes sign sometime between 2000 and 2005 due to the gradual reduction in halocarbons. While ozone concentrations in the upper stratosphere decreased at a rate of 400 ppbv (–6%) per decade during 1980-2000, they are projected to increase at 100 ppbv (1–2%) per decade for 2000–2020 (Austin and Butchart, 2003). On longer timescales, simulations are showing significant changes in ozone and methane relative to current concentrations. The changes are related to a variety of factors, including increased emissions of chemical precursors; changes in gas-phase and heterogeneous chemistry; altered climate conditions due to global warming; and greater transport and mixing across the tropopause. The impacts on methane and ozone from increased emissions are a direct effect of anthropogenic activity, while the impacts of different climate conditions and stratosphere-troposphere exchange represent indirect effects of these emissions (Grewe et al., 2001).

The projections for ozone based upon scenarios with high emissions (IS92a (Leggett et al., 1992) and SRES A2 (Nakicenovic and Swart, 2000)) indicate that the concentrations of tropospheric ozone will increase throughout the 21st century, primarily as a result of these emissions. Simulations for the period 2015 through 2050 find increases in O_3 of 20 to 25% (Grewe et al., 2001; Haglustaine and Brasseur, 2001), and simulations through 2100 indicate that O_3 below 250 mb may grow by 40 to 60% (Stevenson et al., 2000; Grenfell et al., 2003; Zeng and Pyle, 2003). The primary species contributing to the increase in tropospheric O_3 are anthropogenic emissions of NO_x, CH_4, CO, and compounds from fossil fuel combustion. The photochemical reactions that produce smog are accelerated by increases of 2.6× in the flux of NO_x, 2.5× in the flux of CH_4, and 1.8× in CO in the A2 scenario. Approximately 91% of the higher concentrations in O_3 are related to direct effects of these emissions, with the remainder of the increase are attributable to secondary effects of climate change (Zeng and Pyle, 2003). These emissions also lead to higher concentrations of oxidants including OH, leading to a reduction in the lifetime of tropospheric methane by 8% (Grewe et al., 2001).

Since the projected growth in emissions occurs primarily in low latitudes, the ozone increases are largest in the tropics and sub-tropics (Grenfell et al., 2003). In particular, the concentrations in SE Asia, India, and Central America increase by 60 to 80% by 2050 under the A2 scenario. However, the effects of tropical emissions are not highly localized, since the ozone spreads throughout the lower atmosphere in plumes emanating from these regions. As a result, the ozone in remote marine regions in the southern hemisphere grows by 10 to 20% over present-day levels by 2050. The zone is also distributed through vertical transport in tropical convection followed by lateral transport on isentropic surfaces.

The major issues in the fidelity of these simulations for future tropospheric ozone are the sensitivities to the representation of the stratospheric production, destruction, and transport of O_3 and the exchange of species between the stratosphere and troposphere. Few of the models include the effects of non-methyl hydrocarbons (NMHCs), and the sign of the effects of NMHCs on O_3 are not consistent among the models that do (Haglustaine and Brasseur, 2001; Grenfell et al., 2003).

The effect of more stratosphere-troposphere exchange (STE) in response to climate change increases the concentrations of O_3 in the upper troposphere due to the much greater concentrations of O_3 in the lower stratosphere than the upper troposphere. While the sign of the effect is consistent in recent simulations, the magnitude of the change in STE and its effects on O_3 are very model dependent. In a simulation forced by the SRES A1FI scenario, Collins et al. (2003) find that the downward flux of O_3 increases by 37% from the 1990s to the 2090s. As a result, the concentration of O_3 in the upper troposphere at mid-latitudes increases by 5 to 15%. However, Sudo et al. (2003) and Zeng et al. (2003) predict that STE increases by 80% by 2100. The increase in STE is driven by increases in the descending branches of the Brewer-Dobson circulation at mid-latitudes. The effects of the enhanced STE are sensitive to the simulation of processes in the stratosphere, including the effects of lower temperatures and the evolution of chlorine, bromine, and NO_x concentrations. Since the greenhouse effect (GHE) of O_3 is largest in the upper troposphere, the treatment of STE remains a significant source of uncertainty in the calculation of the total GHE of tropospheric O_3.

The effects of climate change, in particular increased tropospheric temperatures and water vapour, tend to offset some of the increase in O_3 driven by emissions. For example, Stevenson et al. (2000) find that the higher water vapour offsets the increase in O_3 by 17%. The water vapour both decelerates the chemical production and accelerates the chemical destruction of O_3. The photochemical production depends on the concentrations of NO_y, and the additional water vapour causes a larger fraction of NO_y to be converted to HNO_3, which can be efficiently removed from the atmosphere in precipitation (Grewe et al., 2001). The vapour also increases the concentrations of OH through reaction with $O(^1D)$, and the removal of $O(^1D)$ from the atmosphere slows the formation of O_3. The increased concentrations of OH and the increased rates of CH_4 oxidation with higher temperature further reduce the lifetime of tropospheric CH_4 by 12%.

10.4.3 Simulations of Future Evolution of Major Aerosol Species

The time-dependent evolution of major aerosol species and the interaction of these species with climate represent some of the major sources of uncertainty in projections of climate change. An increasing number of AOGCMs are included multiple types of tropospheric aerosols including sulphates, nitrates, black and organic carbon, sea salt, and soil dust. Of the twenty-three models represented in the multi-model ensemble of climate-change simulations for IPCC AR4, ten include other tropospheric species besides sulphates. Of these, seven have the non-sulphate species represented with parameterizations that interact with the remainder of the model physics. Nitrates are treated in just two of the models in the ensemble. Recent projections of nitrate and sulphate loading under the SRES A2 scenario suggest that forcing by nitrates may exceed forcing by sulphates by the end of the 21st century (Adams et al., 2001). This result is of course strongly dependent upon the evolution of precursor emissions for these aerosol species.

The black and organic carbon aerosols in the atmosphere include a very complex system of primary organic aerosols (POA) and secondary organic aerosols (SOA), which are formed by oxidation of biogenic volatile organic compounds. The models used for climate projections typically use highly simplified bulk parameterizations for POA and SOA. More detailed parameterizations for the formation of SOA that trace oxidation pathways have only recently been developed and used to estimate the direct radiative forcing by SOA for present-day conditions (Chung and Seinfeld, 2002). The forcing by SOA is an emerging issue for simulations of present-day and future climate since the rate of chemical formation of SOA may be 60% or more of the emissions rate for primary carbonaceous aerosols (Kanakidou et al., 2005). In addition, two-way coupling between reactive chemistry and tropospheric aerosols has not been explored comprehensively in climate-change simulations. Unified models that treat tropospheric ozone-NO_x-hydrocarbon chemistry, aerosol formation, heterogeneous processes in clouds and on aerosols, and gas-phase photolysis have been developed and applied to the current climate (Liao et al., 2003). However, to date these unified models have not yet been used extensively to study the evolution of the chemical state of the atmosphere under future scenarios.

The interaction of soil dust with climate is under active investigation. Whether emissions of soil dust aerosols increase or decrease in response to changes in atmospheric state and circulation is still unresolved (Tegen et al., 2004). Several recent studies have suggested that the total surface area where dust can be mobilized will decrease in a warmer climate with higher concentrations of carbon dioxide (e.g., Harrison et al., 2001). The interaction of and net effects of reductions in dust emissions from natural sources combined with land-use change could potentially be significant but have not been systematically modelled as part of climate-change assessment.

10.5 Quantifying the Range of Climate Change Projections

10.5.1 Sources of Uncertainty and Hierarchy of Models

Uncertainty in predictions of climate change is injected at all stages of the modelling process described in section 10.1. The specification of future emissions of greenhouse gases, aerosols and their precursors is uncertain (e.g. Nakicenovic and Swart, 2000). Following Figure 10.1.1 it is then necessary to convert these emissions into concentrations of radiatively active species, calculate the associated forcing and predict the response of climate system variables such as surface temperature and precipitation, by simulating the relevant physical and biogeochemical processes. At each step uncertainty in the true signal of climate change is introduced both by errors in the representation of processes in models (e.g., Palmer et al., 2005) or by noise associated with unforced internal climate variability (e.g., Nishizawa et al., 2005; Selten et al., 2005). The effects of internal variability can be quantified by running models many times from different initial conditions, assuming that simulated internal variability is consistent with that observed in the real world. The effects of uncertainty in our knowledge of Earth system processes can be partially quantified by constructing ensembles of models, or model versions, which sample different parameterisations of these processes. However some processes may be missing from the set of available models, and the range of options for the parameterisation of other processes may share common systematic biases. Therefore, distributions of future climate responses from ensemble simulations are conditional on the quality of the available models and the range of process uncertainties which they explore.

A range of climate models has been developed, which may be viewed as a spectrum of models of varying complexity (Claussen et al., 2002; Stocker and Knutti, 2003) available to assess the consequences of the uncertainties described above. Simple climate models (SCMs) typically represent the ocean-atmosphere system as a set of global or hemispheric boxes, predicting global surface temperature using an energy balance equation, a prescribed value of climate sensitivity and a basic representation of ocean heat uptake (see Section 8.8.2). Their role is to perform comprehensive analyses of the interactions between global variables, based on prior estimates of uncertainty in their controlling parameters obtained from observations, expert judgement and from tuning to complex models. By coupling SCMs to simple models of biogeochemical cycles they can be used to extrapolate the results of AOGCM simulations to a wide range of alternative forcing scenarios (e.g., Wigley and Raper, 2001) (see Section 10.5.3).

Compared to SCMs, Earth System models of intermediate complexity (EMICs) include more of the processes simulated in AOGCMs, but in a less detailed, more highly parameterised form (see Section 8.8.3), and at coarser resolution. Consequently EMICS are not suitable for examining uncertainties in regional climate change or extreme events, however they can be used to investigate the continental scale effects of coupling between multiple Earth system components in large ensembles or long simulations, which is not yet possible with AOGCMs. To this end, a number of EMICs include biological and geochemical modules such as vegetation dynamics, the terrestrial and ocean carbon cycles and atmospheric chemistry (Claussen et al., 2002), filling a gap in the spectrum of models between AOGCMs and SCMs. Thorough sampling of parameter space is computationally feasible for some EMICs (e.g., Forest et al., 2002; Knutti et al., 2002), as for SCMs (Wigley and Raper, 2001), and is used to obtain probabilistic projections (see Section 10.5.2). In some EMICs climate sensitivity is an adjustable parameter, as in SCMs. In other EMICs climate sensitivity is dependent on multiple model parameters, as in AOGCMs. Probabilistic estimates of climate sensitivity and TCR from SCMs and EMICs are assessed in Section 9.6 and compared with estimates from AOGCMs in Box 10.2.

The high resolution and detailed parameterisations of processes in AOGCMs make them the only modelling tools capable of realistic simulation of internal variability (Section 8.4), extreme events (Section 8.5), and the complex interactions which drive global and regional climate change feedbacks (Boer and Yu, 2003a; Bony and Dufresne, 2005; Soden and Held, 2005). Given that ocean dynamics plays a significant role in determining regional feedbacks (Boer and Yu, 2003b), it is clear that quantification of regional uncertainties in time-dependent climate change requires multi-model ensemble simulations of transient climate change with AOGCMs containing a full, three-dimensional dynamic ocean component.

Uncertainty ranges for 21st century climate change obtained from the AR4 multi-model ensemble of AOGCM simulations and from EMIC simulations are discussed in Section 10.5.2, considering selected forcing scenarios. Section 10.5.3 considers the role of uncertainties in emissions, using SCMs and EMICs calibrated to the multi-model ensemble results. Developments since the TAR in the use of AOGCM ensembles to sample uncertainties and estimate probabilities for climate change are summarised in Section 10.5.4.

10.5.2 Range of Responses from Different Models

10.5.2.1 Comprehensive AOGCMs

The way a climate model responds to changes in external forcing, such as an increase in anthropogenic GHGs, is related to two standard measures: (1) equilibrium climate sensitivity (defined as the increase at equilibrium in the globally averaged surface air temperature when atmospheric CO_2 is doubled), and (2) transient climate response (TCR, defined as the increase in globally averaged surface air temperature in a fully coupled climate model in a 1% per year CO_2 increase experiment at the time of CO_2 doubling). The first measure provides an indication of feedbacks mainly residing in the atmospheric model but also in the land surface and sea ice components, and the latter quantifies the response of the fully coupled climate system including aspects of transient ocean heat uptake (e.g., Sokolov et al., 2003). These two measures have become standard metrics of climate model response to understand how an AOGCM will react to more complicated forcings in scenario simulations.

Historically, the equilibrium climate sensitivity has been given as being likely to be in the range from 1.5°C to 4.5°C. This range has also been reported in the TAR with no indication of a probability distribution within this range. However, considerable recent work has addressed the range of equilibrium climate sensitivity, and attempted to assign probabilities of climate sensitivity.

The two measures are not independent (Figure 10.5.1a). A large ensemble of the Bern2.5D EMIC has been used to explore the relationship of TCR and equilibrium sensitivity over a wide range of ocean heat uptake parameterizations. Good agreement with the available results from AOGCMs is found, and the EMIC covers almost the entire range of structurally different models. Similarly, the percent change in precipitation is closely related to the equilibrium climate sensitivity for the current generation of AOGCMs (Figure 10.5.1b), with values from the current models falling within the range of the models from the TAR . Figure 10.5.1c shows the percent change of globally averaged precipitation at time of CO_2 doubling from 1% per year transient CO_2 increase experiments with AOGCMs as a function of TCR suggesting a broadly positive correlation between these two quantities similar to that for equilibrium climate sensitivity, with these values from the new models also falling within the range of the previous generation of AOGCMs assessed in the TAR.

[INSERT FIGURE 10.5.1 HERE]

Additionally, PDF estimations can be formulated from the models used for IPCC scenarios for probabilistic estimates (Räisänen*,* 2005c), and results for equilibrium climate sensitivity and TCR from 17 current global coupled climate models are shown in Figure 10.5.2. Assuming normal distributions, the resulting 5–95% uncertainty range for equilibrium climate sensitivity is approximately 2.0ºC–4.4ºC and that for TCR 1.2ºC–2.4ºC. The best (median) estimate for climate sensitivity is 3.2ºC and that for TCR 1.8ºC. These numbers are practically the same for both the normal and the log-normal distribution. Therefore, assuming that current global coupled climate models cover the full range of uncertainty and assuming a certain shape of distribution, the "range" of equilibrium climate sensitivity can be modified from an equal probability of any value from 1.5ºC to 4.5ºC, to the 5% to 95% range of 2.0ºC to 4.4ºC, with the most probable value of 3.1ºC. The assumption of a (log)-normal fit is not well supported from the limited sample of AOGCM data. However, most studies aiming to constrain climate sensitivity by observations do indeed indicate a log-normal distribution of climate sensitivity and an approximately normal distribution of the uncertainty in future warming and thus TCR (see Box 10.2). On the other hand, there is a consensus from most studies cited above using observational constraints (see 10.5.4.) that the upper limit of climate sensitivity is very uncertain, with a substantial probability for sensitivity above 4.5°C, and that the current AOGCMs therefore do not cover the full possible range of sensitivities.

[INSERT FIGURE 10.5.2. HERE]

The relationship between TCR and equilibrium climate sensitivity shown in Figure 10.5.1a also indicates that the large uncertainty in the upper limit of sensitivity is not so important for the range of TCR. The implication is that transient climate change is better constrained than the equilibrium climate sensitivity, i.e., models with different sensitivity might still show good agreement for projections on decadal timescales.

Different treatments of boundary layer cloud processes appear to be important for climate sensitivity. In models that have been contributed to CFMIP (AGCMs run to equilibrium with a slab ocean) it was found that the differences in global climate sensitivity are most influenced by two differing geographic areas, the sea ice region (where albedo feedback is dominant) and the actual area covered by model simulated low stratus clouds. Improvements in simulation of low stratus for the current climate in some models have dramatically altered the contribution of changes in low stratus cloud amounts to the climate sensitivity (Webb et al*.,* 2005).

These types of metrics provide information on the possible range and maximum likelihood, and can be related to pdfs from perturbed physics ensembles discussed in Section 10.5.4.

Further indications of equilibrium climate sensitivity can be obtained from other forcing simulations, such as LGM, Pinatubo, or the 20th century, to better constrain model sensitivity (see Chapter 8). A summary of all of the estimates of equilibrium climate sensitivity is given in Box 10.2.

10.5.2.2 Earth system models of intermediate complexity

Over the last few years a range of climate models has been developed that are dynamically simpler and of lower resolution than comprehensive AOGCMs, although they might well be more "complete" in terms of climate system components that are included. The class of such models, usually referred to as Earth System Models of Intermediate Complexity (EMICs, Claussen et al., 2002), is very heterogeneous ranging from zonally averaged ocean models coupled to energy balance models (Stocker et al., 1992a), or coupled to statistical-dynamical models of the atmosphere (Petoukhov et al., 2000), to low resolution 3-dimensional ocean models, coupled to energy balance or simple dynamical models of the atmosphere (Opsteegh et al., 1998; Edwards and Marsh, 2005). Some EMICs have a radiation code and prescribe greenhouse gases, while others prescribe radiative forcing (Joos et al., 2001) (IPCC TAR, 2001, Appendix II, Table II.3.11). Compared to comprehensive models, EMICs place hardly any computational constraint, and therefore many simulations can be performed. This allows for the creation of large ensembles, or the systematic exploration of long-term changes many centuries hence. However, because of the reduced complexity, only results on the largest scales, hemispheric to global, are to be interpreted (Stocker and Knutti, 2003). Table 8.8.2 lists all EMICs used in this section, including their components and resolution.

Illustrative scenarios with a 0.5, 1, and 2% yr^{-1} increase in equivalent CO_2, up to 2× and 4 × CO_2, with radiative forcing kept constant thereafter, have been run (Figure 10.5.3) using various EMICs. In addition, scenarios have been run in which the CO_2 was reduced by 1% yr^{-1} after reaching the 4 × CO_2 level to investigate the possibility of irreversible changes in the climate system. Long-term global warming and sea level rise are all determined by climate sensitivity, whereas the meridional overturning circulation (MOC) strongly depends on the history of the forcing. Most simulations shown in Figure 10.5.3 indicate a reduction of the MOC and a subsequent recovery to nearly initial values. However, depending on the model used, if the forcing is strong enough, and lasts long enough, a complete collapse of the MOC can be induced, as shown by the Bern2D model. This is in line with earlier results with EMICs (Stocker and Schmittner, 1997; Rahmstorf and Ganopolski, 1999), or a coupled model (Stouffer and Manabe, 1999).

[INSERT FIGURE 10.5.3 HERE]

Another set of simulations is used to compare EMICs with AOGCMs for the SRES A1B with stable atmospheric concentrations after year 2100 (Figure 10.5.4). For global mean temperature and sea level, the EMICs generally reproduce the AOGCM behaviour quite well. Two of the EMICs have values for climate sensitivity and transient response below the AOGCM range, and none of the EMICs shows warming as high as some AOGCMs at year 2100. However, climate sensitivity is a tuneable parameter in most EMICs, and no attempt was made here to match the range of response of the AOGCMs. Vertical bars at year 2200 indicate plus/minus two standard deviation uncertainties due to ocean mixing parameterizations where ensembles were available. The transient reduction of the MOC in most EMICs is similar to the AOGCMs (see also Section 10.3.5, Figure 10.5.4), providing support that this class of models can be used for both long-term commitment projections (see Section 10.7) and probabilistic projections involving hundreds to thousands of simulations (see Section 10.5.5)

[INSERT FIGURE 10.5.4 HERE]

10.5.3 Range of Responses from Different Scenarios

10.5.3.1 SRES scenarios from simple models

The TAR projections with a simple climate model presented a range of warming over the 21st century for all the SRES scenarios. The construction of the TAR Figure 9.14 was pragmatic. It used a simple model tuned to AOGCMs that had a climate sensitivity within the long-standing range of 1.5–4.5°C advocated by the IPCC. Models with climate sensitivity outside that range were discussed in the text and allowed the statement that the presented range was not the extreme range indicated by AOGCMs. The figure was based on a single anthropogenic-forcing estimate for 1750 to 2000, which is well within the range of values recommended by TAR Chapter 6, and is also consistent with that deduced from model simulations and the observed temperature record (TAR Chapter 12.). To be consistent with TAR Chapter 3., climate feedbacks on the carbon cycle were included. The resulting range of global mean temperature change from 1990 to 2100 given by the full set of SRES scenarios was 1.4 to 5.8°C.

Since the TAR several studies have examined the TAR projections and attempted probabilistic assessments. Allen et al. (2000) show that the forcing and simple climate model tunings used in the TAR give projections that are in agreement with the observationally constrained probabilistic forecast, reported in TAR Ch 12, stating that under the IS92a scenario anthropogenic warming is likely to lie in the range 0.1° to 0.2°C over the next few decades.

As noted by Moss and Schneider (2000), giving only a range of warming results is potentially misleading unless some guidance is given as to what the range means in probabilistic terms. Wigley and Raper (2001) interpret the warming range in probabilistic terms, accounting for uncertainties in emissions, the climate sensitivity, the carbon cycle, ocean mixing, and aerosol forcing. They give a 90% probability interval for 1990 to 2100 warming of 1.7° to 4°C. As pointed out by Wigley and Raper (2001), such results are only as realistic as the assumptions upon which they are based. Key assumptions in this study were; that each SRES scenario was equally likely, that 1.5 to 4.5°C corresponds to the 90% confidence interval for the climate sensitivity, that carbon cycle feedback uncertainties can be characterised by the full uncertainty range of abundance in 2100 of 490 to 1260 ppm given in the TAR. The aerosol PDFs were based on the uncertainty estimates given in the TAR together with constraints based on fitting the simple climate model to observed global- and hemispheric-mean temperatures.

The most controversial assumption in the Wigley and Raper (2001) probabilistic assessment was the assumption that each SRES scenario was equally likely. Figure 10.5.5 shows results from the study for the individual scenarios A2, A1B and B2. The results show that even if we knew what future emissions were going to be, there are very large uncertainties in future global-mean temperature. Another important result is that PDFs differ very little out to 2030. The A2 scenario has lower temperature at that time than either B1 or A1B, but the differences are very small. By 2070, B1 has become noticeably less than A1B and A2. A1B and A2, however, have almost identical PDFs at 2070. By 2100, all three scenarios have separated, with B1 lowest, then A1B, then A2. Note that these PDFs account for carbon cycle/climate feedbacks (see text below for more details).

[INSERT FIGURE 10.5.5 HERE]

Webster et al. (2003) use the probabilistic emissions projections of Webster et al. (2002), which consider present uncertainty in SO2 emissions, and allow the possibility of continuing increases in SO2 emissions over the 21st century, as well as the declining emissions consistent with SRES. Their main results give a climate sensitivity PDF not unlike that used by Wigley and Raper (2001) but for aerosol forcing their PDF gives substantially smaller forcings compared to both Wigley and Raper (2001) and Knutti et al. (2002). This is likely to be a compensatory effect because they did not explicitly consider natural forcings. Since their climate model PDFs were constrained by observations and are mutually dependant the effect of the lower present day aerosol forcing on the projections is not easy to determine, but there is no doubt that their projections tend to be lower where they admit higher SO_2 emissions.

The aim of this section is to bring together information on emissions scenarios from WGIII, on forcings from Chapter 2, on the carbon cycle from Chapter 7, on attribution from Chapter 8, and on model assessment in Chapter 9, together with the AOGCM responses examined in this chapter and to make projections with simplified models that are consistent with that information. Results for the SRES scenarios are given below. As well as the SRES scenarios there may be new information on post-SRES scenarios from WGIII which will be reported on here in the next draft.

Further to the seven AOGCM model tunings for the simple climate model reported on in the TAR, the simple climate model has been tuned to four models from the IPCC AR4 data set to date (see Section 8.8). This makes a total of eleven models, which have climate sensitivities in the range 1.7 to 4.2°C as before.

Temperature projections with the simple climate model are given in Figure 10.5.6a. For the SRES scenarios, anthropogenic emissions of CO_2 and other gases vary widely (Nakicenovic and Swart, 2000) resulting in a broad range for future temperature projections. For example, the cumulative total (fossil and land-use) CO_2 emissions from 1990 to 2100 vary between 0.75 and 2.6×10^{12} tons of carbon as shown in panel e) of Figure 10.5.6. The relationship between cumulative CO_2 emissions and 2100 temperatures is influenced by differences in non-CO_2 gas emissions and different timing of emissions across the 35 SRES scenarios (compare circle dots in panel e of Figure 10.5.7 and 10.5.8). Considering only the mean of all AOGCM model tunings, the global mean temperature change between 1990 and 2100 spans a range of 2.4°C, from 1.9°C to 4.3°C, for all SRES scenarios. This is the uncertainty in temperatures resulting solely from the uncertainty in emissions (see "All SRES, mean over models" envelope in Figure 10.5.6).

The 'response uncertainty' is comparable in size to the 'emission uncertainty'. For the A2 emission scenario the temperature projections with several models span a range of 2°C, from 2.6 to 4.6°C in 2100. If carbon cycle uncertainties are included, this range widens to 2.4°C, from 2.6°C to 5°C (see panel a and uncertainty bars in panel e in Figure 10.5.6). For lower emission scenarios, this range is smaller. For example, the B1 scenario projections span a range of 1.6°C, from 1.3°C and 2.9° including carbon cycle uncertainties (see panel c and uncertainty bar in panel e of Figure 10.5.6). For at least two reasons, these 'response uncertainties' might be underestimated though. Firstly, no forcing uncertainties are considered in this draft. Secondly, the AOGCM models themselves do not span the full range of possible climate futures. For example, studies that constrain forecasts based on model fits to historic or present day observations generally allow for a much wider 'response uncertainty' (see section 10.5.4.4). The results presented here are a sensitivity study with different model tunings and carbon cycle feedback parameters. The concatenation of all uncertainties requires a probabilistic approach because the extreme ranges have low probability.

The temperature projections in Figure 10.5.6 are based on the anthropogenic and natural (solar & volcanic) forcing shown in Figure 10.5.8, which uses a value of -0.8 W m^{-2} for the indirect aerosol forcing. Solar forcing for the historical period is prescribed according to Lean et al. (1995) and volcanic forcing according to (). The historic solar forcing series is extended into the future by its average over the most recent 22 years. The volcanic forcing is adjusted to have a zero mean over the past 100 years and assumed zero for the future. Model results are shifted to match the mean of the historical observations (Folland et al., 2001; Jones et al., 2001; Jones and Moberg, 2003) over the 1980 to 2000 period.

In the TAR the anthropogenic forcing was used alone even though the projections started in 1765. Advantages of using both natural and anthropogenic forcing for the past is that this it what was done by at least some of the AOGCMs the simple models are emulating. It allows the simulations to be compared with observations and the warming commitments accrued over the instrumental period are reflected in the projections. The disadvantage of including natural forcings is that the warming projections in 2100 are dependent to a few tenths of a degree on the necessary assumptions made about the natural forcings. These assumptions include how the natural forcings are projected into the future and whether to reference the volcanic forcing to a past reference period mean value. Also the choice of data set for volcanic forcing effects the results; the use of Sato et al. (1993) volcanic forcing with its generally higher amplitudes of negative forcing for each volcanic eruption results in a less good match to the observations. Seven different choices have been tried and can be viewed on request.

[INSERT FIGURE 10.5.6 HERE]

[INSERT FIGURE 10.5.7 HERE]

[INSERT FIGURE 10.5.8 HERE]

The major addition here compared to the TAR is the inclusion of carbon cycle uncertainties. In the above presentation for the SRES scenarios the high and low carbon cycle settings are the 90% confidence intervals from the Wigley and Raper (2001) analysis. Their derivation is described as follows. The carbon cycle model in MAGICC includes a number of climate-related carbon cycle feedbacks driven by global-mean temperature. It is not possible to assess the uncertainties in these feedbacks individually. The state of the art only allows us to assess their overall effect, and to quantify this in MAGICC by comparison with more complex and physically realistic models. In Wigley and Raper (2001), the extreme range of such results available at the time was assumed to be the 90% confidence interval. The MAGICC central value, which is close to the average of results from other models, is taken as the 50th percentile. The overall distribution is assumed to be log-normal. This allows MAGICC to produce probabilistic projections of future CO_2 concentration change that are consistent with state-of-the-art carbon cycle model results. When applied to the A2 emissions scenario, MAGICC results are consistent with more recent and comprehensive results from the C4MIP carbon cycle model intercomparison (Friedlingstein et al., 2005). For example, the C4MIP range of 2100 concentrations for A2 is 730 to 1020 ppm, while the 90% confidence interval from MAGICC is 770 to 1090 ppm. MAGICC values are higher because they are driven by the full temperature changes in A2, while the C4MIP values are driven by the component of A2 warming due to CO_2 alone. A more comprehensive comparison of MAGICC with C4MIP will be available shortly, but changes in MAGICC from the present results that may arise from this will be minor.

There are two sources of uncertainty associated with uncertainties in the carbon cycle underlying the projections presented above. First, there are direct uncertainties, those that arise for a single climate sensitivity. In addition, there are uncertainties that arise from uncertainties in the climate sensitivity. If the sensitivity is high, for example, this amplifies the magnitude of the climate feedback on the carbon cycle and so widens the overall uncertainty range considerably. The effect at the other end of the uncertainty range is much smaller. Here, the climate feedback on the carbon cycle is small, so changing the amount of warming by changing the climate sensitivity has little effect.

Figure 10.5.9 illustrates these CO_2 concentration uncertainties for scenario A1B. For low climate feedbacks on the carbon cycle, the projected concentrations in 2100 range from 668 to 682 ppm for sensitivities ranging from 1.5°C to 4.5°C. For high climate feedbacks the corresponding uncertainty range is 737 to 888 ppm. For comparison, the central value is 713 ppm with a climate sensitivity of 2.6°C. (This value is between the projections given in the TAR for the Bern and ISAM models.) At present, it is not possible to assign clear probabilities to the extreme range (668 to 888 ppm), since it concatenates two sources of uncertainty with numbers for each representing individual 90% confidence intervals. A simple assessment would make the probability of lying outside the above range less than 1%.

[INSERT FIGURE 10.5.9 HERE]

Looking at a longer time horizon and for comparison with the EMIC results in the previous section simple climate model results are presented for a scenario that follows A1B to 2100 and then keeps atmospheric composition (and, hence, radiative forcing) constant out to the year 3000. Figure 10.5.10a shows the effect of climate sensitivity uncertainties (with central values for all other model parameters). In 2100, the central warming from 2000 is 2.63°C (for $\Delta T2x = 2.6°C$). For the range $\Delta T2x = 1.5°C$ to $\Delta T2x = 4.5°C$ the warming range is 1.65 to 3.91°C. By 2100, a large warming commitment has been built into the system, which is slowly realized over coming centuries. By the year 3000 the warming range is 2.03 to 6.45°C with a central value of 3.66°C. Figure 10.5.10b shows how these ranges are amplified when one considers carbon cycle uncertainties. At the low end, in both 2100 and 3000, the warming relative to 2000 is reduced by about 4%. At the high end, in both 2100 and 3000, the warming is increased by about 15%.

[INSERT FIGURE 10.5.10 HERE]

10.5.3.2 Long-term integrations: overshoot scenarios and stabilisation

Overshoot scenarios were first considered by Wigley (2004). The original motivation was to extend the WRE concentration stabilization profiles (Wigley et al., 1996) to give less stringent emissions reduction requirements. Overshoot scenarios (or, more correctly, ‘profiles’) are more cost-effective in terms of mitigation, but, because they lead to slightly higher warming, warming rates and sea level rise, they may lead to greater climate damages and an increased risk exceeding some dangerous interference threshold (where the threshold concept must include rates of change as well as absolute warming). The overshoot issue, therefore has extremely important implications for both WG2 (impacts) and WG3 (mitigation). Such scenarios may also be viewed as course-change scenarios, where an initial concentration stabilization target is found to be too high, and a change to a lower target becomes necessary. If such were the case, it is vital to have some idea of the additional mitigation costs. Overshoot scenarios are even more important in the WG3 context, as pointed out by Wigley (2005).

An idealized overshoot scenario has been run in an AOGCM where the concentrations reduce from the A1B stabilized level to the B1 stabilized level between 2150 and 2250 followed by 200 years of integration with that constant B1 level of concentrations (Figure 10.5.11a). This reduction in concentrations would require huge and likely implausible reductions in emissions, but such an experiment illustrates the processes involved with how the climate system would respond to such a large change in emissions and concentrations. Tsutsui et al. (2005) shows there is a relatively fast response in the surface and upper ocean in starting to recover to temperatures at the B1 level after several decades, but a much more sluggish response with more commitment in the deep ocean. That is, as shown in Figure 10.5.11b,c, the overshoot scenario temperatures only slowly reduce to approach the lower temperatures of the B1 experiment, and continue a slow convergence that has still not cooled to the B1 level at the year 2350, or 100 years after the CO_2 concentrations in the overshoot experiment were reduced to equal the concentrations in the B1 experiment. However, Dai et al. (2001b) have shown that reducing emissions to achieve a stabilized level of concentrations in the 21st century reduces warming moderately (less than 0.5°C) by the end of the 21st century in comparison to a business-as-usual scenario, but the warming reduction is about 1.5°C by the end of the 22nd century in that experiment.

[INSERT FIGURE 10.5.11 HERE]

Such stabilization and overshoot scenarios have implications for risk assessment. For example, in a probabilistic study using the MAGICC model and multi-gas scenarios, Meinshausen et al. (2005) estimated that the risk of overshooting a 2°C warming is between 68% and 99% for a stabilization of CO_2 at 550 ppm. They also considered scenarios with peaking CO_2 and subsequent stabilization at lower levels as an alternative pathway and found that if the risk of exceeding a warming of 2°C is not to exceed 30%, it is necessary to peak CO_2 concentrations around 475 ppm before returning to lower concentrations of about 400 ppm. These overshoot and targeted climate change estimations take into account the climate change commitment (see Section 10.7) in the system that must be overcome in the timescale of any overshoot or emissions target calculation. The probabilistic studies also show that when certain thresholds of climate change are to be avoided, emission pathways depend on the certainty required of not overshooting the threshold. Further discussion of the implications of climate change mitigation and adaptation scenarios is given in subsection 10.5.3.3 below.

Intermediate complexity models (EMICs) were used to calculate the long-term climate response to stabilization of atmospheric CO_2. The newly developed stabilization profiles were constructed following Enting et al. (1994) and Wigley et al. (1996) using the most recent atmospheric CO_2 observations, CO_2 projections with the Bern Carbon Cycle-Climate model (Joos et al., 2001) for the A1T scenario over the next few decades, and a ratio of two polynomials (Enting et al., 1994) leading to stabilization at levels of 450, 550, 650, 750 and 1000 ppm atmospheric CO_2 equivalent. Other forcings are not considered. Figure 10.5.12 a) shows the equilibrium surface warming for seven different EMICs and six stabilization levels. Model differences arise mainly from the models having different climate sensitivities. These simulations can be used to determine what CO_2 stabilization level must be targeted when global temperature is to remain below a certain limit. Knutti et al. (2005) explored this further in an EMIC using several published PDFs of climate sensitivity and different ocean heat uptake parameterizations and calculated probabilities of not overshooting a certain temperature threshold given a equivalent CO_2 stabilization level (Figure 10.5.12 b).

[INSERT FIGURE 10.5.12 HERE]

10.5.3.3 Mitigation scenarios

[This section will be added at the second order draft when mitigation scenarios from WG3 have been supplied to WG1 and run with a hierarchy of models.]

10.5.4 Sampling Uncertainty and Estimating Probabilities

Uncertainty in the response of an AOGCM arises from the effects of internal variability, which can be sampled in isolation by creating ensembles of simulations of a single model using alternative initial conditions, and from modelling uncertainties, which arise from errors introduced by the discretisation of the equations of motion on a finite resolution grid, and the consequent need to parameterise the effects of sub-grid scale processes (radiative transfer, cloud formation, convection etc) on the resolved flow. Modelling uncertainties are manifested in alternative structural choices (for example, choices of resolution and the basic physical assumptions on which parameterisations are based), and in the values of poorly-constrained parameters within given parameterisation schemes. Ensemble approaches are used to quantify the effects of uncertainties arising from variations in model structure and parameter settings. These are assessed in Sections 10.5.4.1–10.5.4.3, followed by a discussion of observational constraints in subsection 10.5.4.4 and methods used to obtain probabilistic predictions in subsection 10.5.4.5.

While ensemble predictions carried out to date give a wide range of responses, they do not sample all possible sources of modelling uncertainty. For example, the AR4 multi-model ensemble relies on specified concentrations of CO_2, thus neglecting uncertainties in carbon cycle feedbacks (Section 10.4.1), though this can be partially addressed by using less detailed models to extrapolate the AOGCM results (Section 10.5.3). More generally, climate models may underestimate uncertainty because they implement a restricted approach to the parameterisation of sub-grid scale processes, using deterministic bulk formulae coupled to the resolved flow exclusively at the grid scale. Palmer et al. (2005) argue that this approach should be generalised to allow the outputs of parameterisation schemes to be sampled from statistical distributions consistent with a range of possible sub-grid scale states. Stochastic parameterisation schemes have been tried in numerical weather forecasting (e.g., Buizza et al., 1999; Palmer, 2001), but not yet in climate prediction. The potential for missing factors to broaden the simulated range of future changes is not clear, however this is an important caveat on the results discussed below.

10.5.4.1 The multi-model ensemble approach

The use of ensembles of AOGCMs developed at different modelling centres has become established in climate prediction on both seasonal to interannual and centennial time scales. To the extent that simulation errors in different AOGCMs are independent, the mean of the ensemble can be expected to outperform individual ensemble members, thus providing an improved “best estimate” forecast. Results show this to be the case, both in verification of seasonal forecasts (Hagedorn et al., 2004; Palmer et al., 2004) and of the present day climate from long term simulations (Lambert and Boer, 2001). By sampling modelling uncertainties, ensembles of AOGCMs should provide an improved basis for probabilistic projections compared with ensembles of a single model sampling only uncertainty in the initial state (Palmer et al., 2005). Probabilistic verification of future climate change projections is not possible, however Räisänen and Palmer (2001) used a "perfect model approach" (treating one member of an ensemble as truth and predicting its response using the other members) to show that the hypothetical economic costs associated with climate events can be reduced by calculating the probability of the event across the ensemble, rather than using a deterministic prediction from an individual ensemble member.

However, members of a multimodel ensemble share common systematic errors (Lambert and Boer, 2001), and are not designed to sample the full range of possible model configurations.

10.5.4.2 Perturbed physics ensembles

The AOGCMs featured in Section 10.5.2 are built by selecting components from a pool of alternative parameterisations, each based on a given set of physical assumptions and including a number of uncertain parameters. A comprehensive approach to quantifying the range of predictions consistent with these components would be to construct very large ensembles with systematic sampling of multiple combinations of options for parameterisation schemes and parameter values. SCMs and EMICs have recently adopted such an approach (Wigley and Raper, 2001; Knutti et al., 2002) and Murphy et al. (2004) and Stainforth et al. (2005) describe the first steps in this direction using AOGCMs, constructing large ensembles by perturbing poorly constrained surface and atmospheric parameters in the atmospheric component of HadCM3 coupled to a mixed layer ocean. These experiments quantify the range of equilibrium responses to doubled CO_2 consistent with uncertain parameters in a single GCM, however they do not sample uncertainties associated with changes in ocean circulation, or “structural” model perturbations (see above). Murphy et al (2004) perturbed 29 parameters one at a time and, assuming that effects of individual parameters combine linearly and independently, found a probability distribution for climate sensitivity with a 5–95% range of 2.4–5.4°C when weighting the models with a broadly-based metric of the agreement between simulated and observed climatology, cf 1.9–5.3°C when all model versions are assumed equally reliable (Figure 10.5.13).

[INSERT FIGURE 10.5.13 HERE]

Stainforth et al. (2005) deployed a novel distributed computing approach (suggested by Allen*,* 1999) to run a very large ensemble of 2578 simulations sampling combinations of high, intermediate and low values of six parameters known to affect climate sensitivity. They found climate sensitivities ranging from 2–11°C (Figure 10.5.14a), with 4.2% of model versions giving values exceeding 8°C, and showed that the high sensitivity models could not be ruled out, based on a comparison with surface annual mean climatology. By utilizing multivariate linear relationships between climate sensitivity and spatial fields of several present day observables the 5–95% range of climate sensitivity is estimated at 2.2–6.8°C from the same dataset (Piani et al*.,* 2005) (Figure 10.5.13). Furthermore, in this ensemble, Knutti and Meehl (2005) find a strong relationship between climate sensitivity and the amplitude of the seasonal cycle in surface temperature in the present day simulations (Figure 10.5.14b). Most of the simulations with high sensitivities overestimate the observed amplitude. Using this technique, the 5-95% range of climate sensitivity is estimated at 2–6ºC (Figure 10.5.13). The differences between the PDFs in Figure 10.5.13 reflect uncertainties in methodology arising from choices of uncertain parameters, their expert-specified prior distributions, and alternative applications of observational constraints. It should be noted that those perturbed physics studies are all based on the HadAM3 model. Only Piani et al. (2005) account for structural uncertainties in their statistical method, resulting in a wider range of climate sensitivity, but none of the studies uses a different model.

[INSERT FIGURE 10.5.14 HERE]

Annan et al. (2005a) use an ensemble Kalman Filter technique to obtain uncertainty ranges for model parameters subject to the constraint of minimising simulation errors with respect to a set of climatological observations. This resource-efficient method involves repeat iterations of a cycle of short ensemble integrations and assimilation of observed datasets until a convergent solution is found for parameter ranges. Hargreaves et al. (2005) use this method to explore the range of responses of the Atlantic meridional overturning circulation to increasing CO_2 using an EMIC, finding that the circulation spins down in more than one third of ensemble members. Annan et al. (2005b) apply the method to study the link between climate sensitivity and cooling at the Last Glacial Maximum (see Chapter 8).

10.5.4.3 Diagnosing drivers of uncertainty from ensemble results

Räisänen (2001) analysed the relative roles of internal variability and model differences in explaining differences in the 20 year mean transient response to doubled CO_2 in an ensemble of 15 AOGCMs. The spread in responses is dominated by model differences for surface temperature, whereas internal variability plays a larger (though still subsidiary) role for the other variables. For seasonal changes, internal variability explains more of the ensemble spread, to the extent that it becomes (on average) comparable with model differences as a source of uncertainty in local precipitation and sea level pressure changes, though not for surface temperature. These conclusions are supported by results from the perturbed physics ensemble of Murphy et al. (2004). Räisänen (2001) also analysed the agreement between the responses of different models (Figure 10.5.15), finding that agreement increases with scale for surface temperature and (especially) precipitation, and that the contribution of internal variability to intermodel spread decreases with scale for all variables.

[INSERT FIGURE 10.5.15 HERE]

Selten et al. (2005) report a 62 member initial condition ensemble of simulations of 1940–2080 including natural and anthropogenic forcings. They find an individual member which reproduces the observed trend in the NAO over the past few decades, but no trend in the ensemble-mean, and suggest that the observed change can be explained through internal variability associated with a mode driven by increases in precipitation over the tropical Indian Ocean. Terray et al. (2004) find sensitivity to grid resolution in simulated changes in the residence of the positive phase of the NAO. The coupled ocean-atmosphere version of the ARPEGE model shows small increases in response to SRES A2 and B2 forcing, whereas larger increases are found when SST changes prescribed from the coupled version are used to drive a version of the atmosphere model with enhanced resolution over the North Atlantic and Europe (Gibelin and Déqué*,* 2003).

Collins et al. (2005a) report a perturbed physics ensemble simulation of the transient response to increasing CO_2, created by coupling the ocean component of HadCM3 to 17 versions of the atmospheric component. These are designed to sample a wide range of multiple parameter perturbations and climate sensitivities, subject to the constraint that each version should produce a high quality simulation of present day climate. The results (Figure 10.5.16) show a similar range of global mean surface temperature changes to that found in the AR4 multi-model ensemble. These ensembles are complementary in the sense that the AR4 ensemble partially samples ocean physics uncertainties, and the effects of structural variations in atmospheric model components, whereas the perturbed physics ensemble samples parameter uncertainties for a fixed choice of ocean model and fixed structural choices for atmospheric components. Soden and Held (2005) find that differences in cloud feedback are the dominant source of uncertainty in the transient response of surface temperature in the AR4 ensemble, as in previous IPCC assessments.

[INSERT FIGURE 10.5.16 HERE]

Webb et al. (2005) compare equilibrium radiative feedbacks in a 9 member multi-model ensemble against those simulated in a 128 member perturbed physics ensemble with multiple parameter perturbations. They find that the range of climate sensitivities in the multi-model ensemble is explained mainly by uncertainty in the response of shortwave cloud forcing, while the range found in the perturbed physics ensemble is driven more by uncertainties in the response of longwave cloud forcing, with variations in shortwave cloud forcing playing a lesser role. Given that variations in cloud parameterisation remain a major source of uncertainty in simulations of climate change (Ogura et al., 2005; Tsushima et al., 2005b; Williams et al., 2005b), and that the variations between different schemes remain difficult to resolve using observations, it has been suggested (Palmer et al., 2005) that achieving significant reductions in uncertainty will require much higher resolution climate models, capable of resolving more of the atmospheric processes responsible for the observed distribution of cloud and water vapour. However ensemble approaches will remain necessary for the foreseeable future, given that some of the key parameterisation uncertainties reside in very small scale processes such as cloud microphysics.

10.5.4.4 Observational constraints

A range of observables has been used since the TAR to explore methods for constraining uncertainties in future climate change. These include changes in surface and upper air temperatures and ocean heat content during the past 50–150 years, which have been used in a number of studies with simple climate models, EMICs and AOGCMs to constrain climate sensitivity and TCR (see Section 10.5.4.5). Probabilistic estimates of climate sensitivity have also been obtained using statistical measures of the correspondence of simulated global fields to observations of time averaged present day climate (Murphy et al., 2004; Piani et al., 2005), historical trends in radiative forcing, feedback and surface temperature change (Gregory et al., 2002a; Forster and Gregory, 2005), measures of the variability in present day climate (Bony et al., 2004; Bony and Dufresne, 2005; Knutti and Meehl, 2005; Tsushima et al., 2005a; Williams et al., 2005c), the response to paleoclimatic forcings (Annan et al., 2005b; Hegerl et al., 2005; Schneider von Deimling et al., 2005) and major volcanic eruptions (Wigley et al., 2005; Yokohata et al., 2005) (see Section 9.6).

For the purpose of constraining regional climate change, spatial averages or fields of time averaged regional climate have been used (Giorgi and Mearns, 2003; Laurent and Cai, 2005; Tebaldi et al., 2005b; Tebaldi et al., 2005a), as have regional or continental scale trends in surface temperature (Greene et al., 2005; Stott et al., 2005a). Trends in multiple variables derived from reanalysis datasets are another possibility for future consideration (Lucarini and Russell, 2002).

It is not yet clear to what extent the spread of predicted future changes can be narrowed by combining the above constraints. Additional constraints could also be found, for example from evaluation of ensemble climate prediction systems on shorter time scales for which verification data exists. These could include assessment of the reliability of seasonal to interannual probabilistic forecasts (Hagedorn et al., 2004; Palmer et al., 2004), and the evaluation of model parameterisations in short range weather predictions (Phillips et al., 2004; Palmer, 2005).

10.5.4.5 Probabilistic projections—global mean

A number of methods for providing probabilistic climate change projections, both for global means (discussed in this section) and geographical depictions (discussed in the following section) have emerged since the TAR. These can be grouped into three broad categories, consisting of: (1) methods based on results of AOGCM ensembles without formal application of observational constraints; (2) methods designed to be constrained by observations and their uncertainties and, as far as possible, independent of the spread of outcomes found in AOGCM ensembles; (3) methods designed to give results dependent on both observational constraints and distributions of AOGCM results.

Method 1 above has the advantage of being constrained by the detailed understanding of physical processes built into the models. For example, AOGCM results from both the AR4 multimodel ensemble and from perturbed physics ensembles suggest a very low probability for a climate sensitivity below 2ºC, despite exploring the effects of a wide range of alternative modelling assumptions on the global radiative feedbacks arising from lapse rate, water vapour, surface albedo and cloud (Soden and Held*,* 2005; Webb et al.*,* 2005) (also discussed in Box 10.2 on climate sensitivity in this chapter). However, reliance on AOGCM ensembles can also be questioned on the basis that models share components, and therefore errors, and may not sample the full range of possibilities consistent with our physical understanding (e.g., Allen and Ingram*,* 2002). Also, the results are likely to depend on subjective judgements such as the values or prior distributions chosen for poorly constrained model parameters or alternative choices of parameterisation (Murphy et al.*,* 2004; Ogura et al.*,* 2005; Stainforth et al.*,* 2005). A set of alternative techniques (described below), has been developed in which probabilities are derived on the basis of replicating ranges of historical observations, using models to link historical and future variables while minimising dependence of the results on the models themselves.

Observationally-constrained probability distributions for climate sensitivity (method 2 above) have been derived from physical relationships based on energy balance considerations, and instrumental observations of historical changes including surface and upper air temperatures and ocean heat content during the past 50-150 years, or proxy reconstructions of northern hemisphere extratropical surface temperature during the past millennium (see Chapter 8). The results vary according to the choice of verifying observations, the forcings considered and their specified uncertainties, however all these studies report a high upper limit for sensitivity, the 95th percentile of the distributions invariably exceeding 6ºC (see Chapter 8). Frame et al. (2005) demonstrate that uncertainty ranges for sensitivity are dependent on the choices made for prior distributions of uncertain quantities before the observations are applied. Frame and Allen (2005) and Allen et al. (2002) argue that many observable variables are likely to scale directly with feedback strength and inversely with sensitivity, implying that projections of quantities which are directly related to feedback strength (such as TCR) will be more strongly constrained by observations than climate sensitivity, which will be more dependent on prior assumptions, particularly with respect to the estimated upper limit.

In the case of transient climate change, optimal detection techniques have been used to determine factors by which hindcasts of global surface temperature from AOGCMs can be scaled up or down while remaining consistent with past changes, accounting for uncertainty due to internal variability (see Section 9.4.1). Uncertainty is propagated forward in time by assuming that the fractional error in model projections of global mean temperature change is constant. Stott and Kettleborough (2002) used this approach with HadCM3 to determine probabilistic projections of global mean temperatures for four representative SRES emissions scenarios. Global mean temperature rise was found to be insensitive to differences in emissions scenarios over the first few decades of the 21st century; a temperature rise of 0.91.9°C being predicted by the 2020s relative to pre-industrial conditions (Figure 10.5.17). This uncertainty range is consistent with that obtained by Knutti et al. (2002) by constraining a large ensemble of EMIC simulations using past changes in surface temperature and ocean heat content (Zwiers*,* 2002). Figure 10.5.17 shows that much larger differences between the response to different SRES scenarios emerge by the end of the 21st century. Global mean warming as high as 6.3°C cannot be ruled out at the 95% confidence level in the SRES A2 scenario. Stott et al. (2005b) showed that the results are relatively model-independent, finding that scaling the responses brings three models with different sensitivities into better agreement. Stott et al. (2005a) extend their approach to obtain probabilistic projections of future warming averaged over continental scale regions under the SRES A2 scenario. Fractional errors in the past continental warming simulated by HadCM3 are used to scale future changes, yielding wide uncertainty ranges, notably for North America and Europe where the 5–95% ranges for warming during the 21st century are 2–12°C and 2–11°C respectively. These estimates can be viewed as an upper limit on uncertainty as they do not account for potential constraints arising from regionally differentiated warming rates. Alternatively, a lower limit can be obtained by assuming the simulated spatial patterns of change to be correct, and scaling the regional changes according to fractional errors in global temperature change. This results in tighter ranges of 4–8°C for North America and 4–7°C for Europe.

The third approach to probabilistic projection is to combine information from AOGCM ensembles and observational constraints. One method is described by Allen and Ingram (2002), who suggest that probabilistic projections for some variables may be made by searching for "emergent constraints". These are relationships between variables which can be directly constrained by observations, such as global surface temperature, and variables which may be indirectly constrained by establishing a consistent, physically-based relationship which holds across a wide range of models. They present an example in which future changes in global mean precipitation are constrained using a probability distribution for global temperature obtained from a large EMIC ensemble (Forest et al., 2002) and a relationship between precipitation and temperature obtained from multi-model ensembles of the response to doubled CO_2. Further examples of this approach are those of Knutti and Meehl (2005) and Piani et al. (2005), described in Section 10.5.4.2. Since these methods produce results constrained primarily by observations, they are likely to be robust (Allen et al., 2002; Allen and Stainforth, 2002), changing only as the signal of anthropogenic climate change emerges from the noise of internal variability (Stott and Kettleborough, 2002).

A synthesis of published probabilistic global mean projections for the SRES scenarios B1, A1B and A2 is given in Figure 10.5.17. Probability density functions (PDFs) are given for short-term projections (2020–2030) and the end of the century (2090–2100), and complement the results in Section 10.3.1 for the AOGCMs from the multi-model archive. The four methods are all based on different models and/or methods, described in Section 10.5. In short, Wigley and Raper (2001) used a large ensemble of a simple model with expert priors on climate sensitivity, ocean heat uptake, sulphate forcing and the carbon cycle, without applying constraints. Knutti et al. (2002; 2003) use a large ensemble of EMIC simulations with uninformed priors, consider uncertainties on climate sensitivity, ocean heat uptake, radiative forcing, and the carbon cycle, and apply observational constraints. Neither method considers natural variability explicitly. The fingerprint scaling method (Stott et al., 2005b) implicitly considers uncertainties in forcing, climate sensitivity and internal unforced as well as forced natural variability, but neglects carbon cycle uncertainties. The results based on three different AOGCMs are shown for SRES A2 and illustrate the effect of structural uncertainties. Collins et al. (2005a) and Harris et al. (2005) boost a 17 member perturbed physics ensemble of the HadCM3 model to obtain a PDF, and neglect forcing and carbon cycle uncertainties.

Two key points emerge from Figure 10.5.17: 1) for the projected near-term warming early in this century, there is more agreement among models and methods (narrow width of the PDFs) compared to later in the century (wider PDFs); 2) the near term warming early in this century is similar across different scenarios, compared to later in the century where the choice of scenario makes a real difference in the global warming that is projected to occur.

Additionally, projection uncertainties increase close to linearly with temperature in most studies. The different methods show relatively good agreement in the shape and width of the PDFs, but with some offsets due to structural uncertainties related to the model, setup, forcing and statistics. Kettleborough et al. (2005) project total climate change including variations in natural forcings, resulting in small probability for cooling over the next decades. The other studies project only anthropogenic changes and exclude cooling in the future. The results of Knutti et al. (2003) show wider PDFs and probability for very high warming for the end of the century because they sample uniformly in climate sensitivities (see Chapter 9 and Box 10.2 on climate sensitivity). Resampling uniformly in observables (Frame et al., 2005) would bring those PDFs closer to the others. The other methods explicitly or implicitly exclude high sensitivities. In sum, probabilistic estimates of uncertainties for the next decades seem robust across a variety of models and methods, while results for the end of the century depend on the assumptions made. The range encompassing all PDFs for 2100 is wider than most individual PDFs and exceeds the spread of the multi-model ensemble.

[INSERT FIGURE 10.5.17 HERE]

10.5.4.6 Probabilistic projections—geographical depictions

Several methods have been developed recently to depict probabilistic geographic climate change, such as relying on Bayesian approaches to combine observational constraints and ensemble simulations (e.g., Murphy et al. (2004), described in Section 10.5.4.2). Tebaldi et al. (2005a) update non-informative prior distributions for regional temperature and precipitation using observations and results from AOGCM ensembles to produce probability distributions of future changes for various regions (see more details and discussion in Section 11.2.2.2). Key assumptions are that each model and the observations differ randomly and independently from the true climate, and that the weight given to a model prediction should depend on the bias in its present day simulation and its degree of convergence with the best estimate of the predicted future change. Lopez et al. (2005) apply the Tebaldi et al. (2005a) method to predict future changes in global surface temperature under a 1% per year increase in CO_2, comparing it with the method developed by Allen et al. (2000) and Stott and Kettleborough (2002) (ASK). Lopez et al. find that the Bayesian method (applied to a 15 member ensemble) predicts a much narrower uncertainty range than ASK, which aims to provide model-independent probabilities consistent with observed changes (see above). The results of the Bayesian method are found to be sensitive to choices made in its design, in particular the convergence criterion for upweighting models close to the ensemble mean, relaxation of which substantially increases the predicted uncertainty, reducing the discrepancy with ASK.

Another method by Furrer et al. (2005) employs a hierarchical Bayes model to construct PDFs of temperature change at each grid point from a multi-model dataset. This information can then be displayed in a global geographical map of, for example, the highest temperature change in the A1B scenario by the end of the 21st century with an 80% probability of occurrence (Figure 10.5.18a,b), or as values of probability for a 2°C temperature change by the end of the 21st century (Figure 10.5.18c,d). This technique can be seen as a direct extension of the assumptions of linear regression to the treatment of geographic fields, rather than single scalar values. The temperature differences from each member of the multi-model ensemble, averaged for A1B for 2080–2099 minus 1980–1999 for DJF and JJA, are regressed upon basis functions, i.e., a series of fields that are chosen as starting points to explain the possible common large scale structure of the climate change signal. One of the basis functions is a map of differences of observed temperatures from late minus mid 20th century, and others are spherical harmonics. When linearly combined the spherical harmonics can represent other possible large-scale climate change patterns that are not related to observations.

The statistical model is formulated through a hierachical-Bayes framework, and a Markov Chain Montecarlo algorithm, then calculates estimates of the true coefficients of the regression and the uncertainty around them, plus estimates of the errors. At the lower level of the hierarchical model, the coefficients are AOGCM specific since each model approximates a pattern of change that is a product of its own processes, resolution, parameterization etc. But on average they are assumed to be centered around the true (unknown) coefficients (representing a higher level of the hierarchical structure that is estimated through Bayes theorem) that give the true pattern of climate change as a combination of those basis functions. Weighting by the relative agreement among the models (Tebaldi et al., 2005a) is not assumed in this method. The error in the regression accounts for the remaining spatial correlation that is the deviation in each AOGCM from the common large scale structure. It is then assumed, as is done in a regression, that the errors are Gaussian, in this case Gaussian random fields whose covariance function quantifies the extent of the correlation among grid cells at the small scales.

By recombining the coefficients with the basis functions, an estimate is derived of the true climate change field and of the uncertainty around it. Since the spatial correlation of the large scale (through the basis functions) and of the omitted small scales (through the error covariance) are accounted for, the probabilistic projections derived for the entire globe represent the joint probability of a given climate change at each grid point. In summary, the main assumptions of this method are that large scales can be separated from small scales, that the climate change signal is a common large scale structure represented to some degree in each of the model simulations, and that the signal unexplained by climate change is AOGCM specific in terms of small scale structure, but can be regarded as noise when averaged over all AOGCMs.

[INSERT FIGURE 10.5.18 HERE]

[INSERT FIGURE 10.5.19 HERE]

Räisänen (2005b) fits empirical distributions to multi-model simulations to estimate probabilities for regional surface temperature and precipitation changes. The form of the distribution is calibrated from the ensemble dataset, allowing for possible departures from Gaussian. Cross verification, in which one ensemble member is treated as truth, is used to show that the fitted distributions perform better than Gaussian forms. A key assumption is that the shape of the fitted distribution is unchanged over large spatial regions, in order to give a large enough calibration dataset. Based on this technique, Figure 10.5.19a,b shows the probability of occurrence of at least a 2°C warming by the end of the 21st century for the A1B scenario for DJF and JJA, respectively. This can be compared to a simple calculation in Figure 10.5.19c,d that shows, for the same 21 AOGCMs, the percent of models at each grid point (about 250 km grid) that show a warming at the end of the 21st century in the A1B scenario that is at least 2°C for DJF and JJA, respectively. This calculation is provided as a simple check for the more complicated PDF calculations in Figure 10.5.19a,b, and Figure 10.5.18c,d (though the latter has been interpolated to a more coarse 500 km resolution). All methods show similar results, indicating that the PDF calculations are relatively robust. That is, for DJF all show greater than 80% for a 2°C warming over the high northern latitudes and over most of the northern continents, and less than 50% over the southern oceans. For JJA, there are values greater than 80% over most of the midlatitude continents, with less than 50% over the Arctic and southern oceans.

One consequence of the limited size of multi-model ensembles (typically 10–20 members) is that probabilities derived from them are potentially sensitive to outliers (Räisänen, 2005b). Given that it is currently too expensive to run large ensembles of AOGCMs containing a full dynamic ocean, Harris et al. (2005) propose a method of augmenting the size of AOGCM ensembles using a pattern scaling approach. They obtain frequency distributions of transient regional changes by scaling the equilibrium response patterns of a 128 member perturbed physics ensemble. For a given model version the transient response is emulated by scaling the equilibrium response pattern according to global temperature (predicted from an energy balance model tuned to the relevant climate sensitivity), adding a correction field to account for differences between the equilibrium and transient patterns, and allowing for uncertainty in the emulated result. The correction field and emulation errors are calibrated by comparing the responses of 17 model versions (the black curves in Figure 10.5.16) for which both transient and equilibrium simulations exist. Results are used to estimate uncertainties in the surface temperature and precipitation response to a 1% per year CO_2 increase arising from the combined effects of atmospheric parameter perturbations and internal variability in HadCM3. The spread of predicted changes is found to vary widely around the globe. For annual temperature the 5–95% range is largest at high northern latitudes, qualitatively consistent with results derived from the same forcing scenario applied to a 20 member multi-model ensemble as shown in Figure 10.5.19a,b (Räisänen, 2005b).

In summary, significant progress has been made since the TAR in developing and exploring ensemble approaches to sampling modelling uncertainties and providing uncertainty ranges and probabilities for global and regional climate change. Different methods give different results, because they depend to varying degrees on the nature and use of observational constraints, the nature and design of model ensembles, and the specification of prior distributions for uncertain inputs (see, for example, Table 11.2.1). It is not yet possible to recommend a preferred method, but it is important to communicate to users the assumptions and limitations underlying the various approaches and the sensitivity of the results to them. A good example concerns the treatment of model error in Bayesian methods, the uncertainty in which affects the calculation of the likelihood of different climate model versions, but is difficult to specify and is yet to be properly addressed in the field of climate prediction (Annan and Hargreaves, 2005; Rougier, 2005). These types of depictions of probabilistic climate change, particularly geographic depictions, are new to the field of climate change science and are being facilitated by the recently available multi-model ensembles. Work in this area is almost certain to develop rapidly, and will likely play a major role in how climate change is quantified and communicated in the IPCC AR5.

10.6 Sea-Level Change

10.6.1 Global Average Sea-Level Rise Due to Thermal Expansion

As sea water becomes warmer, its density decreases. This thermal expansion will lead to an increase in volume of the global ocean, producing a (thermosteric) sea level rise (Section 5.5.3), which is expected to be the dominant contribution to the global average during the 21st century. Global average thermosteric sea level rise can be calculated directly from simulated changes in ocean temperature. Results are available from 16 AOGCMs for the 21st century for SRES scenarios A1B, A2 and B1 (Figure 10.6.1), continuing from simulations of the 20th century. The timeseries are rather smooth compared with global average temperature timeseries, because thermal expansion reflects heat storage in the entire ocean, being approximately proportional to the time-integral of temperature change (Gregory et al., 2001). In the control runs (available from a subset of 11 AOGCMs), internally generated variability in the climate system produces a decadal standard deviation of sea level due to thermal expansion in the range 0.4–2.0 mm, with one outlying model giving 3.4 mm.

During 2000–2020 the rate of thermal expansion is 0.6–2.1 mm yr^{-1} (estimated 2.5–97.5% range), similar to the observed rate during 1993-2003, which itself is large compared with that of previous decades (Section 5.5.3). The AOGCMs differ in their treatment of natural forcings during the 20th century (Section 5.5.6, Church et al., 2005; Gleckler et al., 2005; Gregory et al., 2005a); committed response to 20th century forcing may explain some of the spread in the early 21st century.

Thermal expansion from 2000 to 2050 amounts to 50–120 mm. Although each shows a substantial spread across the models, the three scenarios can barely be distinguished. This is because there is less difference in the integral up to 2050 among the scenarios than in the temperature change at 2050.

During 2080–2100 the rate of thermal expansion is 1.3–4.9 mm yr^{1}, more than twice that of 2000–2020, the acceleration being caused by the increased climatic warming. By 2100 thermal expansion has reached 130–340 mm and the scenarios can be distinguished, although the spread across models is still dominant. In SRES A1B for 2080–2100 (for example), there is no correlation of the global average temperature change across models with either thermal expansion or its rate of change, suggesting that spread in thermal expansion is not mainly caused by spread in surface warming, but by model-dependence in ocean heat uptake efficiency (Raper et al., 2002) and the distribution of added heat within the ocean (Russell et al., 2000, and Section 5.5.3).

Thermal expansion beyond 2100 is discussed in Section 10.7.

[INSERT FIGURE 10.6.1 HERE]

10.6.2 Local Sea-Level Change Due to Ocean Dynamics

The geographical pattern (the dynamic topography) of mean sea level relative to the geoid is an aspect of the dynamical balance relating the ocean's density structure and its circulation, which are maintained by air-sea fluxes of heat, fresh water and momentum. Over much of the ocean on multi-annual timescales, a good approximation to local sea level change is given by the steric sea level change, which can be calculated straightforwardly from local temperature and salinity change (Gregory et al., 2001; Lowe and Gregory, 2005). In much of the world, salinity changes are as important as temperature changes in determining the pattern of dynamic topography change in the future, and their contributions can be opposed (Landerer et al., 2005, and as in the past, Section 5.5.4.1). Lowe and Gregory (2005) show that in the HadCM3 AOGCM changes in heat fluxes are the cause of many of the large-scale features of sea level change, but fresh water flux change dominates the north Atlantic and momentum flux change has a signature in the north Pacific and the Southern Ocean. Landerer et al. (2005) find that increased windstress in the Southern Ocean opposes thermosteric sea level change there.

Results are available for local sea level change due to ocean density and circulation change from 14 AOGCMs for the 20th century and the 21st century following SRES scenario A1B. There is substantial spatial variability in all models i.e. sea level change is not uniform, and as the geographical pattern of climate change intensifies, the spatial standard deviation increases (Church et al., 2001; Gregory et al., 2001). Suzuki et al. (2005) show that, in their high-resolution model, enhanced eddy activity contributes to this increase. We consider the difference between the means for 2080–2100 and 1980–2000. The spatial standard deviation lies in the range 0.02–0.57 m, with an average of 0.14 m, smaller values being more common. Across models, it shows no correlation with spatial resolution but has a weak correlation of 0.4 with global average thermal expansion.

The geographical patterns of sea level change from different models are not generally similar in detail, but they have more similarity than those analysed in the TAR by Church et al. (2001). The largest spatial correlation coefficient between any pair is 0.76, but only 20% of correlation coefficients exceed 0.5. To identify common features we examine an ensemble mean (Figure 10.6.2). Like Church et al. (2001) and Gregory et al. (2001) we note smaller than average sea level rise in the Southern Ocean and larger than average in the Arctic, the former possibly due to windstress change (Landerer et al., 2005) or low thermal expansivity (Lowe and Gregory*,* 2005) and the latter to freshening. Another obvious feature is a narrow band of pronounced sea level rise stretching across the southern Atlantic and Indian Oceans and discernible in the southern Pacific. This could be associated with a southward shift in the circumpolar front (Suzuki et al.*,* 2005) or subduction of warm anomalies in the region of formation of sub-Antarctic mode water (Banks et al.*,* 2002), and some similar indications are present in the altimetric and thermosteric patterns of sea level change for 1993–2003 (Figures 5.5.3 and 5.5.13). The model projections do not share other aspects of the observed pattern of sea level rise, such as in the western Pacific, which could be related to interannual variability (Section 5.5.3).

The north Atlantic dipole pattern noted by Church et al. (2001) (reduced rise to the south of the Gulf Stream extension, enhanced to the north, consistent with a weakening of the circulation) is present in some models; a more complex feature is described Landerer et al. (2005). The reverse is apparent in the north Pacific, associated with a wind-driven intensification of the Kuroshio current by Suzuki et al. (2005). Using simplified models, Hsieh and Bryan (1996) and Johnson and Marshall (2002) show how upper-ocean velocities and sea level would be affected in north Atlantic coastal regions within months of a cessation of sinking in the north Atlantic as a result of propagation by coastal and equatorial Kelvin waves, but would take decades to adjust in the central regions and the south Atlantic. Levermann et al. (2005) and Vellinga and Wood (2005) show that a sea level rise of a several tenths of a metre could be realised in coastal regions of the north Atlantic within a few decades (i.e., tens of millimetres per year) of a collapse of the overturning. Such changes to dynamic topography would be much more rapid than global average sea level change. However, it should be emphasised that these studies are sensitivity tests, not projections; the overturning circulation does not collapse in the SRES scenario runs (Section 10.3.4).

The geographical pattern of sea level change is affected also by changes in atmospheric pressure, land movements (elastic and viscous) resulting from the changing loading of the crust by water and ice and the consequent displacement of mantle material, and changes in the gravitational field of the ocean and solid Earth (Section 5.5.4.2). These effects have not been included in Figure 10.6.2.

[INSERT FIGURE 10.6.2 HERE]

10.6.3 Glaciers and Ice Caps

Glaciers and ice caps (G&IC) may change their mass because of changes in ablation (mostly melting) or accumulation (mostly precipitation) (Section 4.5.1). Use of data from climate models to make projections requires a method of downscaling, because individual G&IC are much smaller than typical AOGCM gridboxes, and their mass balance depends strongly on their altitude and aspect. Statistical relations can be developed between GCM and local meteorology (Reichert et al.*,* 2002), but they may not continue to hold in future climates. Hence for projections the approach usually adopted is to assume that GCM simulations of changes in climate parameters can be used locally even though the control values cannot (Schneeberger et al.*,* 2003).

10.6.3.1 Mass balance sensitivity to temperature

For the TAR projections of G&IC outside Greenland and Antarctica, Church et al. (2001) used an empirical relationship (Zuo and Oerlemans*,* 1997) between climatological precipitation and mass balance sensitivity to temperature $\partial b/\partial T$ as determined by energy-balance modelling for a sample of 12 G&IC. (see Section 4.5.1 for discussion of the relation of $\partial b/\partial T$ to climate.) For a temperature change uniform throughout the year, $\partial b/\partial T$ was between –0.14 and –1.00 m yr^{-1} K^{-1}. Oerlemans and Reichert (2000) and Oerlemans (2001)have refined the scheme to include dependence on monthly temperature and precipitation changes, and Oerlemans et al. (2005) have applied this version to a number of Arctic G&IC regions. Using a degree-day method (in which ablation is proportional to the integral of mean daily temperature above freezing point), de Woul and Hock (2005) find somewhat larger sensitivities for Arctic G&IC. Braithwaite et al. (2003) calculated $\partial b/\partial T$ for a set of 61 G&IC using a degree-day method, with results in the range –0.1 to –1.2 m yr^{-1} K^{-1}. Braithwaite and Raper (2002) show there is excellent consistency between the results for $\partial b/\partial T$ of Oerlemans and Fortuin (1992) and Braithwaite et al. (2003). Schneeberger et al. (2000; 2003) use a degree-day method for ablation modified to include incident solar radiation, again obtaining a similar range.

Hansen and Nazarenko (2004) collated measurements of soot (fossil fuel black carbon) in snow and have estimated consequent reductions of snow and ice albedo of between 0.1% for the pristine conditions of Antarctica and over 10% for polluted northern hemisphere land areas. They argue that glacial ablation would be increased by this effect. While it is true that soot has not been explicitly considered in existing sensitivity estimates, it may already be included because the albedo and degree-day parametrisations have been empirically derived from data collected in affected regions.

The sensitivity of global G&IC mass change is estimated by weighting the local sensitivities by land ice area in various regions. For a geographically and seasonally uniform rise in global temperature T_g, Oerlemans and Fortuin (1992) derive a global G&IC mass balance sensitivity $\partial B/\partial T_g$ of –0.40 m yr^{-1} K^{-1}, Braithwaite and Raper (2002) –0.41, Raper and Braithwaite (2005) –0.35. We have extended the scheme of Oerlemans et al. (2001; 2005) worldwide, obtaining a smaller value of –0.32 m yr^{-1} K^{-1}, the reduction being due to the improved treatment of albedo by Oerlemans (2001).There is considerable uncertainty in total G&IC area (Section 4.5.1 and Table 4.5.1). Assuming 530,000 km^2, $\partial B/\partial T_g$ of –0.40 m yr^{-1} K^{-1} is equivalent to 0.58 mm yr^{-1} K^{-1} of sea level rise.

10.6.3.2 Mass balance sensitivity to precipitation

For seasonally uniform temperature rise, Oerlemans et al. (1998) found that an increase in precipitation of 20–50% K^{-1} was required to balance increased ablation, while Braithwaite et al. (2003) reported of 29–41% K^{-1}, in both cases for a sample of G&IC representing a variety of climatic regimes. Oerlemans et al (2005) require 20–43% K^{-1} and de Woul and Hock (2005) ~20% K^{-1} for Arctic G&IC. Although AOGCMs generally indicate larger than average precipitation in northern mid- and high-latitude regions, the global average is less than 5% K^{-1}, so we would expect ablation increases to dominate worldwide. However, precipitation changes may locally be important (Section 4.5.3).

10.6.3.3 Dynamic response

As glacier volume is lost, glacier area declines so the ablation decreases. Oerlemans et al. (1998) calculated that omitting this effect leads to overestimates of ablation of about 25% by 2100. Church et al. (2001) following Bahr et al. (1997) and Van de Wal et al. (2001) made some allowance for it by diminishing the area A of a glacier of volume V according to $V = A^{1.375}$. This is a scaling relation derived for glaciers in a steady state, which may hold approximately during retreat. Schneeberger et al. (2003) found this relation produced a mixture of over- and under-estimates of volume loss for their sample of glaciers by comparison with more detailed modelling.

A further serious difficulty is that $\partial b/\partial T$ of the glacier should change as volume is lost: lowering the ice surface as the glacier thins will tend to make $\partial b/\partial T$ more negative, but the predominant loss of area at lower altitude in the ablation zone will tend to make it less negative (Braithwaite and Raper*,* 2002). The latter effect is more important. Raper et al. (2000) applied a further scaling relation to reduce the width and length of a glacier as its area declines, while keeping its maximum altitude and shape fixed. This treatment includes the main influences on $\partial b/\partial T$, but still excludes the time-dependent effects of glacier dynamics.

The geometrical and dynamical approaches of Raper et al. (2000) and Oerlemans et al. (1998) cannot be applied to all the world's glaciers individually as the required data are unknown for the vast majority of them. Instead, it might be applied to a representative ensemble derived from statistics of size distributions of G&IC. Raper and Braithwaite (2005) have developed such an approach, in which they treat glaciers statistically and ice-caps individually. They find that the reduction of area of glaciers strongly reduces the ablation during the 21st century. The subgrid hypsometry and parametrised dynamics of Marshall and Clarke (1999) could also be used.

10.6.3.4 Global average sea-level change due to glacier and ice-cap changes

We apply the annual mass balance sensitivities, seasonal sensitivity characteristics and glacier area inventory of Oerlemans (2001; 2005), with the area-scaling of Van de Wal and Wild (2001), to temperature and precipitation changes simulated by 17 AOGCMs under scenarios A1B, A2 and B1, using three alternative estimates of world glacier volume (Table 4.5.1). For the AOGCM climate change results, the global mass balance sensitivity to global temperature change $\partial B/\partial T_g$ lies in the range 0.22–0.50 mm yr^{-1} K^{-1}. It is 0.39-0.65 mm yr^{-1} K^{-1} excluding precipitation change, which offsets 25–50% of the melting. This is larger than expected from idealised studies (Section 10.6.3.2) because precipitation increases are projected to be larger than average in glaciated regions.

The projected contribution to sea level change during the 21st century is 26–58 mm. This is considerably less than projected by the TAR, which gave 10–230 mm for scenario IS92a. The TAR neglected precipitation changes, but the difference has several other causes, including smaller warming in the glaciated regions by the AR4 AOGCMs, smaller local sensitivity to temperature, lower estimates of glacier volume and the assumption that the AOGCM control (typically late 19th century) is a steady state for glaciers (cf. Zuo and Oerlemans, 1997). Raper and Braithwaite (2005) project 46 and 51 mm for two of the same AOGCM scenarios, also noting the results are about half the size of the TAR's.

These projections do not include G&IC (separate from the ice sheets) in Antarctica and Greenland. Using a degree-day scheme, Vaughn (2005) estimates that ablation of glaciers in the Antarctic Peninsula presently amounts to 0.055 mm yr^{-1} of sea level. However, Morris and Mulvaney (2004) find that accumulation increases have been larger than ablation increases during 1972–1998, giving a small net negative sea level contribution from the region. Because ablation increases non-linearly with temperature, for future warming the contribution would become positive; they estimate $\partial B/\partial T=0.07 \pm 0.02$ mm yr^{-1} K^{-1} to sea level rise, which is small but not negligible compared with the aggregate of other G&IC.

10.6.4 Ice Sheets

The mass of ice grounded on land in the Greenland and Antarctic ice sheets could change as a result of changes in surface mass balance (accumulation or ablation) or in the flux of ice crossing the grounding line, which is determined by the dynamics of the ice sheet. Mass balance is immediately influenced by climate change. Dynamics has its own timescales, extending to millennia, so the topography and the sea level contribution of the ice sheets will continue to change long after climate has stabilised. An important and controversial question is whether dynamical changes could be important even on decadal timescales (Section 10.6.7).

10.6.4.1 Ice sheet surface mass balance sensitivity to climate change during the 21st century

A good simulation of the ice sheet surface mass balance (SMB) requires a resolution exceeding that of AGCMs used for long climate experiments, because of the steep slopes at the margins of the ice sheet, where the majority of the precipitation and all of the ablation occurs. Orographic forcing is an important influence on the precipitation, which is typically overestimated by AGCMs, whose smooth topography does not present a sufficient barrier to inland penetration (Ohmura et al., 1996b; Glover, 1999; Murphy et al., 2002). Ablation also tends to be overestimated because the area at low altitude around the margins of the ice sheet is exaggerated, where melting preferentially occurs (Glover, 1999; Wild et al., 2003). In addition, AGCMs do not generally have a representation of the refreezing of surface meltwater within the snowpack and may not include albedo variations dependent on snow ageing and its conversion to ice.

To address these issues, several groups have computed SMB at resolutions of tens of kilometres or less, with results that compare acceptably well with observations (e.g., van Lipzig et al., 2002; Wild et al., 2003). Ablation is calculated either by schemes based on temperature (degree-day or other temperature-index methods), calibrated from observations (Braithwaite, 1995; Ohmura et al., 1996a), or by energy-balance modelling.

Changes in SMB have been studied using climate change simulated by high-resolution AGCMs or by perturbing an observational climatology with lower-resolution climate model output. Table 10.6.1 shows that there is considerable uncertainty in accumulation changes (van de Wal et al., 2001; Huybrechts et al., 2004). Precipitation increase could be determined by atmospheric radiative balance (2–3% K^{-1} expected), increase in saturation specific humidity with temperature (6% K^{-1}), circulation changes, retreat of sea ice permitting greater evaporation, or a combination of these (van Lipzig et al., 2002). Accumulation also depends on change in local temperature, which strongly affects whether it falls as solid or liquid (Janssens and Huybrechts, 2000). For Greenland, accumulation derived from the high-resolution time-slices rises increases by 5–9% K^{-1}. Precipitation increases somewhat less in AR4 AOGCMs (typically of lower resolution), by 3–7% K^{-1}. For Antarctica, we have 6-9% K^{-1} in the time-slices and 3–8% K^{-1} in the AOGCMs. Kapsner et al. (1995) do not find a relationship between precipitation and temperature variability inferred from Greenland ice cores for the Holocene, although both show large changes from the LGM to the Holocene. Gregory et al. (2005a) show that in the HadCM3 AOGCM there is a relationship for climate change forced by greenhouse gases and the glacial-interglacial transition, but not for naturally forced variability.

Since there is very little ablation in Antarctica, all studies for 21st century climate change find that Antarctica contributes negatively to sea level, owing to increasing accumulation, consistent with some recent observational analyses (Davis et al., 2005; Wingham et al., 2005). Table 10.6.1 shows uncertainty in the ablation sensitivity of Greenland. Calculations are particularly sensitive to temperature change around the margins and in summer, when melting occurs. In most studies Greenland is a net positive contributor to sea level, again consistent with observations (Rignot and Thomas, 2002). Only Wild et al. (2003) find that the ablation increase is smaller than the precipitation increase, so that Greenland contributes negatively to sea level. Wild et al. (2003) attribute this difference to the reduced ablation area on their higher-resolution grid.

Table 10.6.1. Comparison of ice sheet surface mass balance changes calculated from high-resolution models. $\Delta P/\Delta T$ is the change in accumulation divided by change in temperature over the ice sheet, expressed as sea level equivalent, and $\Delta R/\Delta T$ the corresponding quantity for runoff. To convert to kg yr^{-1} K^{-1}, multiply by 3.6 $\times 10^{14}$ m^2. To convert to mm yr^{-1} K^{-1} averaged over the ice sheet, multiply by 206 for Greenland and 26 for Antarctica. $\Delta P/P\Delta T$ is the fractional change in accumulation divided by the change in temperature.

Study	Climate model	Energy-balance model or temperature index	Greenland $\Delta P/\Delta T$ (mm yr^{-1} K^{-1})	Greenland $\Delta P/P\Delta T$ (% K^{-1})	Greenland $\Delta R/\Delta T$ (mm yr^{-1} K^{-1})	Antarctica $\Delta P/\Delta T$ (mm yr^{-1} K^{-1})	Antarctica $\Delta P/P\Delta T$ (% K^{-1})
Van de Wal et al. (2001)	ECHAM4	20 km EB	0.14	8.5	0.16	–	–
Wild and Ohmura (2000)	ECHAM4	T106 ≈1.1° EB	0.13	8.2	0.22	0.47	7.4
Wild et al. (2003)	ECHAM4	2 km TI			0.04		
Bugnion and Stone (2002)	ECHAM4	20 km EB	0.10	6.4	0.13	–	–
Huybrechts et al. (2004)	ECHAM4	20 km TI	0.13	7.6	~0.2	0.49	7.3
Huybrechts et al. (2004)	HadAM3H	20 km TI	0.09	4.7	~0.2	0.37	5.5
Bugnion and Stone (2002)	MIT 2D	20 km EB	0.04	2.6	0.11	–	–
Van Lipzig et al. (2002)	RACMO	55 km EB	–	–	–	0.53	9.0

10.6.4.2 Global average sea-level rise due to ice-sheet changes

Using the MIT 2D climate model, Bugnion and Stone (2002) calculated the Greenland sea level contribution as –5 to +17 mm during the 21st century, for a range of scenarios. With the ECBILT-CLIO EMIC, Huybrechts et al. (2002) obtained 40 mm from Greenland under the SRES B2 scenario. Huybrechts et al. (2004) used the projections of surface air temperature and precipitation change averaged over the ice sheets from a range of AOGCMs to scale the results of their SMB calculation based on two high-resolution AGCM climate-change simulations. They obtained 20 to 70 mm from Greenland and –20 to –130 mm from Antarctica over the 21st century under the IS92a scenario. Ice sheet dynamical changes were included in the calculation and offset <5% of the SMB change for Antarctica, but 10–20% for Greenland, where thinning of the ice sheet in the ablation area reduces calving, while also steepening the margins, increasing the ice flow there and hence opposing retreat (Huybrechts et al., 2002).

We have used five high-resolution AGCM simulations in the scaling technique of Huybrechts et al. (2004), and found a systematic uncertainty of 30% associated with the geographical and seasonal pattern of climate change over the ice sheets (Section 10.6.3.1) and 15% with the SMB calculation. Mass balance sensitivities (Table 10.6.1) are similar to those calculated by Church et al. (2001). Applying this method to a results from 14 AOGCMs under the SRES A1B, A2 and B1 scenarios, and including an estimate of the effect of dynamics not associated with ice streams (see Section 10.6.7), we project 10 to 70 mm of sea level rise from Greenland and –120 to –20 mm from Antarctica during the 21st century. During 2080–2100 their rates of contribution are 0.2 to 2.1 mm yr^{-1} and –2.1 to –0.3 mm yr^{-1} respectively. The net ice sheet contribution is thus likely to be relatively small.

10.6.5 Projections of Global Average Sea-Level Change for the 21st Century

Combining the results for thermal expansion, glacier and ice sheet mass change obtained in Sections 10.6.1, 10.6.3 and 10.6.4 we project global average sea-level rise with respect to 2000 in the range 10–40 mm by

2020, 50–130 mm by 2050 and 130–380 mm by 2100. This range is considerably less than the TAR range of 90–880 mm by 2100 (with respect to 1990), for several reasons. (1) This range does not cover the SRES range; scenario A1FI gave substantially higher projections than A1B and A2 in the TAR. (2) Glacier projections are smaller than in the TAR, as discussed in Section 10.6.3. (3) We have not yet included some additional terms which were in the TAR projections, pending reassessment of these, namely the ongoing response of the ice sheets to paleoclimate change, runoff from permafrost and sedimentation in the oceans.

The mass of the ocean will also be changed by climatically driven alteration in other water storage, in the forms of atmospheric water vapour, seasonal snow cover, soil moisture, groundwater, lakes and rivers. All of these are expected to be relatively small terms, but there may be substantial contributions from anthropogenic change in terrestrial water storage, through extraction from aquifers and impounding in reservoirs (Section 5.5.5.3).

In the second-order draft the projections will be revised to be consistent with time-dependent PDFs (yet to be made) of global climate change in Section 10.5, taking into account both model and scenario uncertainty, including uncertainty in ocean heat uptake and land ice sensitivity (cf. van der Veen, 2002; Webster et al., 2003). If possible we should also impose a requirement of consistency with past sea level change, within the uncertainties of the budget for the past (Section 5.5.6).

10.6.6 Elimination of the Greenland Ice Sheet by Surface Ablation

The present SMB of Greenland is a net accumulation of 0.6 mm yr^{-1} of sea level equivalent (Church et al., 2001), balanced by calving of icebergs. GCMs suggest that accumulation increases linearly with temperature (van de Wal et al., 2001), whereas ablation increases more rapidly, so sufficient warming will reverse the sign of the SMB. Once it becomes negative, the ice sheet must contract. Huybrechts et al. (1991) found that a seasonally uniform warming of 2.7°C in Greenland would reduce the SMB to zero. Gregory et al. (2004) examined the probability of this threshold being reached under various CO_2 stabilisation scenarios for 450–1000 ppm using TAR projections, finding that it was passed for 34 out of 35 combinations of AOGCM and CO_2 concentration considering seasonally uniform warming, and 24 out of 35 using an upper bound on the threshold and summer warming. From results of Section 10.6.3.2, we find the mass balance becomes negative in about half the combinations of models and scenarios by 2100, and in all cases which continue to 2300 (Figure 10.6.3).

For large warmings, contraction of the ablation area cannot reduce the melting sufficiently to raise the SMB back to zero. As the ice sheet shrinks, its surface altitude falls and the warming is enhanced, providing a positive feedback. If the warm climate is maintained, the ice sheet will eventually be eliminated, except perhaps for remnant glaciers in the mountains. Greve (2000) obtained substantial retreat within 1000 years for seasonally uniform warmings ≥3°C in Greenland, with an average sea-level contribution of 7 mm yr^{-1} for a warming of 12°C, while Huybrechts and De Wolde (1999) reported 3 mm yr^{-1} for 5.5°C and 6 mm yr^{-1} for 8°C. Ridley et al. (2005) carried out an experiment with constant 4×CO_2 in which the HadCM3 AOGCM was coupled to the Greenland ice sheet model of Huybrechts and De Wolde (1999). The annual-average warming in Greenland for a fixed ice sheet was 9.5°C. The sea level contribution was 5.5 mm yr^{-1} over the first 300 years and declined as the ice sheet contracted; after 3000 years the warming reached 18°C and only 4% of the original volume remained (Figure 10.6.4).

Even with pre-industrial or present-day CO_2, the climate of Greenland would be much warmer without the ice sheet, because of lower surface altitude and albedo (Toniazzo et al., 2004). Toniazzo et al. (2004) found that snow does not accumulate anywhere on the ice-free Greenland on account of the warming, implying that Greenland deglaciation and the resulting sea level rise would be irreversible even if global climate change were reversed. Using a higher-resolution model, Lunt et al. () obtained a substantial regenerated ice sheet in east and central Greenland.

[INSERT FIGURE 10.6.3 HERE]

[INSERT FIGURE 10.6.4 HERE]

10.6.7 Rapid Dynamic Response of the Ice Sheets to Climate Change

The TAR concluded that accelerated sea level rise caused by rapid dynamic response of the ice sheets to climate change is very unlikely during the 21st century (Church et al., 2001; Vaughan and Spouge, 2002). Uncertainty concerning this issue has since increased on account of new evidence of rapid recent changes in the ice sheets (see Sections 4.6 and 4.7 for details), because the mechanisms responsible are not completely represented by current state-of-the-art thermomechanical ice dynamics models, such as discussed in Section 10.6.4.

The uncertainty surrounds the degree to which ice shelves can buttress inland ice and reduce the flow across the grounding line. Theoretical studies suggest that the ice shelves can exist without transmitting back-stress to the ice sheets (e.g., Hindmarsh, 1993). Comparisons between measurements and models of streaming and non-streaming flows (Whillans and van der Veen, 1993; Mayer and Huybrechts, 1999) also indicate that back-stress can be insignificant. However, the two-step collapse of Larsen ice shelf, Antarctic Peninsula, substantially increased the rate of grounded glaciers that supplied it with ice (Section 4.6), yielding a strong argument for enhanced flow when the buttress is removed. The onset of disintegration of the ice shelf has been attributed to enhanced fracturing by crevasses promoted by surface meltwater (Scambos et al., 2000). It appears that for ice shelves of the Antarctic Peninsula a mean annual temperature of –5ºC marks the threshold for surface meltwater ponds to form. By this criterion, projected warming at the more southerly latitudes of the Ross and Filchner-Ronne ice shelves indicates that their collapse through this process is unlikely over the next several centuries.

However, the major cause of thinning of the Larsen ice shelf preceding disintegration was bottom melting, not surface melting (Shepherd et al., 2003). Likewise, in the Amundsen Sea sector of West Antarctica, the cause of ice-shelf thinning is bottom melting at the grounding line (Rignot and Jacobs, 2002). Shepherd et al. (2004) give an average ice-shelf thinning rate of 1.5 ± 0.5 m yr^{-1}. Comparison of several ice shelves and modelling studies indicate that basal melt rates depend on water temperature near to the base, with a constant of proportionality of 10 ± 1 m yr^{-1} K^{-1} (Rignot and Jacobs, 2002; Shepherd et al., 2004; Payne et al., 2005). Although there are no direct observations of a correlation between rising temperature and increasing thinning, it is reasonable to assume that such a relationship will apply also to time-dependent changes, implying that small increases in deep water temperature could produce large increases of the thinning rate of ice-shelves.

At the same time as the ice-shelf thinning, accelerated inland flow has been observed for Pine Island, Thwaites and other glaciers in the sector (Rignot, 1998, 2001; Thomas et al., 2004). This suggests that bottom melting of ice shelves, even without complete removal, reduces the buttressing effect, but at present it is unclear how they are quantitatively related. Because the acceleration took place in only a few years (Rignot et al., 2002; Joughin et al., 2003) but appears up to ~150 km inland, it implies that the dynamical response to the reduction of buttressing can propagate rapidly up the ice stream. This conclusion is supported by modelling studies of Pine Island Glacier by Payne et al. (2004) and Dupont and Alley (2005), in which basal or lateral drag at the ice front is reduced in idealised ways. The simulated acceleration and inland thinning are rapid but transient, a new steady state being reached in a few decades. In the study of Payne et al. (2004) the imposed perturbations were designed to resemble loss of drag in the "ice plain", a partially grounded region near the ice front, and produced a velocity increase of ~1 km yr^{-1} there; Tomas et al. (2005) suggest the ice plain will become ungrounded during the next decade and obtain a similar velocity increase using a simplified approach. As the new steady state is attained, the rate of contribution to sea level will decline.

On the other hand, most of inland ice is grounded below sea level so could be floated if it thinned sufficiently; discharge therefore promotes inland retreat of the grounding line, which represents a positive feedback by further reducing basal traction (although it does not itself alter sea level). Grounding-line retreat of the ice streams has been observed recently at up to ~1 km yr^{-1} (Rignot, 1998, 2001; Shepherd et al., 2002) but is difficult to model (Vieli and Payne, 2005).

In view of these quantitative uncertainties, we can only indicate orders of magnitude. The majority of West Antarctic ice discharge is through the ice streams which feed the Ross and Ronne-Filchner ice shelves, but in these regions thinning and acceleration are not currently observed. Excluding these regions, and likewise those parts of the East Antarctic ice sheet which drain into the large Amery ice shelf, the total area of ice streams (areas flowing faster than 100 m yr^{-1}) discharging directly into the sea or via a small ice shelf is 270,000 km^2. Many of these areas show no sign of thinning at present or thinning at small rates, but if they all thinned at 1 m yr^{-1}, the order of magnitude of the larger rates observed in fast-flowing areas, the contribution to sea level rise would be ~0.7 mm yr^{-1}. This is ~5 times greater than the rate of loss of inland ice during the 1990s from accelerated flow, which was 0.13 ± 0.02 mm yr^{1} (Shepherd et al., 2002). It would require simultaneous sustained retreat, and should be taken as an upper limit, not than a projection. For comparison, recall that the projected rate of extra accumulation on Antarctica by the end of the 21st century amounts to 0.3 to 2.1 mm yr^{-1} of sea level lowering (Section 10.6.4.1). It therefore seems likely that the net contribution of Antarctica to sea level rise during the 21st century will be negative even with accelerated dynamic discharge.

The maximum loss of ice in this way would be the volume in excess of flotation in the regions occupied by these ice streams, which is 120,000 km^3, equivalent to ~0.3 m of sea level. If all ice streams were affected, including those discharging into large ice shelves, these totals would be doubled, but would still be only ~1% of the mass of the Antarctic ice sheet, most of which does not flow in ice streams. Using a model without explicit modelling of ice streams, Huybrechts and De Wolde (1999) found that basal thinning of Antarctic ice shelves at 10 m yr^{-1} would result in a sea level rise contribution of 2.5 mm yr^{-1}, this being an upper limit of the rate of discharge that could be sustained over centuries.

Analysis of changes in the velocity of Jakobshavn Isbræ, the largest outlet glacier of the Greenland ice sheet, suggests again that discharge may be accelerated by the removal of floating ice tongues (Joughin et al., 2004). The observation in west-central Greenland of seasonal variation in ice flow rate and of a correlation with summer temperature variation (Zwally et al., 2002) has prompted speculation that surface meltwater is able to penetrate more than 1200 m of subfreezing ice to join a subglacially routed drainage system lubricating the ice flow. However, other studies (Echelmeyer and Harrison, 1990; Joughin et al., 2004) found no evidence for seasonal fluctuations in the flow rate of nearby Jakobshavn Isbræ despite a substantial supply of surface meltwater; thus other explanations for flow variability cannot be discounted. Parizek and Alley (2004) undertook a sensitivity study of how increased surface melting might amplify the response to warming by accelerating ice-flow dynamics. Their best estimate was that it could add 0.15–0.40 m by 2500, compared with the contribution of 0.4–3.2 m calculated by Huybrechts and De Wolde (1999). This reinforces the conclusion (Section 10.6.6) that the Greenland ice sheet is likely to be a large contributor to sea level rise on the timescale of centuries.

10.7 Climate Change Commitment

10.7.1 Climate Change Commitment Out to Year 2300 Based on AOGCMs

Climate change commitment can be defined as the further increase of temperature, or any other quantity in the climate system that changes in response to an external forcing that continues to change if the forcing stops increasing and is held at a constant value (over and above the increase that has already been experienced). The concept that the climate system has this property, mainly due to the thermal inertia of the oceans, was first introduced independently by Wigley (1984) and Hansen et al. (1984). In the TAR this was illustrated in idealized scenarios of doubling and quadrupling CO_2, and stabilization at 2050 and 2100 after an IS92a forcing scenario. Various warming commitment values were reported (about 0.3°C per century with much model-dependency), and EMIC simulations were used to illustrate long-term influence of the ocean owing to long mixing times and meridional overturning circulation. Subsequent studies have confirmed this behavior of the climate system and ascribed it to the inherent property of the climate system that the thermal inertia of the ocean introduces a lag to the warming of the climate system after concentrations of greenhouse gases are stabilized (Mitchell et al., 2000; Wetherald et al., 2001; Wigley and Raper, 2003; Hansen et al., 2005; Meehl et al., 2005d).

Three climate change commitment experiments have recently been performed by the global coupled climate modeling community: (1) stabilizing concentrations of GHGs at year 2000 values after a 20th century climate simulation, and running an additional 100 years; (2) stabilizing concentrations of GHGs at year 2100 values after a 21st century B1 experiment and running an additional 100 years (with some models run to 200 years); and (3) stabilizing concentrations of GHGs at year 2100 values after a 21st century A1B experiment, and running an additional 100 years (and some models to 200 years). Multi-model mean warming in these experiments is depicted in Figure 10.3.2. Time series of the globally averaged surface temperature and percent precipitation change after stabilization are shown for all the models in Figure 10.7.1. The multi-model average warming in the first experiment (reported earlier for several of the models) (Hansen et al., 2005; Meehl et al., 2005d) is about 0.5°C at year 2100, nearly the magnitude of warming simulated in the 20th century. For the B1 commitment run, the additional warming after 100 years is also about 0.5°C, and roughly the same for the A1B commitment (Figure 10.7.1). These new results quantify what was postulated in the TAR in that warming commitment after stabilizing concentrations is about 0.5°C for the first century, and considerably smaller after that, with most of the warming commitment occurring in the first several decades of the 22nd century.

[INSERT FIGURE 10.7.1 HERE]

Precipitation commitment for the multi-model ensemble average is about 1.1% by 2100 for the 20th century commitment experiment, and for the B1 commitment experiment by 2200 is 0.8% and by 2300 is 1.5%, while for the A1B commitment experiment by 2200 is 1.5% and 2% by 2300.

The patterns of change in temperature in the B1 and A1B experiments, relative to pre-industrial, do not change greatly after stabilization, as is quantified in Table 10.3.2. (Maps of warming can be seen in the supplementary material[1].) Even the 20th century stabilization case warms with some similarity to the A1B pattern (Table 10.3.2). However, there is some contrast in the land and ocean warming rates, as seen from Figure 10.3.3. Mid and low latitude land warms at rates closer to the global mean that for A1B, while high latitude ocean warming is larger.

The commitment to sea level rise due to thermal expansion has much longer timescales than the warming commitment, owing to the slow processes which mix heat into the deep ocean (Church et al., 2001). Despite stabilisation of concentrations, thermal expansion in the 22nd and 23rd centuries is greater than in the 21st century in most models, as noted by Meehl et al. (2005e), reaching 0.3–0.8 m by 2300 in A1B (Figure 10.7.2). There is a wide spread among the models for the thermal expansion commitment due partly to climate sensitivity, partly to differences in the parameterization of vertical mixing affecting ocean heat uptake, as shown by Weaver and Wiebe (1999) for instance. If there is deep water formation in the final steady state as in the present day, the ocean will eventually warm up fairly uniformly by the amount of the global average surface temperature change (Stouffer and Manabe, 2003), which would give about 0.5 m K^{-1} of thermal expansion. If deep water formation is weakened or suppressed, the deep ocean will warm up more (Knutti and Stocker, 2000). For instance, in the $3 \times CO_2$ experiment of Bi et al. (2001) with the CSIRO AOGCM, both NADW and AABW formation cease, and the steady-state thermosteric sea level rise is 4.5 m.

[INSERT FIGURE 10.7.2 HERE]

10.7.2 Climate Change Commitment Out to Year 3000 Based on EMICs

Projections for the SRES scenario A1B discussed in Section 10.5.2 (Figure 10.5.4) were extended to year 3000 with EMICs and are shown in Figure 10.7.3. While surface temperatures are approximately stable after 2200 (i.e. 100 yrs after the forcing is stabilized), sea level continues to rise for many centuries.

Five of the intermediate complexity climate models presented in Section 10.5.2 include interactive representations of the marine and terrestrial carbon cycle, and therefore can be used to assess carbon cycle – climate feedbacks and effects of carbon emission reductions on atmospheric CO_2 and climate. Although carbon cycle processes in these models are highly simplified, global-scale quantities are in good agreement with more complex models (Doney et al., 2004).

Results for one carbon emission scenario are shown in Figure 10.7.4 where anthropogenic emissions follow a path towards stabilization of atmospheric CO_2 at 750 ppm but at year 2100 are reduced to zero. The prescribed emissions were calculated from the SP750 profile (Knutti et al., 2005) using the Bern Carbon Cycle Model (Joos et al., 2001). Although unrealistic, such a scenario permits the calculation of committed climate change due to 21st century emissions. Even though emissions are instantly reduced to zero at year 2100, it takes about 100 to 400 years in the different models for the atmospheric CO_2 concentration to drop from the maximum (ranges between 650 to 700 ppm) to below the level of two times preindustrial CO_2 (~560 ppm) owing to a continuous transfer of carbon from the atmosphere into the terrestrial and oceanic reservoirs. Emissions effected in the 21st century continue to have an impact even at year 3000 when both surface temperature and sea level rise due to thermal expansion are still substantially higher than preindustrial. Also shown are atmospheric CO_2 concentrations and ocean/terrestrial carbon inventories at year 3000 versus total emitted carbon for similar emission pathways targeting 450, 550, 750 and 1000 ppm atmospheric CO_2 and with carbon emissions reduced to zero at year 2100. Atmospheric CO_2 at year 3000 is approximately linearly related to the total amount of carbon emitted in each model, but with a substantial spread among the models in both slope and absolute values, because the redistribution of carbon between the different reservoirs is model-dependant. In summary, the model results show that 21st century emissions represent a minimum commitment of climate change for several centuries, irrespective of later emissions. A reduction of this "minimum" commitment is possible only if CO_2, in addition to cutting emissions after 2100, were actively removed from the atmosphere.

[INSERT FIGURE 10.7.3 HERE]

[INSERT FIGURE 10.7.4 HERE]

Using a similar approach, Friedlingstein and Solomon (2005) showed that even if emissions were immediately cut to zero, the climate change commitment dictates that the system would continue to warm for several more decades before starting to cool. It is important also to note that climate change commitment goes beyond rapidly responding quantities such as temperature and precipitation: ocean heat content and changes in the cryosphere evolve on time scales extending over centuries. Most of their evolution is determined by emissions in this century.

Box 10.1: Future Abrupt Climate Change and "Climate Surprises"

Theoretical studies and model simulations, as well as the abundant evidence of high-resolution proxy data from numerous paleoclimatic archives (Chapter 6) have established the fact that changes in the climate system can be abrupt and widespread. A working definition of "abrupt climate change" was given in Alley et al. (2002): "Technically, an abrupt climate change occurs when the climate system is forced to cross some threshold, triggering a transition to a new state at a rate determined by the climate system itself and faster than the cause". More generally, a gradual change in some determining quantity of the climate system (e.g., radiation balance, land surface properties, sea ice, etc.) can cause a variety of structurally different responses (Box 10.1, Figure 1). The response of a purely linear system scales with the forcing, and at stabilisation of the forcing, a new equilibrium is achieved which is structurally similar, but not necessarily close to the original state. However, if the system contains more than one stable equilibrium state, transitions to structurally different states are possible. Upon the crossing of a bifurcation point the evolution of the system is no longer controlled by the time scale of the forcing, but rather determined by its internal dynamics, which can either be much faster than the forcing, or significantly slower. Only the former case would be termed "abrupt climate change", but the latter case is of equal importance. For the long-term evolution of a climate variable one must distinguish between reversible and irreversible changes. When one speaks in popular terms about "climate surprises", one usually refers to abrupt transitions and temporary or permanent transitions to a different state of parts of the climate system.

[INSERT BOX 10.1, FIGURE1 HERE]

Atlantic meridional overturning circulation and other ocean circulation changes:
The best documented type of abrupt climate change in the paleoclimatic archives is that associated with changes in the ocean circulation. The climate system has thus demonstrated, that such changes were physically possible in the past. Since TAR many new results from climate models of different complexity have provided a more detailed view on the anticipated changes of the Atlantic meridional overturning circulation (MOC) in response to global warming. Most models agree that the MOC weakens over the next 100 years (Figure 10.3.14). This weakening evolves on the time scale of the warming and can achieve up to 60% by 2100. None of the AOGCM simulations shows an abrupt change when forced with the SRES emissions scenarios until 2100, but some long-term model simulations suggest that a complete cessation can result for large forcings (Stouffer and Manabe, 2003). Models of intermediate complexity have been used to explore parameter space more completely and indicate that thresholds in MOC may be present but that they depend on the amount and rate of warming for a given model. More importantly, the existence of such thresholds crucially depends on model parameterisations, e.g. the amount of vertical and horizontal mixing that is simulated in the ocean model components (Manabe and Stouffer, 1999; Knutti et al., 2000; Longworth et al., 2005). The few long-term simulations of AOGCMs indicate that even complete shutdowns of the MOC may be reversible (Stouffer and Manabe, 2003; Nakashiki et al., 2005). However, until millenial simulations with AOGCMs are available, the important question of potential irreversibility of an MOC shutdown remains unanswered. Both simplified models and AOGCMs agree, however, that a potential spin-down of the MOC, induced by global warming, would not be abrupt, but would evolve on the time scale of the forcing, i.e. would take many decades to more than a century to fully spin down. Therefore, there is no model evidence to support speculations, that the MOC could collapse within years or a few decades in response to global warming. This is not inconsistent with the paleoclimate records which suggest much faster transitions evolving over only a few decades, because the forcing factors in the past, thought to be associated with large ice sheet instabilities, are not comparable to the present (Chapter 6).

Recent simulations with models, whose ocean components resolve topography in sufficient detail, obtain a consistent pattern of a strong to complete reduction of convection in the Labrador Sea (Wood et al., 1999; Schweckendiek and Willebrand, 2005). Such changes in the convection, with implications to the atmospheric circulation, can develop within a few years (Schaeffer et al., 2002). The long-term and hemispheric to global scale effects of such changes in water mass properties have not yet been investigated.

With a reduction of the MOC, the meridional heat flux also reduces in the subtropical and mid latitudes with large-scale effects on the atmospheric circulation. In consequence, the warming of the North Atlantic surface proceeds more slowly. Even for strong reductions in MOC towards the end of the 21st century, no cooling is observed in the regions around the North Atlantic because it is overwhelmed by the radiative forcing that caused the ocean response in the first place. In the high latitudes, an increase in the oceanic meridional heat flux is simulated by these models. This increase is due to both an increase in the overturning circulation in the Arctic and the advection of warmer waters from lower latitudes and thus contributes significantly to continuing sea ice reduction in the Atlantic sector of the Arctic (Hu et al., 2004a). Few simulations have also addressed the changes to overturning in the South Atlantic and Southern Ocean. In addition to water mass modifications, this also has an effect on the transport by the Antarctic Circumpolar Current, but results are not yet conclusive.

Arctic sea ice:
Arctic sea ice is responding sensitively to global warming. While changes in winter sea ice cover are moderate, late summer sea ice is projected to disappear almost completely towards the end of the 21st century. A number of positive feedbacks in the climate system accelerate the melt back of sea ice. The ice albedo feedback allows open water to receive more heat from the sun during summer, and the increase of ocean heat transport to the Arctic through the advection of warmer waters and stronger circulation further reduce ice cover. Minimum Arctic sea ice cover is observed in September. Model simulations indicate that the September sea ice cover reduces substantially in response to global warming. The reduction generally evolves on the time scale of the warming. However, a recent model simulation suggests that sea ice cover can significantly and rapidly reduce within a few years, owing to a coupling to the ocean heat transport from the northern North Atlantic into the Arctic (M. Holland, 2005, pers. comm.). Such changes are abrupt and develop much faster than the forcing. With sustained warming, the late summer disappearance of a major fraction of Arctic sea ice is permanent.

Glaciers and ice caps:
Glaciers and ice caps are sensitive to changes in temperature and precipitation. Observations point to a reduction in volume over the last 20 years (Section 4.5.2), the rate of which during 1993–2003 was twice the average for 1961–1998. Rapid changes are therefore already under way and enhanced by positive feedbacks associated with the surface energy balance of shrinking glaciers and newly exposed land surface in periglacial areas. Acceleration of glacier loss over the next few decades is likely (Section 10.6.3). Based on simulations of 11 glaciers in various regions, a volume loss of 60% of these glaciers is projected by the year 2050 (Schneeberger et al., 2003). Glaciated areas in the Americas are also affected. A comparative study including 7 GCM simulations at $2 \times CO_2$ conditions inferred that many glaciers may disappear completely due to an increase of the equilibrium line altitude (Bradley et al., 2004). The disappearance of these ice bodies is much faster than a potential reglaciation several centuries hence, and may, in some areas actually be irreversible.

Greenland and West Antarctic Ice Sheets:
Satellite and in situ measurement networks have demonstrated the increasing melting around the periphery and on the surface of the Greenland Ice Sheet (GIS) over the past 25 years (Section 4.6.2). The few simulations of long-term ice sheet simulations suggest that the Greenland Ice Sheet (GIS) will significantly reduce in volume and area over the coming centuries if warming is sustained (Gregory et al., 2004; Huybrechts et al., 2004; Toniazzo et al., 2004). A threshold of global mean warming of (2.7 ± 0.5) °C was estimated for elimination of the GIS (Gregory et al., 2004). The melting would not proceed abruptly but take many centuries to complete. Even if temperatures were to decrease later, the reduction of the GIS to a much smaller extent might be irreversible, because the climate of an ice-free Greenland could be too warm for accumulation; however, this result is model-dependent (Ridley et al., 2005). The positive feedbacks involved here are that once the ice sheet gets thinner, temperatures in the accumulation region are higher, causing more precipitation to fall as rain rather than snow, and that the lower albedo of the exposed ice-free land causes a local climatic warming.

A collapse of the West Antarctic Ice Sheet (WAIS) has been discussed as a potential response to global warming for many years (Bindschadler, 1998; Oppenheimer, 1998). The observation of accelerated inland flow behind ice shelves which have disintegrated due to surface melting. or which are thinning as a result of ocean warming, has renewed these concerns (De Angelis and Skvarca, 2003; Rignot et al., 2004), since it indicates that ice-shelves tend to "buttress" the icesheet inland. A complete disintegration of the WAIS would cause a global sea level rise of about 6 m. However, the fast-flowing areas are limited in extent, and could discharge only a small fraction of this. There is no information available from current ice sheet models about the possibility of sustained discharge or accelerated flow in areas which are not currently thinning.

However, an order of magnitude estimate suggests that Antarctica is likely to make a net negative contribution to sea level during the 21st century, since increasing precipitation will be the dominant effect.

A collapse of the West Antarctic Ice Sheet (WAIS) has been discussed as a potential response to global warming for many years (Bindschadler, 1998; Oppenheimer, 1998). A complete disintegration of the WAIS would cause a global sea level rise of about 4 to 6 meters. The observed frequency of ice shelf breakups and the rapidity of propagation of signals upstream has renewed these concerns (De Angelis and Skvarca, 2003; Rignot et al., 2004). The break-off of big ice shelves has caused the acceleration of the flow of ice streams which fed the shelves. This indicates that the presence of ice shelves tends to stabilize the ice sheet, at least regionally. Therefore, in addition to the creation of surface meltwater ponds and bottom melting by a warmer ocean, the disappearance of large ice shelves contributes to a potential destabilization of the WAIS. There is no information available from ice sheet models about possible thresholds of a WAIS disintegration, nor about the speed of and extent of it. However, there is no evidence for a disintegration of WAIS within the next few decades.

Vegetation cover:
Irreversible and relatively rapid changes in vegetation cover and composition have occurred frequently in the past. The most prominent example is the desertification of the Sahara region about 5000 years ago (Claussen et al., 1999). The reason for this behaviour is believed to lie in the limitation of plant communities with respect to temperature and precipitation. Once critical levels are crossed, certain species can no longer compete within their ecosystem. Areas close to vegetation boundaries will experience particularly large and rapid changes due to the slow migration of these boundaries induced by global warming. A climate model simulation into the future shows that drying and warming in South America leads to a continuous reduction in the forest of Amazonia (Cox et al., 2000; Cox et al., 2004). While evolving continuously over the 21st century, such a change and ultimate disappearance could be irreversible.

One of the possible "climate surprises" concerns the role of the soil in the global carbon cycle. As the concentration of CO_2 is increasing, the soil is acting, in the global mean, as a carbon sink by assimilating carbon due to accelerated growing of the terrestrial biosphere. However, by about 2050, a model simulation suggests that the soil changes to a source of carbon by releasing previously accumulated carbon due to increased respiration (Cox et al., 2000), induced by increasing temperature and precipitation. This represents a positive feedback to the increase in atmospheric CO_2. While different models agree regarding the sign of the feedback, large uncertainties exist regarding the strength (Cox et al., 2000; Friedlingstein et al., 2001; Dufresne et al., 2002). However, the respiration increase is caused by warmer and wetter climate. The switch from moderate sink to strong source of atmospheric carbon is rather rapid and occurs within two decades (Cox et al., 2004), but the timing of the onset is uncertain (Huntingford et al., 2004). A model intercomparison reveals that once set in motion, the increase in respiration continues even after the CO_2 levels are held constant (Cramer et al., 2001). Although considerable uncertainties still exist, it is clear that feedback mechanisms between the terrestrial biosphere and the physical climate system exist, which can qualitatively and quantitatively alter the response to an increase in radiative forcing.

Atmospheric and ocean-atmosphere regimes:
Changes in weather patterns and regimes can be abrupt processes which might occur spontaneously due to dynamical interactions in the atmosphere-ice-ocean system, or they manifest the crossing of a threshold in the system due to slow external forcing. Such shifts have been reported in SST in the tropical Pacific leading into a phase of more ENSO (Trenberth, 1990), or in the stratospheric polar vortex (Christiansen, 2003), a shut-down of deep convection in the Greenland Sea (Bönisch et al., 1997; Ronski and Budeus, 2005) and an abrupt freshening of the Labrador Sea (Dickson et al., 2002). The freshening evolves in the entire depth but the shift in salinity was particularly rapid: the 34.87 isohaline plunges from seasonally surface to 1600 meters within 2 years with no return since 1973.

In a long, unforced model simulation, a period of a few decades with anomalously cold temperatures (up to 10 standard deviations below average) in the region south of Greenland was found (Hall and Stouffer, 2001). It was caused by persistent winds which changed the stratification of the ocean and inhibited convection thereby reducing heat transfer from the ocean to the atmosphere. Similar results were found in a different model in which the major convection site in the North Atlantic spontaneously switched to a more southerly location for several decades to centuries (Goosse et al., 2002). Other simulations show that the slowly increasing radiative forcing is able to cause transitions in the convective activity in the GIN Sea which has an influence on the atmospheric circulation over Greenland and western Europe (Schaeffer et al., 2002). The changes unfold within a few years and indicate that the system has crossed a threshold.

A multi-model analysis of regimes of polar variability (NAO, AO, and AAO) reveals that the simulated trends in the 21st century are significant for the AO and AAO and point towards more zonal circulation (Rauthe et al., 2004b). Temperature changes associated with changes in atmospheric circulation regimes such as NAO can easily exceed in certain regions (e.g., Northern Europe) the long-term global warming which cause the regime shifts (Dorn et al., 2003).

Box 10.2: Climate Sensitivity

The range for equilibrium climate sensitivity was estimated in the TAR (2001) to be about 1.5 to 4.5°C, almost identical to an early report of the National Research Council (Charney, 1979), and the two previous IPCC assessment reports (FAR, 1990; SAR, 1995). These estimates were expert assessments largely based on climate sensitivities simulated by atmospheric GCMs coupled to a non-dynamic slab ocean. The mean plus-minus one standard deviation of the model sensitivities was (3.8 ± 0.78) °C in the SAR (17 models), 3.5 ± 0.92 in the TAR (15 models) and now amounts to (3.2 ± 0.72) °C in the AR4 models. However, these numbers provide only general guidance concerning how large climate sensitivity could be. Previous assessments noted that there was an equal probability for climate sensitivity in the range of about 1.5°C to 4.5°C, and that it was not possible to estimate the probability that climate sensitivity might fall outside that range. Considerable work has been done since the TAR (2001) to estimate climate sensitivity based on new methods, and to provide a better quantification of relative probabilities, including a most likely value, rather than just a simple range with all values in the range assigned an equal probability. Since climate sensitivity of the real climate system cannot be measured directly, a variety of new methods have been used since the TAR (2001) to establish a relationship between sensitivity and some observable quantity (either directly or through a model), and to estimate a range or probability density function (PDF) of climate sensitivity consistent with observations. These methods have been summarized separately in Chapters 9 and 10, and here we synthesize that information into an assessment.

Constraints from the observed warming of the 20th century and the last millennium

A first category of methods uses the historical transient evolution of surface temperature, upper air temperature, ocean temperature and radiation, or a combination thereof, to constrain climate sensitivity (discussed in Section 9.6). A summary of all PDFs of climate sensitivity from those methods is shown in Figure 9.6.1 and in Box 10.2, Figure 1a. Median values, maximum values and 5–95% confidence ranges are shown in Figure Box 10.2, Figure 1b for each PDF. Those studies used the observed surface, upper air and ocean warming over the 20th century, estimates of the radiative forcing, satellite data, proxy data over the last millennium, or a subset thereof to calculate ranges or PDFs for sensitivity (e.g., Wigley et al., 1997; Tol and De Vos, 1998; Andronova and Schlesinger, 2001; Forest et al., 2002; Gregory et al., 2002a; Knutti et al., 2002; Knutti et al., 2003; Forest et al., 2005; Forster and Gregory, 2005; Frame and Allen, 2005; Frame et al., 2005; Hegerl et al., 2005). Most of the results confirm previous judgements that the lower limit of climate sensitivity is very unlikely below 1°C. The upper bound is difficult to constrain because of the limited length of the observational record and uncertainties in the observations, which are particularly large for ocean heat uptake and for the magnitude of the aerosol radiative forcing. Studies that take all the important uncertainties in observed historical trends into account cannot rule out the possibility that the climate sensitivity exceeds 4.5°C, though high values have a lower probability of occurrence than the more likely values of around 2.0 to 3.5°C. A further difficulty is that observations of transient climate change make it difficult to tightly constrain the equilibrium climate sensitivity, but provide better constraints for the transient climate response (see Section 9.6.1.3)

Constraints from the Last Glacial Maximum

Two recent studies use the relation between climate sensitivity and tropical sea surface temperatures (SST) in the Last Glacial Maximum (LGM) and proxy records of the latter to estimate ranges of climate sensitivity (Annan et al., 2005b; Schneider von Deimling et al., 2005). While both of these estimates overlap partially with results from the instrumental period and results from other AOGCMS, the results differ substantially due to the different relationships between LGM SSTs and sensitivity in the models used. Therefore, it is not yet possible to conclude that LGM proxy data constrains the range of climate sensitivity beyond our knowledge from the last century.

Constraints from volcanic eruptions

Studies comparing the observed transient surface temperature after large volcanic eruptions with model results obtained for different climate sensitivities (see Chapter 9) do not provide PDFs, but find best agreement with sensitivities around 3°C, and reasonable agreement within the 1.5–4.5°C range (Wigley et al., 2005; Yokohata et al., 2005). They are not able to fully exclude sensitivities above 4.5°C.

Constraints based on model climatology

Climate sensitivity is not a tuneable quantity in AOGCMs, and depends on many parameters related mainly to atmospheric processes and feedbacks. The observed present-day climatology (spatial structure of the mean climate and its variability) provides a constraint on model climate sensitivity. Three studies (see Chapter 10) have calculated PDFs of climate sensitivity by comparing different variables of the simulated present-day climate against observations in an ensemble of an atmospheric GCM HadAM3 with perturbed parameters coupled to a slab ocean model (Murphy et al.*,* 2004; Knutti and Meehl*,* 2005; Piani et al.*,* 2005). The results are shown in ,Box 10.2, Figure 1c/d and show most likely values of equilibrium climate sensitivity of about 3.2°C. They constrain the lower bound at about 2°C, while the upper bound depends on the method used. Those types of analysis need to be repeated with different models to estimate the contribution of structural uncertainties to the results.

Raw distributions without observational constraints
Box 10.2, Figure 1e and f show the frequency distributions obtained by different methods when perturbing parameters in the HadAM3 model but before weighting with observations (Chapter 10). Murphy et al. (2004)(unweighted) calculated climate sensitivities by sampling a uniform distribution for 29 parameters whose individual effects were assumed to combine linearly, while Stainforth et al. (2005) simulated multiple combinations of high, standard, and low values of a subset of key parameters, finding significant nonlinearities in the response. Most likely equilibrium climate sensitivity values are grouped around 3°C . Although some of the high sensitivities reported by Stainforth et al. (2005) are downweighted by using observational constraints (Knutti and Meehl*,* 2005; Piani et al.*,* 2005), climate sensitivities above 4.5°C cannot be excluded, though they have low probabilities attached to them.

The climate sensitivities of the AR4 AOGCMs (represented by an atmospheric GCM coupled to a slab ocean and sea ice to calculate sensitivity) are given for comparison (Chapter 10). These estimates come from models that represent the current best efforts from the international global coupled climate modelling community at simulating climate. A normal and log-normal fit yield 5–95% ranges of about 2 to 4.5°C (Räisänen*,* 2005c), with median values of equilibrium climate sensitivity of about 3.2°C. It is important to note that the results shown in this category (Box 10.2, Figure 1e and f) should not be interpreted as observationally-constrained probabilities, because each model version obtained is assumed to be equally credible and is given the same weight.

Summary
The TAR (2001) estimated a range of 1.5–4.5°C for climate sensitivity, but provided no information about the probability of the distribution within that range, or about the likelihood of being outside that range. Since then, improved models have been developed to provide new estimates of climate sensitivity, and our understanding of the constraints on climate sensitivities from a variety of observations has increased significantly. For a synthesis, we show the nine PDFs of Box 10.2, Figure 1a/c as cumulative distributions in Box 10.2, Figure 2.

Based on the currently available evidence, summarized in Figure Box 10.2, Figure 1 and Box 10.2, Figure 2 we conclude:

1. The current generation of AOGCMs covers a range of climate sensitivity from 2.1–4.4°C, similar to the TAR (2001), with a mean value of 3.2°C. The AOGCMs do not sample the full range of sensitivities constrained from observations, in particular not the high values.
2. Though studies performed to date have not been able to strongly constrain the 5% and 95% bounds of climate sensitivity, confidence in the shape of the PDF of climate sensitivity and the lower bound has increased significantly. The PDF of climate sensitivity is very likely right-skewed, with maximum probabilities for each PDF between 1 and 4°C, on average around 3°C, and lower probabilities of higher values such that those higher climate sensitivities cannot be ruled out. The lower bound is well constrained and provides a lower limit on the projected climate change. A definitive quantification of the 95% bound is not possible at this stage.
3. Based on a conservative estimate satisfying each of the individual observational constraints in Box 10.2, Figure 2, climate sensitivity is very unlikely to be below 1°C, and it is unlikely (<33%) to be above 6°C, given several independent lines of evidence from climate models and climate change in different periods.

4. There is no formal way of estimating a single PDF from the individual results due to different assumptions in each study. Nevertheless, an expert judgement can be based on the average of the nine PDFs shown in Box 10.2, Figure 2 such that best agreement with observations is found for a sensitivity of 3.0°C, with a median value of 3.4°C, similar to the centre of the TAR range and close to the AOGCM average. The average of the nine PDFs suggests that climate sensitivity is very unlikely below 1.5°C (8% probability) and unlikely above 4.5°C (28% probability).

[INSERT BOX 10.2, FIGURE 1 HERE]

[INSERT BOX 10.2, FIGURE 2 HERE]

Question 10.1: Are Extreme Events, Like Heat Waves, Droughts, or Floods, Expected to Change as the Earth's Climate Changes?

Yes, extreme events are expected to change as Earth's climate changes. These changes could occur even with relatively small mean climate changes, with the impacts from the changed extreme events having profound influences on human society, ecosystems and wildlife.

In a future warmer climate, most models simulate summer dryness and winter wetness in most parts of northern middle and high latitudes. Going along with the risk of drying is also an increased chance of intense precipitation and flooding. Though somewhat counter-intuitive, this is because precipitation is concentrated into more intense events, with longer periods of little precipitation in between. Therefore, intense and heavy episodic rainfall events are interspersed with longer relatively dry periods. Another aspect of these changes has been related to the mean changes of precipitation, with wet extremes becoming more severe in many areas where mean precipitation increases, and dry extremes where the mean precipitation decreases.

Going along with the results for increased extremes of intense precipitation, even if the storms in future climate did not change much in intensity, there would be an increase in extreme rainfall intensity with the extra-tropical surface lows, particularly over Northern Hemisphere land with an increase in the likelihood of very wet winters over much of central and northern Europe due to the increase of intense precipitation. These events would be associated with midlatitude storms suggesting increasing floods over Europe and other midlatitude regions. Similar results apply for summer precipitation with implications for more flooding in the Asian monsoon region and other tropical areas. The increased risk of floods in a number of major river basins in a future warmer climate have been related to an increase in river discharge with an enhanced risk for future intense storm-related precipitation events and flooding.

There is a very likely risk of increased temperature extremes, with more extreme heat episodes in a future climate. Furthermore, it has been shown that warm extremes correspond to increases in daily maximum temperature, but cold extremes warm up faster than daily minimum temperatures. For a future warmer climate, it is likely that there will be a decline in frequency of cold air outbreaks of 50 to 100% in NH winter in most areas, with the smallest reductions occurring in western N. America, the North Atlantic, and southern Europe and Asia due to atmospheric circulation changes associated with the increase of GHGs.

In a future climate there is an increased risk of more intense, longer-lasting and more frequent heat waves . The European 2003 heat wave has been used as an example of the type of heat wave that are likely to become more common in a future warmer climate. A related aspect of temperature extremes is that there could be a decrease in diurnal temperature range in most regions in a future warmer climate. It is also likely that a future warmer climate would be characterized by a decrease in frost days (e.g., nights where the temperature dips below freezing). A quantity related to frost days is growing season length, and this has been projected to increase in future climate.

Future tropical cyclones are likely become more severe with greater wind speeds and more intense precipitation. Some modelling studies have projected a decrease in tropical cyclone numbers globally but with a regional increase over the North Atlantic, and more mean and extreme precipitation from the tropical cyclones simulated in the future. One study has projected that tropical cyclones could decrease 30% globally (but increase in the North Atlantic), with the strongest tropical cyclones with extreme surface winds increasing in number while weaker storms decrease. The tracks would not be appreciably altered, and there would be about a 10% increase in maximum wind speeds in future simulated tropical cyclones in that model.

There could be a future tendency for more intense extratropical storms, though the numbers could be less, with a tendency towards more extreme wind events in association with those deepened cyclones for several regions. Several studies have shown a possible reduction of midlatitude storms but an increase in intense storms Regionally, models project a poleward shift of cyclone density, with a decrease in DJF extratropical cyclone density in East Asia around Japan (south of 50°N) and an increase north of that latitude. More regional aspects of these changes show a more active storm track in the western Pacific in the future but weaker elsewhere, with increased storm track activity over the North Atlantic and North Pacific, and lowered over Canada and poleward of 70°N. These regional features have been generalized in studies that have documented a poleward shift in midlatitude storm tracks. For most regions of the midlatitude oceans, an increase of extreme wave height is likely to occur in a future warmer climate. This is related to increased wind speed associated with midlatitude storms, resulting in higher waves produced by these storms, and is consistent with the studies noted above that showed decreased numbers of midlatitude storms but more intense storms.

Question 10.2: How Likely are Major or Abrupt Climate Changes, such as Loss of Ice Sheets or Changes in Global Ocean Circulation?

Physical, chemical and biological analyses from Greenland ice cores, marine sediments from the North Atlantic and elsewhere, and many other paleoclimatic archives have demonstrated that local temperature, wind regimes, and the water cycle can change rapidly within just a few years. The comparison of results from records in different locations of the world shows that in the past such changes were hemispheric to global in extent. This has led to the notion of an unstable climate in the past which underwent phases of abrupt swings. Therefore, an important question we must address is whether the continuing growth of greenhouse gas concentrations in the atmosphere constitutes a perturbation sufficiently strong to trigger abrupt changes in the climate system. If this is the case, such interference with the climate system is dangerous because it would have major global consequences.

Based on currently available results from a hierarchy of models, we conclude that abrupt climate changes, such as the loss of the Greenland ice sheet or large-scale changes of ocean circulation systems, are unlikely in the 21st century, but their occurrence becomes more likely as the perturbation of the climate system progresses.

Before the discussion of the different possibilities of such changes, we must say what we mean by "abrupt". There is no rigorous definition, but "abrupt" conveys the meaning that the changes occur much faster than the perturbation which is inducing the change. For example, if the extension of the Gulf Stream in the Atlantic Ocean, which delivers substantial amounts of heat into the northern latitudes, changed course, or if deepwater formation in the North Atlantic even ceased within a few years in response to the continuing warming, this would clearly be considered an abrupt change.

On more local scales, abrupt changes are a common characteristic of natural climate variability. Here, we do not consider isolated, short lived events which are more appropriately referred to as "extreme events", but rather changes that evolve rapidly and are to stay for several years to decades. For instance, the shift in sea surface temperatures in the Eastern Pacific of the mid 1970’s, or the freshening of the upper 1000 meters of the Labrador Sea since the mid 1980ies are typical examples of abrupt events with local to regional consequences.

In the public, the most widely discussed abrupt change is the shut-down of the Gulf Stream. The Gulf Stream is a primarily horizontal current driven by the zonal wind system, which is ultimately caused by the large-scale meridional temperature contrasts at the Earth's surface. Although variable through millennia, these temperature contrasts are very stable, and therefore the Gulf Stream cannot shut down. However, its northern extension which feeds deep water formation in the Greenland-Norwegian-Iceland Seas and thereby delivers heat to these areas, is shown to be strongly influenced by changes in density of the surface waters in these areas. This current constitutes the northern end of a basin-scale meridional overturning circulation (MOC) which is established along the western boundary of the Atlantic basin. A firm result of the entire hierarchy of climate models is that if the density of the surface waters in the North Atlantic decreases by warming or freshening, the MOC is reduced, and with it the delivery of heat into these areas. Strong sustained freshening induces substantial reductions, or complete shut-downs, of the MOC in all climate models. Such changes have indeed happened in the past. According to the paleoclimatic records, the MOC has shut down repeatedly during the last ice age, likely in response to massive discharges of ice from the circum-Atlantic ice sheets.

The issue now is, whether anthropogenic forcing constitutes a strong enough perturbation to the MOC that such a change can be induced. The increase of greenhouse gases in the atmosphere leads to a warming and an acceleration of the hydrological cycle, with the latter making the surface waters in the Atlantic fresher. Both effects reduce the density of the surface waters and lead to a reduction of the MOC in the 21st century. This reduction proceeds in lockstep with the warming: none of the current models simulates an abrupt reduction or shut-down. There is still a large spread in the simulated reduction of the MOC, ranging from virtually no response to a reduction of 60% by the end of the 21st century. This is due to various strengths of the ocean, and atmosphere-ocean feedback mechanisms simulated in these models.

Uncertainty also exists about the long-term fate of the MOC. Many models show a recovery of the MOC once the warming is stabilized. But some models have thresholds of the MOC, and they are passed when the forcing is strong enough and lasts long enough. Such simulations then show a slow spin-down of the MOC which continues after the warming is stabilized. A quantification of likelihood for a long-term spin-down of the Atlantic MOC is not possible at this stage. However, even if such a scenario were to happen, Europe will still experience warming since radiative forcing overwhelms the cooling associated with the MOC reduction. In consequence, catastrophic scenarios about the beginning of an ice age triggered by a shut-down of the MOC are mere speculations, and no climate model simulation exists that would produce such an outcome. In fact, the processes leading to an ice age are sufficiently well understood and completely different from those discussed here, that we can confidently exclude this scenario.

Irrespective of the long term evolution of the MOC, model simulations agree that the warming and freshening will reduce deep and intermediate water formation in the Labrador Sea significantly during the next few decades. This will alter the characteristics of the intermediate water masses in the North Atlantic and eventually affect the deep ocean. The long term effects of such a change are unknown.

Other widely discussed examples of climate surprises are the loss of the Greeland ice sheet, or the abrupt disintegration of the West Antarctic Ice Sheet (WAIS). Model simulations indicate that warming in the high latitudes of the northern hemisphere accelerates the melting of the Greenland ice sheet, and that the increased meridional transport of moisture is unable to compensate for this. In consequence, the possibility exists that the Greenland ice sheet may reduce its size substantially in the coming centuries. Moreover, the results also suggest that there may exist a critical warming beyond which, if sustained, the Greenland ice sheet may disappear completely. The reduction of the Greenland ice sheet, however, is a slow process taking many hundreds of years to complete.

Recent satellite and in situ observations of ice streams behind disintegrating ice shelves highlight the rapid reaction of such systems. This raises new concern about the overall stability of the West Antarctic Ice Sheet. While these streams appear buttressed by the shelves before them, it is currently unknown whether a reduction or failure of this buttressing of relatively limited areas of the ice sheet could actually trigger a wide spread discharge of many ice streams and hence a destabilization of the entire WAIS. Ice sheet models are only beginning to capture such small-scale dynamical processes which involve complicated interactions with the glacier bed and the ocean at the perimeter of the ice sheet. Therefore, we have no quantitative information available as to the likelihood of such an event.

References

ACIA, 2004: Arctic Climate Impact Assessment (ACIA): Impacts of a warming Arctic. Cambridge University Press, 140 pp.

Adams, P.J., J.H. Seinfeld, D. Koch, L. Mickley, and D. Jacob, 2001: General circulation model assessment of direct radiative forcing by the sulfate-nitrate-ammonium-water inorganic aerosol system. J. Geophys. Res., **106**, 1097-1111.

Allen, M.R., 1999: Do-it-yourself climate prediction. Nature, **401**, 627.

Allen, M.R., P.A. Stott, J.F.B. Mitchell, R. Schnur, and T.L. Delworth, 2000: Quantifying the uncertainty in forecasts of anthropogenic climate change. Nature, **407**, 617-620.

Allen, M.R., and D.A. Stainforth, 2002: Towards objective probabilistic climate forcasting. Nature, **419**, 228.

Allen, M.R., and W.J. Ingram, 2002: Constraints on future changes in climate and the hydrologic cycle. Nature, **419**, 224-232.

Allen, M.R., J.A. Kettleborough, and D.A. Stainforth, 2002: Model error in weather and climate forecasting. In: 2002 ECMWF Predicatibility Seminar [T.N. Palmer (ed.), Reading, UK.

Alley, R.B., et al., 2002: Abrupt Climate Change: Inevitable Surprises. US. National Research Council Report. National Academy Press, Washington, DC, 230 pp.

Andronova, N.G., and M.E. Schlesinger, 2001: Objective estimation of the probability density function for climate sensitivity. J. Geophys. Res., **106**, 22605-22612.

Annan, J.D., and J.C. Hargreaves, 2005: Climate prediction with imperfect models. Quart. J. Roy. Met. Soc., submitted.

Annan, J.D., J.C. Hargreaves, N.R. Edwards, and R. Marsh, 2005a: Parameter estimation in an intermediate complexity earth system model using an ensemble Kalman filter. Oc. Model., **8**, 135-154.

Annan, J.D., J.C. Hargreaves, R. Ohgaito, A. Abe-Ouchi, and S. Emori, 2005b: Efficiently constraining climate sensitivity with paleoclimate simulations. SOLA, submitted.

Arblaster, J.M., and G.A. Meehl, 2005: Contributions of external forcings to Southern Annular Mode trends. J. Clim., submitted.

Arora, V.K., and G.J. Boer, 2001: Effects of simulated climate change on the hydrology of major river basins. J. Geophys. Res., **106**, 3335-3348.

Arzel, O., T. Fichefet, and H. Goosse, 2005: Sea ice evolution over the 20th and 21st centuries as simulated by current AOGCM. Oc. Model., submitted.

Ashok, K., Z. Guan, and T. Yamagata, 2001: Impact of the Indian Ocean dipola on the relationship between the Indian monsoon rainfall and ENSO. Geophys. Res. Lett., **28**, 4499-4502.

Ashrit, R.G., K. Rupa Kumar, and K. Krishna Kumar, 2001: ENSO-monsoon relationships in a greenhouse warming scenario. Geophys. Res. Lett., **28**, 1727-1730.

Ashrit, R.G., H. Douville, and K. Rupa Kumar, 2003: Response of the Indian monsoon and ENSO-monsoon teleconnection to enhanced greenhouse effect in the CNRM coupled model. J. Met. Soc. Japan, **81**, 779-803.

Ashrit, R.G., A. Kitoh, and S. Yukimoto, 2005: Transient response of ENSO-monsoon teleconnection in MRI.CGCM2 climate change simulations. J. Met. Soc. Japan, **83**, 273-291.

Austin, J., and N. Butchart, 2003: Coupled chemistry-climate model simulations for the period 1980 to 2020: Ozone depletion and the start of ozone recovery. Quart. J. Roy. Met. Soc., **129**, 3225-3249.

Bahr, D.B., M.F. Meier, and S.D. Peckham, 1997: The physical basis of glacier volume-area scaling. J. Geophys. Res., **102**, 20355-20362.

Banks, H., R.A. Wood, and J.M. Gregory, 2002: Changes to Indian Ocean subantarctic mode water in a coupled climate model as CO_2 forcing increases. J. Phys. Oceanogr., **32**, 2816-2827.

Bengtsson, L., K.I. Hodges, and E. Roeckner, 2005: Storm tracks and climate change. J. Clim., submitted.

Beniston, M., 2004: The 2003 heat wave in Europe: A shape of things to come? An analysis based on Swiss climatological data and model simulations. Geophys. Res. Lett., **31**, L02202.

Berger, A., and M.F. Loutre, 2002: An exceptionally long interglacial ahead? Science, **297**, 1287-1288.

Berthelot, M., P. Friedlingstein, P. Ciais, P. Monfray, J.L. Dufresne, H. Le Treut, and L. Fairhead, 2002: Global response of the terrestrial biosphere to CO_2 and climate change using a coupled climate-carbon cycle model. Glob. Biogeochem. Cyc., **16**.

Bi, D.H., W.F. Budd, A.C. Hirst, and X.R. Wu, 2001: Collapse and reorganisation of the Southern Ocean overturning under global warming in a coupled model. Geophys. Res. Lett., **28**, 3927-3930.

Bindschadler, R., 1998: Geoscience - Future of the west Antarctic ice sheet. Science, **282**, 428-429.

Bitz, C.M., and G.H. Roe, 2004: A mechanism for the high rate of sea-ice thinning in the Arctic Ocean. J. Clim., **18**, 3622-3631.

Bitz, C.M., P.R. Gent, R.A. Woodgate, A. Hall, M.M. Holland, and R. Lindsay, 2005: The influence of sea ice on ocean heat uptake in response to increasing CO_2. J. Clim., submitted.

Boer, G.J., and B. Yu, 2003a: Climate sensitivity and response. Clim. Dyn., **20**, 415-429.

Boer, G.J., and B. Yu, 2003b: Dynamical aspects of climate sensitivity. Geophys. Res. Lett., **30**, 1135.

Boer, G.J., B. Yu, S.-J. Kim , and G.M. Flato, 2004: Is there observational support for an El Niño-like pattern of future global warming? Geophys. Res. Lett., **31**, L06201.

Bond, T.C., D.G. Streets, K.F. Yarber, S.M. Nelson, J.H. Woo, and Z. Klimont, 2004: A technology-based global inventory of black and organic carbon emissions from combustion. J. Geophys. Res., **109**, D14203, doi:10.1029/2003JD003697.

Bönisch, G., J. Blindheim, J.L. Bullister, P. Schlosser, and D.W.R. Wallace, 1997: Long-term trends of temperature, salinity, density, and transient tracers in the central Greenland Sea. J. Geophys. Res., **102**, 18553-18571.

Bony, S., J.-L. Dufresne, H. Le Treut, J.-J. Morcrette, and C.A. Senior, 2004: On dynamic and thermodynamic components of cloud changes. Clim. Dyn., **22**, 71-86.

Bony, S., and J.-L. Dufresne, 2005: Marine boundary layer clouds at the heart of cloud feedback uncertainties in climate models. in preparation.

Bosilovich, M.G., S.D. Schubert, and G.K. Walker, 2005: Global changes of the water cycle intensity. J. Clim., **18**, 1591-1608.

Bradley, R.S., F.T. Keimig, and H.F. Diaz, 2004: Projected temperature changes along the American cordillera and the planned GCOS network. Geophys. Res. Lett., **31**.

Braithwaite, R.J., 1995: Positive degree-day factors for ablation on the Greenland ice sheet studied by energy-balance modeling. J. Glaciol., **41**, 153-160.

Braithwaite, R.J., and S.C.B. Raper, 2002: Glaciers and their contribution to sea level change. Phys. Chem. Earth, **27**, 1445-1454.

Braithwaite, R.J., Y. Zhang, and S.C.B. Raper, 2003: Temperature sensitivity of the mass balance of mountain glaciers and ice caps as a climatological characteristic. Z. Gletscherk. Glazialgeol., **38**, 35-61.

Bryan, F.O., G. Danabasoglu, N. Nakashiki, Y. Yoshida, D.-H. Kim, J. Tsutsui, and S.C. Doney, 2005: Response of the North Atlantic thermohaline circulation and ventilation to increasing carbon dioxide in CCSM3. J. Clim., submitted.

Bugnion, V., and P.H. Stone, 2002: Snowpack model estimates of the mass balance of the Greenland ice sheet and its changes over the twentyfirst century. Clim. Dyn., **20**, 87-106.

Buizza, R., M. Miller, and T.N. Palmer, 1999: Stochastic representation of model uncertainties in the ECMWF ensemble prediction system. Quart. J. Roy. Met. Soc., **125**, 2887-2908.

Burke, E.J., and S.J. Brown, 2005: Modelling the recent evolution of global drought and projections for the 21st century with the Hadley Centre climate model. J. Hydromet., submitted.

Camberlin, P., F. Chauvin, H. Douville, and Y. Zhao, 2004: Simulated ENSO-tropical rainfall teleconnections in present-day and under enhanced greenhouse gases conditions. Clim. Dyn., **23**, 641-657.

Carmichael, G.R., D.G. Streets, G. Calori, M. Amann, M.Z. Jacobson, J. Hansen, and H. Ueda, 2002: Changing trends in sulfur emissions in Asia: Implications for acid deposition, air pollution, and climate. Env. Sci. Tech., **36**, 4707-4713.

Cassano, J.J., P. Uotila, and A. Lynch, 2005: Changes in synoptic weather patterns in the polar regions in the 20th and 21st centuries, Part 1: Arctic. Int. J. Clim., submitted.

Chang, C.-P., P. Harr, and J. Ju, 2001: Possible roles of Atlantic circulations on the weakening Indian monsoon rainfall-ENSO relationship. J. Clim., **14**, 2376-2380.

Charney, J.G., 1979: Carbon dioxide and climate: a scientific assessment. . Natl. Acad. Sci, Washington, DC, 22 pp.

Chiang, J.C.H., and A.H. Sobel, 2002: Tropical tropospheric temperature variations caused by ENSO and their influence on the remote tropical climate. J. Clim., **15**, 2616-2631.

Christensen, J.H., and O.B. Christensen, 2003: Severe summertime flooding in Europe. Nature, **421**, 805-806.

Christensen, O.B., and J.H. Christensen, 2004: Intensification of extreme European summer precipitation in a warmer climate. Glob. Planet. Change, **44**, 107-117.

Christiansen, B., 2003: Evidence for Nonlinear climate change: Two stratospheric regimes and a regime shift. J. Clim., **16**, 3681-3690.

Chung, S.H., and J.H. Seinfeld, 2002: Global distribution and climate forcing of carbonaceous aerosols. J. Geophys. Res., **107**, 4407, doi:10.1029/2001JD001397.

Church, J.A., J.M. Gregory, P. Huybrechts, M. Kuhn, K. Lambeck, M.T. Nhuan, D. Qin, and P.L. Woodworth, 2001: Changes in sea level. In: Climate Change 2001: The Scientific Basis. Contribution of Working Group I to the Third Assessment Report of the Intergovernmental Panel on Climate Change [J.T. Houghton, et al. (eds.)]. Cambridge University Press, pp. 639-693.

Church, J.A., N.J. White, and J.M. Arblaster, 2005: Significant decadal-scale impact of volcanic eruptions on sea level and ocean heat content. Nature, submitted.

Clark, R., S. Brown, and J. Murphy, 2005: Modelling boreal summer heat extreme changes and their uncertainties using a physics ensemble of climate sensitivity experiments. J. Clim., submitted.

Claussen, M., C. Kubatzki, V. Brovkin, A. Ganopolski, P. Hoelzmann, and H.-J. Pachur, 1999: Simulation of an abrupt change in Saharan vegetation in the mid-Holocene. Geophys. Res. Lett., **26**, 2037-2040.

Claussen, M., et al., 2002: Earth system models of intermediate complexity: closing the gap in the spectrum of climate system models. Clim. Dyn., **18**, 579-586.

Collins, W.J., R.G. Derwent, B. Garnier, C.E. Johnson, M.G. Sanderson, and D.S. Stevenson, 2003: Effect of stratosphere-troposphere exchange on the future tropospheric ozone trend. J. Geophys. Res., **108**, doi:10.1029/2002JD002617.

Collins, M., and The CMIP Modelling Groups, 2005: El Niño- or La Niña-like climate change? Clim. Dyn., **24**, 89-104.

Collins, M., B.B.B. Booth, G. Harris, J.M. Murphy, D.M.H. Sexton, and M.J. Webb, 2005a: Towards quantifying uncertainty in transient climate change. Clim. Dyn., submitted.

Collins, W.D., et al., 2005b: Radiative forcing by well-mixed greenhouse gases: Estimates from climate models in the IPCC AR4. J. Geophys. Res., submitted.

Cooke, W.F., and J.J.N. Wilson, 1996: A global black carbon aerosol model. J. Geophys. Res., **101**, 19395-19409.

Covey, C., K.M. AchutaRao, U. Cubasch, P. Jones, S.J. Lambert, M.E. Mann, T.J. Phillips, and K.E. Taylor, 2003: An overview of results from the Coupled Model Intercomparison Project. Glob. Planet. Change, **37**, 103-133.

Cox, P.M., R.A. Betts, C.D. Jones, S.A. Spall, and I.J. Totterdell, 2000: Acceleration of global warming due to carbon-cycle feedbacks in a coupled climate model. Nature, **408**, 184-187.

Cox, P.M., R.A. Betts, M. Collins, P.P. Harris, C. Huntingford, and C.D. Jones, 2004: Amazonian forest dieback under climate-carbon cycle projections for the 21st century. Theor. Appl. Clim., **78**, 137-156.

Cramer, W., et al., 2001: Global response of terrestrial ecosystem structure and function to CO_2 and climate change: results from six dynamic global vegetation models. Glob. Change Biol., **7**, 357-373.

Crucifix, M., and M.F. Loutre, 2002: Transient simulations over the last interglacial period (126-115 kyr BP): feedback and forcing analysis. Clim. Dyn., **19**, 417-433.

Dai, A., T.M.L. Wigley, B.A. Boville, J.T. Kiehl, and L.A. Buja, 2001a: Climates of the twentieth and twenty-first centuries simulated by the NCAR Climate System Model. J. Clim., **14**, 485-519.

Dai, A.G., T.M.L. Wigley, G.A. Meehl, and W.M. Washington, 2001b: Effects of stabilizing atmospheric CO_2 on global climate in the next two centuries. Geophys. Res. Lett., **28**, 4511-4514.

Dai, A.G., and K.E. Trenberth, 2004: The diurnal cycle and its depiction in the Community Climate System Model. J. Clim., **17**, 930-951.

Dai, A., A. Hu, G.A. Meehl, W.M. Washington, and W.G. Strand, 2005: Atlantic thermohaline circulation in a coupled general circulation model: Unforced variations vs. forced changes. J. Clim., in press.

Daikaru, K., and S. Emori, 2005: Projected dynamic and thermodynamic changes in precipitation under enhanced greenhouse gases over Asian monsoon region. in preparation.

Davis, C.H., Y. Li, J.R. McConnell, M.M. Frey, and E. Hanna, 2005: Snowfall-Driven Growth in East Antarctic Ice Sheet Mitigates Recent Sea-Level Rise. Science, **308**, 1898-1901.

De Angelis, H., and P. Skvarca, 2003: Glacier surge after ice shelf collapse. Science, **299**, 1560-1562.

de Viron, O., H. Goosse, M. Crucifix, V. Dehant, and Participating CMIP Modeling Groups, 2002: Effect of the global warming on the length-of-day. Geophys. Res. Lett., **29**, 1146, doi:10.1029/2001GL013672.

de Woul, M., and R. Hock, 2005: Static mass balance sensitivity of Arctic glaciers and ice caps using a degree-day approach. Ann. Glaciol., in press.

Defries, R.S., L. Bouboua, and G.J. Collatz, 2002: Human modification of the landscape and surface climate in the next fifty years. Glob. Change Biol., **8**, 438-458.

Delworth, T.L., and K.W. Dixon, 2000: Implications of the recent trend in the Arctic/north Atlantic Oscillation for the North Atlantic thermohaline circulation. J. Clim., **13**, 3721-3727.

Déqué, M., C. Dreveton, A. Braun, and D. Cariolle, 1994: The ARPEGE/IFS atmosphere model: a contribution to the French community climate modelling. Clim. Dyn., **10**, 249-266.

Dethloff, K., W. Dorn, A. Rinke, K. Fraedrich, M. Junge, E. Roeckner, V. Gayler, U. Cubasch, and J.H. Christensen, 2004: The impact of Greenland's deglaciation on the Arctic circulation. Geophys. Res. Lett., **31**, L19201.

Dickson, B., I. Yashayaev, J. Meincke, B. Turrell, S. Dye, and J. Holfort, 2002: Rapid freshening of the deep North Atlantic Ocean over the past four decades. Nature, **416**.

Dixon, K.W., T.L. Delworth, M.J. Spelman, and R.J. Stouffer, 1999: The influence of transient surface fluxes on North Atlantic overturning in a coupled GCM climate change experiment. Geophys. Res. Lett., **26**, 2749-2752.

Doney, S.C., et al., 2004: Evaluating global ocean carbon models: The importance of realistic physics. Glob. Biogeochem. Cyc., **18**, GB3017.

Dorn, W., K. Dethloff, A. Rinke, and E. Roeckner, 2003: Competition of NAO regime changes and increasing greenhouse gases and aerosols with respect to Arctic climate projections. Clim. Dyn., **21**, 447-458.

Dufresne, J.-L., J. Quaas, O. Boucher, S. Denvil, and L. Fairhead, 2005: Contrasts in the effects on climate of anthropogenic sulfate aerosols between the 20th and the 21st century. Geophys. Res. Lett., submitted.

Dufresne, J.L., P. Friedlingstein, M. Berthelot, L. Bopp, P. Ciais, L. Fairhead, H. Le Treut, and P. Monfray, 2002: On the magnitude of positive feedback between future climate change and the carbon cycle. Geophys. Res. Lett., **29**.

Dupont, T.K., and R.B. Alley, 2005: Assessment of the importance of ice-shelf buttressing to ice-sheet flow. Geophys. Res. Lett., **32**, L04503, doi:10.1029/2004GL022024.

Echelmeyer, K., and W.D. Harrison, 1990: Jakobshavn Isbræ, West Greenland: Seasonal variations in velocity - or lack thereof. J. Glaciol., **36**, 82-88.

Edwards, N.R., and R. Marsh, 2005: An efficient climate model with three-dimensional ocean dynamics. Clim. Dyn., in press.

Eichelberger, S., and J.R. Holton, 2002: A mechanistic model of the Northern Annular Mode. J. Geophys. Res., **107**, doi: 10.1029/2001JD001092.

Emori, S., and S.C. Brown, 2005: Dynamic and thermodynamic changes in mean and extreme precipitation under changed climate. Geophys. Res. Lett., submitted.

Emori, S., K. Daikaru, and S.C. Brown, 2005: Validation and future projection of modeled extreme daily precipitation: A multi-model analysis. in preparation.

Enting, I.G., T.M.L. Wigley, and M. Heimann, 1994: Future emissions and concentrations of carbon dioxide: key ocean/ atmosphere/ land analyses. Technical Report 31, CSIRO, Div. of Atmos. Res., Australia, Melbourne.

Fedorov, A.V., and S.G. Philander, 2001: A stability analysis of tropical ocean-atmosphere interactions: Bridging measurements and theory for El Nino. J. Clim., **14**, 3086-3101.

Fichefet, T., C. Poncin, H. Goosse, P. Huybrechts, I. Janssens, and H. Le Treut, 2003: Implications of changes in freshwater flux from the Greenland ice sheet for the climate of the 21st century. Geophys. Res. Lett., **30**.

Findell, K.L., and T.R. Knutson, 2005: Weak Simulated Extratropical Responses to Complete Tropical Deforestation. J. Clim., submitted.

Flato, G.M., and Participating CMIP modeling groups, 2004: Sea-ice and its response to CO_2 forcing as simulated by global climate change studies. Clim. Dyn., **23**, 220-241.

Foell, W., et al., 1995: Energy use, emissions, and air pollution reduction strategies. Water, Air Soil Pollut., **85**, 2277-2282.

Folland, C.K., N.A. Rayner, S.J. Brown, T.M. Smith, S.S.P. Shen, D.E. Parker, and I. Macadam, 2001: Global temperature change and its uncertainties since 1861. Geophys. Res. Lett., **28**, 2621-2624.

Forest, C.E., P.H. Stone, A.P. Sokolov, M.R. Allen, and M.D. Webster, 2002: Quantifying uncertainties in climate system properties with the use of recent climate observations. Science, **295**, 113-117.

Forest, C.E., P. Stone, and A. Sokolov, 2005: Estimated PDFs of climate system properties including natural and anthropogenic forcings. Geophys. Res. Lett., submitted.

Forster, P.M.D., and K.P. Shine, 2002: Assessing the climate impact of trends in stratospheric water vapor. Geophys. Res. Lett., **29**.

Forster, P.M.D., 2005: Climate forcings and climate sensitivities diagnosed from coupled climate model integrations. J. Clim., accepted.

Forster, P.M.D., and J.M. Gregory, 2005: The climate sensitivity and its components diagnosed from Earth radiation budget data. J. Clim., submitted.
Frame, D.J., and M.R. Allen, 2005: Challenging climate sensitivity. Nature, submitted.
Frame, D.J., B.B.B. Booth, J.A. Kettleborough, D.A. Stainforth, J.M. Gregory, M. Collins, and M.R. Allen, 2005: Constraining climate forecasts: The role of prior assumptions. Geophys. Res. Lett., **32**, L09702.
Frei, C., C. Schär, D. Lüthi, and H.C. Davies, 1998: Heavy precipitation processes in a warmer climate. Geophys. Res. Lett., **25**, 1431-1434.
Frich, P., L.V. Alexander, P. Della-Marta, B. Gleason, M. Haylock, A.M.G. Klein Tank, and T. Pearson, 2002: Observed coherent changes in climatic extremes during the second half of the twentieth century. Clim. Res., **19**, 193-212.
Friedlingstein, P., L. Bopp, P. Ciais, J.L. Dufresne, L. Fairhead, H. LeTreut, P. Monfray, and J. Orr, 2001: Positive feedback between future climate change and the carbon cycle. Geophys. Res. Lett., **28**, 1543-1546.
Friedlingstein, P., and S. Solomon, 2005: Contributions of past and present human generations to committed warming caused by carbon dioxide. Proc. Natl. Acad. Sci., USA, **102**, 10832-10836.
Friedlingstein, P., et al., 2005: Climate-carbon cycle feedback analysis, results from the C4MIP model intercomparison. J. Clim., submitted.
Furrer, R., S.R. Sain, D. Nychka, C. Tebaldi, and G.A. Meehl, 2005: Multivariate Bayesian analysis of atmosphere-ocean general circulation models. Env. Ecol. Stat., submitted.
Fyfe, J.C., 2003: Extratropical southern hemisphere cyclones: Harbingers of climate change? J. Clim., **16**, 2802-2805.
Fyfe, J.C., and O.A. Saenko, 2005: Human-induced change in the Antarctic Circumpolar Current. J. Clim., in press.
Ganachaud, A., 2003: Large-scale mass transports, water mass formation, and diffusivities estimated from World Ocean Circulation Experiment (WOCE) hydrographic data. J. Geophys. Res., **108**.
Gauss, M., et al., 2003: Radiative forcing in the 21st century due to ozone changes in the troposphere and the lower stratosphere. J. Geophys. Res., **108**.
Geng, Q., and M. Sugi, 2003: Possible change of extratropical cyclone activity due to enhanced greenhouse gases and sulfate aerosols - Study with a high-resolution AGCM. J. Clim., **16**, 2262-2274.
Giannini, A., R. Saravanan, and P. Chang, 2003: Oceanic forcing of Sahel rainfall on interannual to interdecadal time scales. Science, **302**, 1027-1030.
Gibelin, A.-L., and M. Déqué, 2003: Anthropogenic climate change over the Mediterranean region simulated by a global variable resolution model. Clim. Dyn., **20**, 327-339.
Gillett, N.P., M.R. Allen, R.E. McDonald, C.A. Senior, D.T. Shindell, and G.A. Schmidt, 2002: How linear is the Arctic Oscillation response to greenhouse gases? J. Geophys. Res., **107**.
Gillett, N.P., and D.W.J. Thompson, 2003: Simulation of recent Southern Hemisphere climate change. Science, **302**, 273-275.
Gillett, N.P., M.R. Allen, and K.D. Williams, 2003: Modeling the atmospheric response to doubled CO_2 and depleted stratospheric ozone using a stratosphere-resolving coupled GCM. Quart. J. Roy. Met. Soc., **129**, 947-966.
Giorgi, F., P.H. Whetton, R.G. Jones, J.H. Christensen, L.O. Mearns, B. Hewitson, H. Von Storch, R. Francisco, and C. Jack, 2001: Emerging patterns of simulated regional climatic changes for the 21st century due to anthropogenic forcings. Geophys. Res. Lett., **28**, 3317-3320.
Giorgi, F., and L.O. Mearns, 2003: Probability of regional climate change based on the Reliability Enseble Averaging (REA) method. Geophys. Res. Lett., **30**, 1629.
Gleckler, P.J., T.M.L. Wigley, B.D. Santer, J.M. Gregory, K. AchutaRao, and K.E. Taylor, 2005: Krakatau lives: The effect of volcanic eruptions on ocean heat content and thermal expansion. Science, submitted.
Glover, R.W., 1999: Influence of spatial resolution and treatment of orography on GCM estimates of the surface mass balance of the Greenland ice sheet. J. Clim., **12**, 551-563.
Goosse, H., H. Renssen, F.M. Selten, R.J. Haarsma, and J.D. Opsteegh, 2002: Potential causes of abrupt climate events: a numerical study with a three-dimensional climate model. Geophys. Res. Lett., **29**, DOI: 10.1029/2002GL014993.
Gordon, H.B., and S.P. O'Farrell, 1997: Transient climate change in the CSIRO coupled model with dynamic sea ice. Mon. Wea. Rev., **125**, 875-907.
Greene, A.M., L. Goddard, and U. Lall, 2005: Performance-based multimodel climate change scenarios 1: Low-frequency temperature variations. J. Clim., submitted.

Gregory, J.M., 2000: Vertical heat transport in the ocean and their effect on time-dependent climate change. Clim. Dyn., **16**, 501-515.
Gregory, J.M., et al., 2001: Comparison of results from several AOGCMs for global and regional sea-level change 1900-2100. Clim. Dyn., **18**, 241-253.
Gregory, J.M., R.J. Stouffer, S.C.B. Raper, P.A. Stott, and N.A. Rayner, 2002a: An observationally based estimate of the climate sensitivity. J. Clim., **15**, 3117-3121.
Gregory, J.M., P.A. Stott, D.J. Cresswell, N.A. Rayner, C. Gordon, and D.M.H. Sexton, 2002b: Recent and future changes in Arctic sea ice simulated by the HadCM3 AOGCM. Geophys. Res. Lett., **29**.
Gregory, J.M., P. Huybrechts, and S.C.B. Raper, 2004: Threatened loss of the Greenland ice-sheet. Nature, **428**, 616.
Gregory, J.M., J.A. Lowe, and S.F.B. Tett, 2005a: Simulated global-mean sea-level changes over the last half-millennium. in preparation.
Gregory, J.M., et al., 2005b: A model intercomparison of changes in the Atlantic thermohaline circulation in response to increasing atmospheric CO_2 concentration. Geophys. Res. Lett., **32**, L12703.
Grenfell, J.L., D.T. Shindell, and V. Grewe, 2003: Sensitivity studies of oxidative changes in the troposphere in 2100 using the GISS GCM. Atm. Chem. Phys., **3**, 1267-1283.
Greve, R., 2000: On the response of the Greenland ice sheet to greenhouse climate change. Clim. Change, **46**, 283-289.
Grewe, V., M. Dameris, R. Hein, R. Sausen, and B. Steil, 2001: Future changes of the atmospheric composition and the impact of climate change. Tellus, **53B**, 103-121.
Guilyardi, E., 2005: El Niño-mean state-seasonal cycle interactions in a multi-model ensemble. Clim. Dyn., submitted.
Haarsma, R.J., F. Selten, N. Weber, and M. Kliphuis, 2005: Sahel rainfall variability and response to greenhouse warming. Geophys. Res. Lett., submitted.
Hagedorn, R., F.J. Doblas-Reyes, and T.N. Palmer, 2004: The rationale behind the success of multi.model ensembles in seasonal forecasting. Part I: Basic concept. Tellus, in press.
Haglustaine, D.A., and G.P. Brasseur, 2001: Evolution of tropospheric ozone under anthropogenic activities and associated radiative forcing of climate. J. Geophys. Res., **106**, 32337-32360.
Hall, A., and R.J. Stouffer, 2001: An abrupt climate event in a coupled ocean-atmosphere simulation without external forcing. Nature, **409**, 171-174.
Hanna, E., P. Huybrechts, and T.L. Mote, 2002: Surface mass balance of the Greenland ice sheet from climate-analysis data and accumulation/runoff models. Ann. Glaciol., **35**, 67-72.
Hansen, J., A. Lacis, D. Rind, G.L. Russell, P. Stone, I. Fung, R. Ruedy, and J. Lerner, 1984: Climate sensitivity: Analysis of feedback mechanisms. In: Climate Processes and Climate Sensitivity [J. Hansen, and T. Takahashi (eds.)]. Vol. 29. American Geophysical Union, Washington, D.C.
Hansen, J., and L. Nazarenko, 2004: Soot climate forcing via snow and ice albedos. Proc. Natl. Acad. Sci., USA, **101**, 423-428.
Hansen, J., et al., 2005: Earth's Energy Imbalance: Confirmation and Implications. Science, **308**, 1431-1435.
Hargreaves, J.C., J.D. Annan, N.R. Edwards, and R. Marsh, 2005: Climate forecasting using an intermediate complexity Earth System Model and the Ensemble Kalman Filter. Clim. Dyn.
Harris, G., D.M.H. Sexton, B.B.B. Booth, M. Collins, J.M. Murphy, and M.J. Webb, 2005: Frequency distributions of transient regional climate change from perturbed ensembles of general circulation models. Clim. Dyn., submitted.
Harrison, S.P., K.E. Kohfeld, C. Roelandt, and T. Claquin, 2001: The role of dust in climate changes today, at the last glacial maximum, and in the future. Earth Sci. Rev., **54**, 43-80.
Harvey, L.D.D., 2004: Characterizing the annual-mean climatic effect of anthropogenic CO_2 and aerosol emissions in eight coupled atmosphere-ocean GCMs. Clim. Dyn., **23**, 569-599.
Hasegawa, A., and S. Emori, 2005: Tropical cyclones and associated precipitation over the western North Pacific in present and doubled CO_2 climates simulated by a T106 atmospheric GCM. SOLA, submitted.
Hazeleger, W., 2005: Does global warming affect tropical ocean heat transport? Geophys. Res. Lett., submitted.
Hegerl, G.C., T.J. Crowley, and W.T. Hyde, 2005: Estimating climate sensitivity from paleo-data. Nature, submitted.
Hindmarsh, R.C.A., 1993: Qualitative dynamics of marine ice sheets. In: Ice in the Climate System [W.R. Peltier (ed.), pp. 67-99.
Hoerling, M.P., J.W. Hurrell, T. Xu, G.T. Bates, and A. Phillips, 2004: Twentieth century North Atlantic climate change. Part II: Understanding the effect of Indian Ocean warming. Clim. Dyn., **23**, 391-405.

Holland, M.M., and C.M. Bitz, 2003: Polar amplification of climate change in the Coupled Model Intercomparison Project. Clim. Dyn., **21**, 221-232.
Hosaka, M., D. Nohara, and A. Kitoh, 2005: The changes of snow coverage and snow amount due to global warming simulated by a 20km-mesh global atmospheric model. SOLA, submitted.
Houghton, R.A., and J.L. Hackler, 2000: Changes in terrestrial carbon storage in the United States. 1: The roles of agriculture and forestry. Global Ecol. Biogeogr., **9**, 125-144.
Hsieh, W.W., and K. Bryan, 1996: Redistribution of sea level rise associated with enhanced greenhouse warming: A simple model study. Clim. Dyn., **12**, 535-544.
Hu, A.X., G.A. Meehl, W.M. Washington, and A.G. Dai, 2004a: Response of the Atlantic thermohaline circulation to increased atmospheric CO_2 in a coupled model. J. Clim., **17**, 4267-4279.
Hu, Z.Z., L. Bengtsson, E. Roeckner, M. Christoph, A. Bacher, and J.M. Oberhuber, 2001: Impact of global warming on the interannual and interdecadal climate modes in a coupled GCM. Clim. Dyn., **17**, 361-374.
Hu, Z.-Z., and A. Wu, 2004: The intensification and shift of the annual North Atlantic Oscillation in a global warming scenario simulation. Tellus, **56A**, 112-124.
Hu, Z.Z., E.K. Schneider, U.S. Bhatt, and B.P. Kirtman, 2004b: Potential mechanism for response of El Niño-Southern Oscillation variability to change in land surface energy budget. J. Geophys. Res., **109**, D21113, 10.1029/2004JD004771.
Huntingford, C., P.P. Harris, N. Gedney, P.M. Cox, R.A. Betts, J.A. Marengo, and J.H.C. Gash, 2004: Using a GCM analogue model to investigate the potential for Amazonian forest dieback. Theor. Appl. Clim., **78**, 177-185.
Hurrell, J.W., M.P. Hoerling, A. Phillips, and T. Xu, 2004: Twentieth century North Atlantic climate change. Part I: Assessing determinism. Clim. Dyn., **23**, 371-389.
Huybrechts, P., A. Letréguilly, and N. Reeh, 1991: The Greenland ice sheet and greenhouse warming. Palaeogeogr. Palaeoclim. Palaeoec., **89**, 399-412.
Huybrechts, P., and J. De Wolde, 1999: The dynamic response of the Greenland and Antarctic ice sheets to multiple-century climatic warming. J. Clim., **12**, 2169-2188.
Huybrechts, P., I. Janssens, C. Poncin, and T. Fichefet, 2002: The response of the Greenland ice sheet to climate changes in the 21st century by interactive coupling of an AOGCM with a thermomechanical ice-sheet model. Ann. Glaciol., **35**, 409-415.
Huybrechts, P., J. Gregory, I. Janssens, and M. Wild, 2004: Modelling Antarctic and Greenland volume changes during the 20th and 21st centuries forced by GCM time slice integrations. Glob. Planet. Change, **42**, 83-105.
Inatsu, M., and M. Kimoto, 2005: Two types of interannual variability of the mid-winter storm-track and their relationship to global warming. SOLA, **1**, 61-64.
Jacobson, M.Z., 2001: Strong radiative heating due to the mixing state of black carbon in atmospheric aerosols. Nature, **409**, 695-697.
Janicot, S., A. Harzallah, B. Fontaine, and V. Moron, 1998: West African monsoon dynamics and eastern equatorial Atlantic and Pacific SST anomalies (1970-88). J. Clim., **11**, 1874-1882.
Janicot, S., S. Trzaska, and I. Poccard, 2001: Summer Sahel-ENSO teleconnection and decadal time scale SST variations. Clim. Dyn., **18**, 303-320.
Janssens, I., and P. Huybrechts, 2000: The treatment of meltwater retention in mass-balance parameterizations of the Greenland ice sheet. Ann. Glaciol., **31**, 133-140.
Jin, F.-F., Z.-Z. Hu, M. Latif, L. Bengtsson, and E. Roeckner, 2001: Dynamical and cloud-radiation feedbacks in El Niño and greenhouse warming. Geophys. Res. Lett., **28**, 1539-1542.
Johns, T.C., et al., 2003: Anthropogenic climate change for 1860 to 2100 simulated with the HadCM3 model under updated emissions scenarios. Clim. Dyn., **20**, 583-612.
Johnson, H.L., and D.P. Marshall, 2002: A theory for surface Atlantic response to thermohaline variability. J. Phys. Oceanogr., **32**, 1121-1132.
Jones, P.D., T.J. Osborn, K.R. Briffa, C.K. Folland, E.B. Horton, L.V. Alexander, and D.E. Parker, 2001: Adjusting for sampling density in grid box land and ocean surface temperature time series. J. Geophys. Res., **106**, 3371-3380.
Jones, P.D., and A. Moberg, 2003: Hemispheric and large-scale surface air temperature variations: An extensive revision and an update to 2001. J. Clim., **16**, 206-223.
Joos, F., I.C. Prentice, S. Sitch, R. Meyer, G. Hooss, G.-K. Plattner, S. Gerber, and K. Hasselmann, 2001: Global warming feedbacks on terrestrial carbon uptake under the Intergovernmental Panel on Climate Change IPCC emission scenarios. Glob. Biogeochem. Cyc., **15**, 891-907.

Joughin, I., E. Rignot, C.E. Rosanova, B.K. Lucchitta, and J. Bohlander, 2003: Timing of recent accelerations of Pine Island Glacier, Antarctica. Geophys. Res. Lett., **30**, 1706, doi:10.1029/2003GL017609.

Joughin, I., W. Abdalati, and M. Fahnestock, 2004: Large fluctuations in speed on Greenland's Jakobshavn Isbræ. Nature, **432**, 608-610.

Kanakidou, M., et al., 2005: Organic aerosol and global climate modelling: a review. Atm. Chem. Phys., **5**, 1053-1123.

Kapsner, W.R., R.B. Alley, C.A. Shuman, S. Anandakrishnan, and P.M. Grootes, 1995: Dominant influence of atmospheric circulation on snow accumulation in Greenland over the past 18,000 years. Nature, **373**, 52-54.

Kattsov, V., J.E. Walsh, W.L. Chapman, V.A. Govorkova, T. Pavlova, and X. Zhang, 2005: Simulation and projection of Arctic freshwater budget components by the IPCC AR4 global climate models. J. Hydromet., submitted.

Kawamura, R., T. Matsuura, and S. Iizuka, 2003: Equatorially symmetric impact of El Niño-Southern Oscillation on the South Asian summer monsoon system. J. Met. Soc. Japan, **81**, 1329-1352.

Kettleborough, J.A., B.B.B. Booth, P.A. Stott, and M.R. Allen, 2005: Estimates of uncertainty in predictions of global mean surface temperature. in preparation.

Kharin, V.V., and F.W. Zwiers, 2005: Estimating extremes in transient climate change simulations. J. Clim., **18**, 1156-1173.

Kiilsholm, S., J.H. Christensen, K. Dethloff, and A. Rinke, 2003: Net accumulation of the Greenland ice sheet: High resolution modeling of climate changes. Geophys. Res. Lett., **30**.

Kitoh, A., and O. Arakawa, 2005: Reduction in tropical rainfall diurnal variation by global warming simulated by a 20-km mesh climate model. Geophys. Res. Lett., submitted.

Knight, J., J. Allan, R., C. Folland, M. Vellinga, and M. Mann, 2005: A signature of persistent natural thermohaline circulation cycles in observed climate. Geophys. Res. Lett., accepted.

Knutson, T.R., and S. Manabe, 1995: Time-mean Rrsponse over the tropical Pacific to increased CO_2 in a cupled Ocon-amosphere mdel. J. Clim., **8**, 2181-2199.

Knutson, T.R., and R.E. Tuleya, 2004: Impact of CO_2-induced warming on simulated hurricane intensity and precipitation: Sensitivity to the choice of climate model and convective parameterization. J. Clim., **17**, 3477-3495.

Knutti, R., and T.F. Stocker, 2000: Influence of the thermohaline circulation on projected sea level rise. J. Clim., **13**, 1997-2001.

Knutti, R., T.F. Stocker, and D.G. Wright, 2000: The effects of sub-grid-scale parameterizations in a zonally averaged ocean model. J. Phys. Oceanogr., **30**, 2738-2752.

Knutti, R., T.F. Stocker, F. Joos, and G.-K. Plattner, 2002: Constraints on radiative forcing and future climate change from observations and climate model ensembles. Nature, **416**, 719-723.

Knutti, R., T.F. Stocker, F. Joos, and G.-K. Plattner, 2003: Probabilistic climate change projections using neural networks. Clim. Dyn., **21**, 257-272.

Knutti, R., and G.A. Meehl, 2005: Constraining climate sensitivity from the seasonal cycle in surface temperature. J. Clim., submitted.

Knutti, R., F. Joos, S.A. Müller, G.-K. Plattner, and T.F. Stocker, 2005: Probabilistic climate change projections for stabilization profiles. Geophys. Res. Lett., submitted.

Koch, D., 2001: Transport and direct radiative forcing of carbonaceous and sulfate aerosols in the GISS GCM. J. Geophys. Res., **106**, 20311-20332.

Krabill, W., et al., 2000: Greenland ice sheet: High-elevation balance and peripheral thinning. Science, **289**, 428-430.

Kripalani, R.H., and A. Kulkarni, 1997: Rainfall variability over southeast Asia - connections with Indian monsoon ad ENSO extremes: New perspectives. Int. J. Clim., **17**, 1155-1168.

Krishna Kumar, K., B. Rajagopalan, and M.A. Cane, 1999: On the weakening relationship between the Indian monsoon and ENSO. Science, **284**, 2156-2159.

Kunkel, K.E., and X.Z. Liang, 2005: GCM simulations of climate in the central United States. J. Clim., in press.

Kutzbach, J.E., J.W. Williams, and S.J. Vavrus, 2005: Simulated 21st century changes in regional water balance of the USA Upper Midwest (Great Lakes Basin) and links to changes in global temperature and poleward moisture transport. J. Clim., submitted.

Kuzmina, S.I., L. Bengtsson, O.M. Johannessen, H. Drange, L.P. Bobylev, and M.W. Miles, 2005: The North Atlantic Oscillation and greenhouse-gas forcing. Geophys. Res. Lett., **32**.

Lambert, S.J., and G.J. Boer, 2001: CMIP1 evaluation and intercomparison of coupled climate models. Clim. Dyn., **17**, 83-106.
Lambert, S.J., and J.C. Fyfe, 2005: Changes in winter cyclone frequencies and strengths simulated in enhanced greenhouse warming experiments: results from the models participating in the IPCC diagnostic exercise. Clim. Dyn., submitted.
Land, C., and J. Feichter, 2003: Stratosphere-troposphere exchange in a chaning climate simulated with the general circulation model MAECHAM4. J. Geophys. Res., **108**, 8523.
Landerer, F.W., J.H. Jungclaus, and J. Marotzke, 2005: Regional dynamic and steric sea level change in response to the IPCC-A1b scenario. J. Phys. Oceanogr., submitted.
Laurent, R., and X. Cai, 2005: Uncertainty quantification for global climate models using the maximum entropy method. J. Clim., submitted.
Lean, J., J. Beer, and R.S. Bradley, 1995: Reconstruction of solar irradience since 1610: Implications for climate change. Geophys. Res. Lett., **22**, 3195-3198.
Leckebusch, G.C., and U. Ulbrich, 2004: On the relationship between cyclones and extreme windstorm events over Europe under climate change. Glob. Planet. Change, **44**, 181-193.
Leemans, R., et al., 1998: The IMAGE User Support System: Global Change Scenarios from IMAGE 2.1. 4815006, National Institute of Public Health and the Environment (RIVM), Bilthoven, The Netherlands.
Leggett, J., W.J. Pepper, and R. Swart, 1992: Emissions scenarios for IPCC: An update. In: Climate Change 1992. The Supplementary Report to the IPCC Scientific Assessment [J.T. Houghton, et al. (eds.)]. Cambridge University Press, Cambridge.
Levermann, A., A. Griesel, M. Hofmann, and S. Rahmstorf, 2005: Dynamic sea level changes following changes in the thermohaline circulation. Clim. Dyn., in press.
Liao, H., P.J. Adams, S.H. Chung, J.H. Seinfeld, L.J. Mickley, and D.J. Jacob, 2003: Interactions between tropospheric chemistry and aerosols in a unified general circulation model. J. Geophys. Res., **108**, 4001, doi:10.1029/2001JD001260.
Liu, P., G.A. Meehl, and G. Wu, 2003: Multi-model trends in the Sahara induced by increasing CO_2. Geophys. Res. Lett., **29**, DOI 10.1029/2002GL015923.
Liu, Z., S.J. Vavrus, F. He, N. Wen, and Y. Zhong, 2005: Rethink tropical ocean response to global warming: the enhanced equatorial warming. J. Clim., in press.
Longworth, H., J. Marotzke, and T.F. Stocker, 2005: Ocean gyres and abrupt change in thermohaline circulation and climate. J. Clim., in press.
Lopez, A., C. Tebaldi, M. New, D.A. Stainforth, M.R. Allen, and J.A. Kettleborough, 2005: Two approaches to quantifying uncertainty in global temperature changes under different forcing scenarios. J. Clim., submitted.
Lowe, J.A., and J.M. Gregory, 2005: Understanding projections of sea level rise in a Hadley Centre coupled climate model. in preparation.
Lucarini, V., and G.L. Russell, 2002: Comparison of mean climate trends in the northern hemisphere between National Centers for Environmental Prediction and two atmosphere-ocean model forced runs. J. Geophys. Res., **107**, 4269.
Lumpkin, R., and K. Speer, 2003: Large-scale vertical and horizontal circulation in the North Atlantic Ocean. J. Phys. Oceanogr., **33**, 1902-1920.
Lynch, A., P. Uotila, and J.J. Cassano, 2005: Changes in synoptic weather patterns in the polar regions in the 20th and 21st centuries, Part 2: Antarctic. Int. J. Clim., submitted.
Mahowald, N.M., and C. Luo, 2003: A less dusty future? Geophys. Res. Lett., **30**, 1903.
Manabe, S., and R.J. Stouffer, 1980: Sensitivity of a global climate model to an increase of CO_2 concentration in the atmosphere. J. Geophys. Res., **85**, 5529-5554.
Manabe, S., and R.J. Stouffer, 1994: Multiple-century response of a coupled ocean-atmosphere model to an increase of atmospheric carbon dioxide. J. Clim., **7**, 5-23.
Manabe, S., and R.J. Stouffer, 1999: Are two modes of the thermohaline circulation stable? Tellus, **51A**, 400-411.
Marland, G., T.A. Boden, and R.J. Andres, 2005: Global, Regional and National Fossil Fuel CO_2 Emissions. In: Trends: A Compendium of Data on Global Change. Carbon Dioxide Information Analysis Center, Oak Ridge National Laboratory, U.S. Department of Energy, Oak Ridge, TN.
Marquart, S., M. Ponater, F. Mager, and R. Sausen, 2003: Future development of contrail cover, optical depth, and radiative forcing: Impacts of increasing air traffic and climate change. J. Clim., **16**, 2890-2904.

Marshall, S.J., and G.K.C. Clarke, 1999: Ice sheet inception: Subgrid hypsometric parametrization of mass balance in an ice sheet model. Clim. Dyn., **15**, 533-550.

Mayer, C., and P. Huybrechts, 1999: Ice-dynamics conditions across the grounding zone, Ekströmisen, East Antarctica. J. Glaciol., **45**, 384-393.

Maykut, G.A., and N. Untersteiner, 1971: Some results from a time-dependent thermodynamic model of sea ice. J. Geophys. Res., **76**, 1550-1575.

Maynard, K., and J.-F. Royer, 2004: Effects of "realistic" land-cover change on a greenhouse-warmed African climate. Clim. Dyn., **22**, 343-358.

McCabe, G.J., M.P. Clark, and M.C. Serreze, 2001: Trends in Northern Hemisphere surface cyclone frequency and intensity. J. Clim., **14**, 2763-2768.

McDonald, R.E., D.G. Bleaken, D.R. Cresswell, V.D. Pope, and C.A. Senior, 2005: Tropical storms: Representation and diagnosis in climate models and the impacts of climate change. Clim. Dyn., in press.

McHugh, M.J., and J.C. Rogers, 2005: Multi-model respresentation of the North Atlantic Oscillation in the 20^{th} and 21^{st} centuries. Geophys. Res. Lett., submitted.

Meehl, G.A., and C. Tebaldi, 2004: More intense, more frequent, and longer lasting heat waves in the 21st century. Science, **305**, 994-997.

Meehl, G.A., C. Tebaldi, and D. Nychka, 2004a: Changes in frost days in simulations of twentyfirst century climate. Clim. Dyn., **23**, 495-511.

Meehl, G.A., W.M. Washington, J.M. Arblaster, and A.X. Hu, 2004b: Factors affecting climate sensitivity in global coupled models. J. Clim., **17**, 1584-1596.

Meehl, G.A., J.M. Arblaster, and C. Tebaldi, 2005a: Understanding future patterns of precipitation extremes in climate model simulations. Geophys. Res. Lett., in press.

Meehl, G.A., H. Teng, and G.W. Branstator, 2005b: Future changes of El Nino in two global coupled climate models. Clim. Dyn., submitted.

Meehl, G.A., C. Covey, B. McAvaney, M. Latif, and R.J. Stouffer, 2005c: Overview of the coupled model intercomparison project. Bull. Am. Met. Soc., **86**, 89-93.

Meehl, G.A., W.M. Washington, W.D. Collins, J.M. Arblaster, A. Hu, L.E. Buja, W.G. Strand, and H. Teng, 2005d: How much more global warming and sea level rise? Science, **307**, 1769-1772.

Meehl, G.A., et al., 2005e: Climate change projections for the 21^{st} century and climate change commitment in the CCSM3. J. Clim., in press.

Merryfield, W., 2005: Changes to ENSO under CO_2 doubling in the IPCC AR4 coupled climate models. J. Clim., submitted.

Mikolajewicz, U., and R. Voss, 2000: The role of the individual air-sea flux components in CO_2-induced changes of the ocean's circulation and climate. Clim. Dyn., **16**, 627-642.

Miller, R.L., G.A. Schmidt, and D.T. Shindell, 2005: Forced variations of annular modes in the 20th century IPCC AR4 simulations. J. Geophys. Res., submitted.

Milly, P.C.D., R.T. Wetherald, K.A. Dunne, and T.L. Delworth, 2002: Increasing risk of great floods in a changing climate. Nature, **415**, 514-517.

Milly, P.C.D., K.A. Dunne, and A.V. Vecchia, 2005: The global fingerprint of externally forced hydroclimatic changes on land during the 20th and 21st centuries. Science, submitted.

Mitchell, J.F.B., T.C. Johns, W.J. Ingram, and J.A. Lowe, 2000: The effect of stabilising atmospheric carbon dioxide concentrations on global and regional climate change. Geophys. Res. Lett., **27**, 2977-2980.

Mitchell, T.D., 2003: Pattern scaling **-** An examination of the accuracy of the technique for describing future climates. Clim. Change, **60**, 217-242.

Moron, V., N. Philippon, and B. Fontaine, 2003: Skill of Sahel rainfall variability in four atmospheric GCMs forced by prescribed SST. Geophys. Res. Lett., **30**.

Morris, E.M., and R. Mulvaney, 2004: Recent variations in surface mass balance of the Antarctic Peninsula ice sheet. J. Glaciol., **50**, 257-267.

Moss, R.H., and S.H. Schneider, 2000: Uncertainties in the IPCC TAR: Recommendations to Lead Authors for more consistent assessment and reporting. In: Guidance Papers on the Cross-Cutting Issues of the Third Assessment Report of the IPCC [R. Pachauri, et al. (eds.)]. Intergovernmental Panel on Climate Change, Geneva, pp. 33-51.

Mote, T.L., 2003: Estimation of the runoff rates, mass balance, and elevation changes on the Greeland ice sheet from passive microwave observations. J. Geophys. Res., **108**, 4056.

Murphy, B.F., I. Marsiat, and P. Valdes, 2002: Atmospheric contributions to the surface mass balance of Greenland in the HadAM3 atmospheric model. J. Geophys. Res., **107**, 4556-.

Murphy, J.M., D.M.H. Sexton, D.N. Barnett, G.S. Jones, M.J. Webb, M. Collins, and D.A. Stainforth, 2004: Quantification of modelling uncertainties in a large ensemble of climate change simulations. Nature, **429**, 768-772.
Myhre, G., and F. Stordal, 2001: On the tradeoff of the solar and thermal infrared radiative impact of contrails. Geophys. Res. Lett., **28**, 3119-3122.
Myhre, G., T.F. Berglen, C.E.L. Myhre, and I.S.A. Isaksen, 2004: The radiative effect of the anthropogenic influence on the stratospheric sulfate aerosol layer. Tellus, **56B**, 294-299.
Nakashiki, N., D.-H. Kim, F.O. Bryan, Y. Yoshida, D. Tsumune, K. Maruyama, and H. Kitabata, 2005: Recovery of thermohaline circulation and sea ice area under CO_2 stabilization and overshoot scenarios. Oc. Model., submitted.
Nakicenovic, N., and R. Swart, 2000: Special Report on Emissions Scenarios. Cambridge University Press.
Nanjundiah, R.S., V. Vidyunmala, and J. Srinivasan, 2005: The tropical biennial oscillation in coupled model simulations of pre-industrial and doubled CO_2 IPCC AR4 scenarios. Atm. Sci. Lett., submitted.
Nishizawa, K., H. Kitabata, J. Tsutsui, Y. Yoshida, and K. Maruyama, 2005: Ensemble projections of regional climate changes to the late 21st century under the IPCC SRES scenarios: Comparison of water budgets over East Asia and Australia. J. Met. Soc. Japan, submitted.
Nohara, D., A. Kitoh, M. Hosaka, and T. Oki, 2005: Impact of climate change on river runoff using multi-model ensemble. J. Hydromet., submitted.
Oerlemans, J., and J.P.F. Fortuin, 1992: Sensitivity of glaciers and small ice caps to greenhouse warming. Science, **258**, 115-117.
Oerlemans, J., et al., 1998: Modeling the response of glaciers to climate warming. Clim. Dyn., **14**, 267-274.
Oerlemans, J., and B.K. Reichert, 2000: Relating glacier mass balance to meteorological data by using a seasonal sensitivity characteristic. J. Glaciol., **46**, 1-6.
Oerlemans, J., 2001: Glaciers and climate change. A.A. Balkema Publishers, Rotterdam, Netherlands, 148pp.
Oerlemans, J., R.P. Bassford, W. Chapman, J.A. Dowdeswell, A.F. Glazosky, J.-O. Hagen, K. Melvold, M. de Ruyter de Wildt, and R.S.W. van de Wal, 2005: Estimating the contribution from Arctic glaciers to sea-level change in the next hundred years. Ann. Glaciol., in press.
Ogura, T., S. Emori, Y. Tsushima, S. Yokohata, A. Abe-Ouchi, and M. Kimoto, 2005: Climate sensitivity of a general circulation model with different cloud modelling assumptions. Clim. Dyn., submitted.
Ohmura, A., M. Wild, and L. Bengtsson, 1996a: A possible change in mass balance of Greenland and Antarctic ice sheets in the coming century. J. Clim., **9**, 2124-2135.
Ohmura, A., M. Wild, and L. Bengtsson, 1996b: Present and future mass balance of the ice sheets simulated with GCM. Ann. Glaciol., **23**, 187-193.
Oouchi, K., J. Yoshimura, H. Yoshimura, R. Mizuta, K. S., and A. Noda, 2005: Tropical cyclone climatology in a global-warming climate as simulated in a 20km-mesh global atmospheric model. J. Met. Soc. Japan, submitted.
Oppenheimer, M., 1998: Global warming and the stability of the West Antarctic Ice Sheet. Nature, **393**, 325-332.
Opsteegh, J.D., R.J. Haarsma, F.M. Selten, and A. Kattenberg, 1998: ECBILT: A dynamic alternative to mixed boundary conditions in ocean models. Tellus, **50A**, 348-367.
Osborn, T.J., 2004: Simulating the winter North Atlantic Oscillation: The roles of internal variability and greenhouse forcing. Clim. Dyn., **22**, 605-623.
Pal, J.S., F. Giorgi, and X. Bi, 2004: Consistency of recent European summer precipitation trends and extremes with future regional climate projections. Geophys. Res. Lett., **31**, L13202.
Palmer, T.N., 2001: A non-linear dynamical perspective on model error: A proposal for non local stochastic dynamic parameterization in weather and climate prediction models. Quart. J. Roy. Met. Soc., **127**, 279-303.
Palmer, T.N., and J. Räisänen, 2002: Quantifying the risk of extreme seasonal precipitation events in a changing climate. Nature, **415**, 514-517.
Palmer, T.N., et al., 2004: Development of a European multimodel ensemble system for seasonal-to-interannual prediction (DEMETER). Bull. Am. Met. Soc., **85**, 853-872.
Palmer, T.N., 2005: Global warming in a nonlinear climate - Can we be sure? Europhys. News, **36**, 42-46.
Palmer, T.N., G.J. Shutts, R. Hagedorn, F.J. Doblas-Reyes, T. Jung, and M. Leutbecher, 2005: Representing model uncertainty in weather and climate prediction. Ann. Rev. Earth Planet. Sci., **33**, 4.1-4.31.
Parizek, B.R., and R.B. Alley, 2004: Implications of increased Greenland surface melt under global-warming scenarios: Ice-sheet simulations. Quat. Sci. Rev., **23**, 1013-1027.

Paterson, W.S.B., and N. Reeh, 2001: Thinning of the ice sheet in northwest Greeland over the past forty years. Nature, **414**, 60-62.
Payne, A.J., A. Vieli, A.P. Shepherd, D.J. Wingham, and E. Rignot, 2004: Recent dramatic thinning of largest West Antarctic ice stream triggered by oceans. Geophys. Res. Lett., **31**, L23401, doi: 10.1029/2004GL021284.
Payne, A.J., P.R. Holland, A.P. Shepherd, A. Jenkins, and D.L. Feltham, 2005: Numerical modelling of ocean-ice interactions under Pine Island Bay's ice shelf. submitted.
Penner, J.E., D.H. Lister, D.J. Griggs, D.J. Dokken, and M. McFarland (eds.), 1999: Aviation and the global atmospheres. Cambridge University Press.
Petoukhov, V., A. Ganopolski, V. Brovkin, M. Claussen, A. Eliseev, C. Kubatzki, and S. Rahmstorf, 2000: CLIMBER-2: a climate system model of intermediate complexity. Part I: model description and performance for present climate. Clim. Dyn., **16**, 1-17.
Phillips, T.J., et al., 2004: Evaluating parameterizations in general circulation models. Bull. Am. Met. Soc., **85**, 1903-1915.
Phillips, T.J., and P.J. Gleckler, 2005: Evaluation of continental precipitation in 20th century climate simulations: The utility of multi-model statistics. Water Resour. Res., submitted.
Piani, C., D.J. Frame, D.A. Stainforth, and M.R. Allen, 2005: Constraints on climate change from a multi-thousand member ensemble of simulations. Geophys. Res. Lett., submitted.
Pitari, G., E. Mancini, V. Rizi, and D.T. Shindell, 2002: Impact of future climate and emission changes on stratospheric aerosols and ozone. J. Atm. Sci., **59**, 414-440.
Prospero, J.M., D.L. Savoie, and R. Arimoto, 2003: Long-term record of nss-sulfate and nitrate in aerosols on Midway Island, 1981-2000: Evidence of increased (now decreasing?) anthropogenic emissions from Asia. J. Geophys. Res., **108**.
Rahmstorf, S., and A. Ganopolski, 1999: Long-term global warming scenarios computed with an efficient coupled climate model. Clim. Change, **43**, 353-367.
Räisänen, J., 2001: CO_2-induced climate change in CMIP2 experiments: Quantification of agreement and role of internal variability. J. Clim., **14**, 2088-2104.
Räisänen, J., and T.N. Palmer, 2001: A probability and decision.model analysis of a multimodel ensemble of climate change simulations. J. Clim., **14**, 3212-3226.
Räisänen, J., 2003: CO_2-induced changes in angular momentum in CMIP2 experiments. J. Clim., **16**, 132-143.
Räisänen, J., 2005a: Impact of increasing CO_2 on monthly-to-annual precipitation extremes: Analysis of the CMIP2 experiments. Clim. Dyn., submitted.
Räisänen, J., 2005b: Model-based probability distributions of climate change: A semi-analytic approach. Clim. Dyn., submitted.
Räisänen, J., 2005c: Probability distributions of CO_2-induced global warming as inferred directly from multimodel ensemble simulations. Geophysica, submitted.
Ramanathan, V., and R.E. Dickinson, 1979: Role of Stratospheric Ozone in the Zonal and Seasonal Radiative Energy-Balance of the Earth-Troposphere System. J. Atm. Sci., **36**, 1084-1104.
Ramanathan, V., P.J. Crutzen, J.T. Kiehl, and D. Rosenfeld, 2001: Aerosols, climate, and the hydrologic cycle. Science, **294**, 2119-2124.
Randall, D.A., et al., 1996: A revised land surface parameterization (SiB2) for GCMs. Part III: The greening of the Colorado State University General Circulation Model. J. Clim., **9**, 738-763.
Raper, S.C.B., O. Brown, and R.J. Braithwaite, 2000: A geometric glacier model for sea-level change calculations. J. Glaciol., **46**, 357-368.
Raper, S.C.B., J.M. Gregory, and R.J. Stouffer, 2002: The role of climate sensitivity and ocean heat uptake on AOGCM transient temperature response. J. Clim., **15**, 124-130.
Raper, S.C.B., and R.J. Braithwaite, 2005: The potential for sea level rise: New estimates from glacier and ice cap area and volume distributions. Geophys. Res. Lett., submitted.
Rauthe, M., A. Hense, and H. Paeth, 2004a: A model intercomparison study of climate change signals in extratropical circulation. Int. J. Clim., **24**, 643-662.
Rauthe, M., A. Hense, and H. Paeth, 2004b: A model intercomparison study of climate change-signals in extratropical circulation. Int. J. Clim., **24**, 643-662.
Reichert, B.K., L. Bengtsson, and J. Oerlemans, 2002: Recent glacier retreat exceeds internal variability. J. Clim., **15**, 3069-3081.

Ridley, J., P. Huybrechts, J.M. Gregory, and J.A. Lowe, 2005: Future changes in the Greenland ice sheet: A 3000 year simulation with a high resolution ice sheet model interactively coupled to an AOGCM. J. Clim., in press.

Rignot, E., 1998: Fast recession of a West Antarctic glacier. Science, **281**, 549.551.

Rignot, E., 2001: Evidence for a rapid retreat and mass loss of Thwaites Glacier, West Antarctica. J. Glaciol., **47**, 213-222.

Rignot, E., and R.H. Thomas, 2002: Mass balance of polar ice sheets. Science, **297**, 1502-1506.

Rignot, E., and S.S. Jacobs, 2002: Rapid bottom melting widespread near Antarctic ice sheet grounding lines. Science, **296**, 2020-2023.

Rignot, E., D.G. Vaughan, M. Schmeltz, T. Dupont, and D. MacAyeal, 2002: Acceleration of Pine Island and Thwaites Glaciers, West Antarctica. Ann. Glaciol., **34**, 189-194.

Rignot, E., G. Casassa, P. Gogineni, W. Krabill, A. Rivera, and R. Thomas, 2004: Accelerated ice discharge from the Antarctic Peninsula following the collapse of Larsen B ice shelf. Geophys. Res. Lett., **31**, L19401.

Rind, D., R.J. Healy, C. Parkinson, and D. Martinson, 1995: The role of sea ice in $2\times CO_2$ climate model sensitivity. 1. The total influence of sea ice thickness and extent. J. Clim., **8**, 449-463.

Rind, D., J. Perlwitz, and P. Lonergan, 2005a: AO/NAO response to climate change. Part I: The respective influences of stratospheric and tropospheric climate changes. J. Geophys. Res., submitted.

Rind, D., J. Perlwitz, P. Lonergan, and J. Lerner, 2005b: AO/NAO response to climate change. Part II: The relative importance of low and high latitude temperature changes. J. Geophys. Res., submitted.

Rodwell, M.J., D.P. Rowell, and C.K. Folland, 1999: Oceanic forcing of the wintertime North Atlantic oscillation and European climate. Nature, **398**, 320-323.

Roesch, A., 2005: Evaluation of surface albedo and snow cover in AR4 coupled climate models. J. Geophys. Res., submitted.

Ronski, S., and G. Budeus, 2005: Time series of winter convection in the Greenland Sea. J. Geophys. Res., **110**, C04015.

Rothrock, D.A., Y. Yu, and G.A. Maykut, 1999: Thinning of the Arctic sea-ice cover. Geophys. Res. Lett., **26**, 3469-3472.

Rougier, J.C., 2005: Probabilistic inference for future climate using an ensemble of simulator evaluations. Clim. Change, submitted.

Rowell, D.P., and R.G. Jones, 2005: The Causes and uncertainty of future summer drying over Europe. Clim. Dyn., submitted.

Russell, G.L., V. Gornitz, and J.R. Miller, 2000: Regional sea-level changes projected by the NASA/Giss atmosphere-ocean model. Clim. Dyn., **16**, 789-797.

Saenko, O.A., A.J. Weaver, and J.M. Gregory, 2003: On the link between the two modes of the ocean thermohaline circulation and the formation of global-scale water masses. J. Clim., **16**, 2797-2801.

Saenko, O.A., 2005: Influence of global warming on baroclinic Rossby radius in the ocean: a model intercomparison. J. Clim., submitted.

Saenko, O.A., J.C. Fyfe, and M.H. England, 2005: On the response of the oceanic wind-driven circulation to atmospheric CO_2 increase. Clim. Dyn., in press.

Sato, M., J. Hansen, M.P. McCornick, and J.B. Pollack, 1993: Stratospheric aerosol optical depths. J. Geophys. Res., **98**, 22987-22994.

Scambos, T.A., C. Hulbe, M.A. Fahnestock, and J. Bohlander, 2000: The link between climate warming and break-up of ice shelves in the Antarctic Peninsula. J. Glaciol., **46**, 516-530.

Schaeffer, M., F.M. Selten, J.D. Opsteegh, and H. Goosse, 2002: Intrinsic limits to predictability of abrupt regional climate change in IPCC SRES scenarios. Geophys. Res. Lett., **29**.

Schaeffer, M., F.M. Selten, J.D. Opsteegh, and H. Goosse, 2004: The influence of ocean convection patterns on high-latitude climate projections. J. Clim., **17**, 4316-4329.

Schär, C., P.L. Vidale, D. Lüthi, C. Frei, C. Häberli, M.A. Liniger, and C. Appenzeller, 2004: The role of increasing temperature variability in European summer heat waves. Nature, **427**, 332-336.

Schneeberger, C., O. Albrecht, H. Blatter, M. Wild, and R. Hoeck, 2000: Størglacieren in doubling CO_2 climate. Clim. Dyn., **17**, 825-834.

Schneeberger, C., H. Blatter, A. Abe-Ouchi, and M. Wild, 2003: Modelling changes in the mass balance of glaciers of the northern hemisphere for a transient $2\times CO_2$ scenario. J. Hydrol., **282**, 145-163.

Schneider von Deimling, T., H. Held, A. Ganopolski, and S. Rahmstorf, 2005: Climate sensitivity estimated from ensemble simulations of glacial climate. Clim. Dyn., submitted.

Schweckendiek, U., and J. Willebrand, 2005: Mechanisms for the overturning response in global warming simulations. J. Clim., in press.
Selten, F.M., G.W. Branstator, H.A. Dijkstra, and M. Kliphuis, 2005: Tropical origins for recent and future northern hemisphere climate change. Geophys. Res. Lett., in press.
Semenov, V.A., and L. Bengtsson, 2002: Secular trends in daily precipitation characteristics: Greenhouse gas simulation with a coupled AOGCM. Clim. Dyn., **19**, 123-140.
Shepherd, A., D. Wingham, A. Payne, and P. Skvarca, 2003: Larsen ice shelf has progressively thinned. Science, **302**, 856-859.
Shepherd, A., D. Wingham, and E. Rignot, 2004: Warm ocean is eroding West Antarctic ice sheet. Geophys. Res. Lett., **31**, L23402, doi:10.1029/2004GL021106.
Shepherd, A., D.J. Wingham, and J.A.D. Mansley, 2002: Inland thinning of the Amundsen Sea sector, West Antarctica. Geophys. Res. Lett., **29**, 1364, 10.1029/2001GL014183.
Shindell, D.T., G.A. Schmidt, R.L. Miller, and D. Rind, 2001: Northern hemisphere winter climate response to greenhouse gas, ozone, and volcanic forcing. J. Geophys. Res., **106**, 7193-7210.
Shindell, D.T., and G.A. Schmidt, 2004: Southern hemisphere climate response to ozone changes and greenhouse gas increases. Geophys. Res. Lett., **31**, doi: 10.1029/2004GL020724.
Sigmond, M., P.C. Siegmund, E. Manzini, and H. Kelder, 2004: A simulation of the separate climate effects of middle-atmosphere and tropospheric CO_2 doubling. J. Clim., **17**, 2352-2367.
Smethie, W.M., and R.A. Fine, 2001: Rates of North Atlantic Deep Water formation calculated from chlorofluorocarbon inventories. Deep-Sea Res. I, **48**, 189-215.
Smith, S.J., H. Pitcher, and T.M.L. Wigley, 2001: Global and regional anthropogenic sulfur dioxide emissions. Glob. Planet. Change, **29**, 99-119.
Soden, B.J., and I.M. Held, 2005: An assessment of climate feedbacks in coupled ocean-atmosphere models. J. Clim., submitted.
Sokolov, A., C.E. Forest, and P.H. Stone, 2003: Comparing oceanic heat uptake in AOGCM transient climate change experiments. J. Clim., **16**, 1573-1582.
Stainforth, D.A., et al., 2005: Uncertainty in predictions of the climate response to rising levels of greenhouse gases. Nature, **433**, 403-406.
Stevenson, D.S., C.E. Johnson, W.J. Collins, R.G. Derwent, and J.M. Edwards, 2000: Future estimates of tropospheric ozone radiative forcing and methane turnover - the impact of climate change. Geophys. Res. Lett., **27**, 2073-2076.
Stocker, T.F., D.G. Wright, and L.A. Mysak, 1992a: A zonally averaged, coupled ocean-atmosphere model for paleoclimate studies. J. Clim., **5**, 773-797.
Stocker, T.F., D.G. Wright, and W.S. Broecker, 1992b: The influence of high-latitude surface forcing on the global thermohaline circulation. Paleoceanogr., **7**, 529-541.
Stocker, T.F., and A. Schmittner, 1997: Influence of CO_2 emission rates on the stability of the thermohaline circulation. Nature, **388**, 862-865.
Stocker, T.F., and R. Knutti, 2003: Do simplified climate models have any useful skill? CLIVAR Exchanges, **8**, 7-10.
Stocker, T.F., and C.C. Raible, 2005: Climate change - Water cycle shifts gear. Nature, **434**, 830-833.
Stone, D.A., and A.J. Weaver, 2002: Daily maximum and minimum temperature trends in a climate model. Geophys. Res. Lett., **29**, doi: 10.1029/2001GL014556.
Stone, D.A., and J.C. Fyfe, 2005: The effect of ocean mixing parametrisation on the enhanced CO_2 response of the Southern Hemisphere midlatitude jet. Geophys. Res. Lett., in press.
Stott, P.A., and J.A. Kettleborough, 2002: Origins and estimates of uncertainty in predictions of twenty-first century temperature rise. Nature, **416**, 723-726.
Stott, P.A., D.A. Stone, and M.R. Allen, 2004: Human contribution to the European heatwave of 2003. Nature, **432**, 610-613.
Stott, P.A., J.A. Kettleborough, and M.R. Allen, 2005a: Uncertainty in predictions of continental scale temperature rise. in preparation.
Stott, P.A., J.F.B. Mitchell, J.M. Gregory, B.D. Santer, G.A. Meehl, T. Delworth, and M.R. Allen, 2005b: Observational constraints on past attributable warming and predictions of future global warming. J. Clim., submitted.
Stouffer, R.J., and S. Manabe, 1999: Response of a coupled ocean-atmosphere model to increasing atmospheric carbon dioxide: sensitivity to the rate of increase. J. Clim., **12**, 2224-2237.
Stouffer, R.J., and S. Manabe, 2003: Equilibrium response of thermohaline circulation to large changes in atmospheric CO_2 concentration. Clim. Dyn., **20**, 759-773.

Stouffer, R.J., et al., 2005: Investigating the causes of the response of the thermohaline circulation to past and future climate changes. J. Clim., submitted.

Stowasser, M., and K. Hamilton, 2005: Relationship between shortwave cloud radiative forcing and local meteorological variables compared in observations and several climate models. J. Clim., submitted.

Streets, D.G., K.J. Jiang, X.L. Hu, J.E. Sinton, X.Q. Zhang, D.Y. Xu, M.Z. Jacobson, and J.E. Hansen, 2001: Recent reductions in China's greenhouse gas emissions. Science, **294**, 1835-1837.

Sudo, K., M. Takahashi, and H. Akimoto, 2003: Future changes in stratosphere-troposphere exchanges and their impacts on future tropospheric ozone simulations. Geophys. Res. Lett., **30**, doi:10.1029/2003GL018526.

Sugi, M., A. Noda, and N. Sato, 2002: Influence of the global warming on tropical cyclone climatology: An experiment with the JMA global model. J. Met. Soc. Japan, **80**, 249-272.

Sugi, M., and J. Yoshimura, 2004: A mechanism of tropical precipitation change due to CO_2 increase. J. Clim., **17**, 238-243.

Suzuki, T., H. Hasumi, T.T. Sakamoto, T. Nishimura, A. Abe-Ouchi, T. Segawa, N. Okada, A. Oka, and S. Emori, 2005: Future projection of sea level and its variability in a high resolution climate model. Geophys. Res. Lett., submitted.

Takemura, T., T. Nakajima, T. Nozawa, and K. Aoki, 2001: Simulation of future aerosol distribution, radiative forcing, and long-range transport in East Asia. J. Met. Soc. Japan, **79**, 1139-1155.

Talley, L.D., 2003: Shallow, intermediate, and deep overturning components of the global heat budget. J. Phys. Oceanogr., **33**, 530-560.

Tanaka, H.L., N. Ishizaki, and D. Nohara, 2005: Intercomparison of the intensities and trends of Hadley, Walker and monsoon circulations in the global warming predictions. SOLA, submitted.

Tebaldi, C., J.M. Arblaster, K. Hayhoe, and G.A. Meehl, 2005b: Going to the extremes: An intercomparison of model-simulated historical and future changes in extreme events. Clim. Change, submitted.

Tebaldi, C., L.O. Mearns, D. Nychka, and R.W. Smith, 2005a: Regional probabilities of precipitation change: A Bayesian analysis of multimodel simulations. Geophys. Res. Lett., submitted.

Tegen, I., M. Werner, S.P. Harrison, and K.E. Kohfeld, 2004: Reply to comment by N. M. Mahowald et al. on "Relative importance of climate and land use in determining present and future global soil dust emission". Geophys. Res. Lett., **31**.

Terray, L., M.-E. Demory, M. Déqué, G. de Coetlogon, and E. Maisonnave, 2004: Simulation of late twenty-first century changes in wintertime atmospheric circulation over Europe de to anthtopogenic causes. J. Clim., **17**, 4630-4635.

Thomas, R., E. Rignot, P. Kanagaratnam, W. Krabill, and G. Casassa, 2005: Force-perturbation analysis of Pine Island Glacier, Antarctica, suggests cause for recent acceleration. Ann. Glaciol., in press.

Thomas, R., et al., 2004: Accelerated sea level rise from West Antarctica. Science, **306**, 255-258.

Thompson, D.W., and S. Solomon, 2002: Interpretation of recent Southern Hemisphere climate change. Science, **296**, 895-899.

Tol, R.S.J., and A.F. De Vos, 1998: A Bayesian statistical analysis of the enhanced greenhouse effect. Clim. Change, **38**, 87-112.

Toniazzo, T., J.M. Gregory, and P. Huybrechts, 2004: Climatic impact of Greenland deglaciation and its possible irreversibility. J. Clim., **17**, 21-33.

Trenberth, K.E., 1990: Recent observed interdecadal climate changes in the Northern Hemisphere. Bull. Am. Met. Soc., **71**, 988-993.

Tsushima, Y., A. Abe-Ouchi, and S. Manabe, 2005a: Radiative damping of annual temperature variation: Observational constraint on simulated feedback. Clim. Dyn., in press.

Tsushima, Y., S. Emori, T. Ogura, M.J. Webb, K.D. Williams, M.A. Ringer, B. Soden, B. Li, and N.G. Andronova, 2005b: A multi-model analysis of the distribution of mixed-phase clouds in AGCMs, for control and doubled carbon dioxide simulations. Clim. Dyn., submitted.

Tsutsui, J., Y. Yoshida, D.-H. Kim, H. Kitabata, and K. Maruyama, 2005: Long-time climate responses to CO_2 stabilization and overshoot scenarios.

Uchiyama, T., R. Mizuta, K. Kamiguchi, A. Kitoh, and A. Noda, 2005: Changes in temperature-based extremes indices due to global warming projected by a global 20-km-mesh atmospheric model. SOLA, submitted.

Ulbrich, U., G.C. Leckebusch, T. Spangehl, J. Pinto, and M. Royer, 2005: Changing Northern Hemisphere storm tracks in climate change simulations. Geophys. Res. Lett., submitted.

van de Wal, R.S.W., and M. Wild, 2001: Modelling the response of glaciers to climate change by applying volume-area scaling in combination with a high resolution GCM. Clim. Dyn., **18**, 359-366.

van de Wal, R.S.W., M. Wild, and J. de Wolde, 2001: Short-term volume change of the Greenland ice sheet in response to doubled CO_2 conditions. Tellus, **53B**, 94-102.

van der Veen, C.J., 2002: Polar ice sheets and global sea level: how well can we predict the future? Glob. Planet. Change, **32**, 165-194.

van Lipzig, N.M., E. van Meijgaard, and J. Oerlemans, 2002: Temperature sensitivity of the Antarctic surface mass balance in a regional atmospheric climate model. J. Clim., **15**, 2758-2774.

van Oldenborgh, G.J., S. Philip, and M. Collins, 2005: El Niño in a changing climate: a multi-model study. Oc. Sci., submitted.

Vaughan, D.G., and J.R. Spouge, 2002: Risk estimation of collapse of the West Antarctic Ice Sheet. Clim. Change, **52**, 65-91.

Vaughn, D.G., 2005: Recent trends in melting conditions on the Antarctic Peninsula and their implications for ice-sheet mass balance. Arct. Antarct. Alp. Res., in press.

Vavrus, S.J., J.E. Walsh, W.L. Chapman, and D. Portis, 2005: The behavior of extreme cold air outbreaks under greenhouse warming. Int. J. Clim., submitted.

Vellinga, M., and R.A. Wood, 2005: Impacts of thermohaline circulation shutdown in the twenty-first century. in preparation.

Vieli, A., and A.J. Payne, 2005: Assessing the ability of numerical ice sheet models to simulate grounding line migration. Geophys. Res. Lett., **110**, F01003, doi:10.1029/2004JF000202.

Voss, R., and U. Mikolajewicz, 2001: Long-term climate changes due to increased CO_2 concentration in the coupled atmosphere-ocean general circulation model ECHAM3/LSG. Clim. Dyn., **17**, 45-60.

Voss, R., W. May, and E. Roeckner, 2002: Enhanced resolution modeling study on anthropogenic climate change: changes in the extremes of the hydrological cycle. Int. J. Clim., **22**, 755-777.

Wang, G., 2005: Agricultural drought in a future climate: Results from fifteen models participating in the IPCC 4th Assessment. Clim. Dyn., submitted.

Wang, H., 2002: The instability of the East Asian summer monsoon-ENSO relations. Advances in Atmospheric Sciences, **19**, 1-11.

Wang, X.L., and V.R. Swail, 2004: Historical and possible future changes of wave heights in northern hemisphere ocean. In: Atmosphere-Ocean Interactions [W. Perrie (ed.). Vol. 2. Wessex Institute of Technology Press, Southampton, pp. 300.

Wang, X.L., F.W. Zwiers, and V.R. Swail, 2004: North Atlantic ocean wave climate change scenarios for the twenty-first century. J. Clim., **17**, 2368-2383.

Wang, X.L., and V.R. Swail, 2005: Climate change signal and uncertainty in projections of ocean wave heights. Clim. Dyn., submitted.

Watanabe, S., T. Nagashima, and S. Emori, 2005: Response of gravity wave momentum flux to the global warming in the lower stratosphere. Geophys. Res. Lett., submitted.

Watterson, I.G., 1996: Non-dimensional measures of climate model performance. Int. J. Clim., **16**, 379-391.

Watterson, I.G., 2003: Effects of a dynamic ocean on simulated climate sensitivity to greenhouse gases. Clim. Dyn., **21**, 197-209.

Watterson, I.G., and M.R. Dix, 2003: Simulated changes due to global warming in daily precipitation means and extremes and their interpretation using the gamma distribution. J. Geophys. Res., **108**, 4379, doi:10.1029/2002JD002928, 2003.

Watterson, I.G., 2005: The intensity of precipitation during extra-tropical cyclones in global warming simulations: A link to cyclone intensity? Tellus, in press.

Watterson, I.G., and M.R. Dix, 2005: Effective sensitivity and heat capacity in the response of climate models to greenhouse gas and aerosol forcings. Quart. J. Roy. Met. Soc., **131**, 259-279.

Weaver, A.J., and E.C. Wiebe, 1999: On the sensitivity of projected oceanic thermal expansion to the parameterisation of sub-grid scale ocean mixing. Geophys. Res. Lett., **26**, 3461-3464.

Weaver, A.J., O.A. Saenko, P.U. Clark, and J.X. Mitrovica, 2003: Meltwater pulse 1A from Antarctica as a trigger of the Bølling-Allerød warm interval. Science, **299**, 1709-1713.

Weaver, A.J., and C. Hillaire-Marcel, 2004a: Ice growth in the greenhouse: A seductive paradox but unrealistic scenario. Geosci. Canada, **31**, 77-85.

Weaver, A.J., and C. Hillaire-Marcel, 2004b: Global warming and the next ice age. Science, **304**, 400-402.

Webb, M.J., et al., 2005: On uncertainty in feedback mechanisms controlling climate sensitivity in two GCM ensembles. Clim. Dyn., submitted.

Webster, M.D., M. Babiker, M. Mayer, J.M. Reilly, J. Harnisch, M.C. Sarofim, and C. Wang, 2002: Uncertainty in emissions projections for climate models. Atmos. Env., **36**, 3659-3670.

Webster, M., et al., 2003: Uncertainty analysis of climate change and policy response. Clim. Change, **61**, 295-320.

Weisheimer, A., and T.N. Palmer, 2005: Changing frequency of occurrence of extreme seasonal temperatures under global warming. Geophys. Res. Lett., submitted.

Wetherald, R.T., R.J. Stouffer, and K.W. Dixon, 2001: Committed warming and its implications for climate change. Geophys. Res. Lett., **28**, 1535-1538.

Wetherald, R.T., and S. Manabe, 2002: Simulation of hydrologic changes associated with global warming. J. Geophys. Res., **107**.

Whillans, I.M., and C.J. van der Veen, 1993: New and improved determinations of velocity of Ice Streams B and C, West Antarctica. J. Glaciol., **39**, 483-490.

Wigley, T.M.L., 1984: Carbon dioxide, trace gases and global warming. Climate Monitor, **13**, 133-148.

Wigley, T.M.L., R. Richels, and J.A. Edmonds, 1996: Economic and environmental choices in the stabilization of atmospheric CO_2 concentrations. Nature, **379**, 240-243.

Wigley, T.M.L., A.K. Jain, F. Joos, B.S. Nyenzi, and P.R. Shukla, 1997: Technical Paper IV. Implications of Proposed CO_2 Emissions Limitations. Intergovernmental Panel on Climate Change.

Wigley, T.M.L., and S.C.B. Raper, 2001: Interpretation of high projections for global-mean warming. Science, **293**, 451-454.

Wigley, T.M.L., and S.C.B. Raper, 2003: Future changes in global-mean temperature and sea level. In: Climate and Sea Leel Change: Observations, Projections and Implications [R.A. Warrick, et al. (eds.)]. Cambridge University Press, Cambridge, pp. 111-133.

Wigley, T.M.L., 2004: Modeling climate change under no-policy and policy emissions pathways. In: The Benefits of Climate Change Policies: Analytical and Framework Issues. OECD Publications, Paris, pp. 221-248.

Wigley, T.M.L., 2005: The climate change commitment. Science, **307**, 1766-1769.

Wigley, T.M.L., C.M. Ammann, B.D. Santer, and S.C.B. Raper, 2005: Effect of climate sensitivity on the response to volcanic forcing. J. Geophys. Res., **110**, D09107, doi:10.1029/2004JD005557.

Wilby, R.L., and T.M.L. Wigley, 2002: Future changes in the distribution of daily precipitation totals across North America. Geophys. Res. Lett., **29**, 1135.

Wild, M., and A. Ohmura, 2000: Changes in mass balance of the polar ice sheets and sea level from high resolution GCM simulations of global warming. Ann. Glaciol., **30**, 197-203.

Wild, M., P. Calanca, S. Scherrer, and A. Ohmura, 2003: Effects of polar ice sheets on global sea level in high resolution greenhouse scenarios. J. Geophys. Res., **108**, 4165, doi:10.1029/2002JD002451.

Williams, J.W., S.T. Jackson, and J.E. Kutzbach, 2005a: Projected Distributions of Novel and Disappearing Climates by 2100AD. Nature, submitted.

Williams, K.D., M. Crucifix, C.A. Senior, and M.J. Webb, 2005b: On differences in climate change feedbacks between HadGEM1 and HadCM3. Atm. Sci. Lett., submitted.

Williams, K.D., et al., 2005c: Evaluation of a component of the cloud response to climate change in an intercomparison of climate models. Clim. Dyn., submitted.

Wingham, D.J., A. Muir, and A.P. Shepherd, 2005: The Antarctic ice sheet is growing. submitted.

Wood, R.A., A.B. Keen, J.F.B. Mitchell, and J.M. Gregory, 1999: Changing spatial structure of the thermohaline circulation in response to atmospheric CO_2 forcing in a climate model. Nature, **399**, 572-575.

Wu, P., R. Wood, and P. Stott, 2005: Human influence on increasing Arctic river discharge. Geophys. Res. Lett., **32**, L02703.

Xu, Y., Z.-C. Zhao, Y. Luo, and X. Gao, 2005: Climate change projections for the 21st century by the NCC/IAP T63 with SRES scenarios. Acta Meteorol. Sin., submitted.

Yamaguchi, K., and A. Noda, 2005: Global warming patterns over the North Pacific: ENSO versus AO. J. Met. Soc. Japan, submitted.

Yeh, S.-W., and B.P. Kirtman, 2005: Pacific decadal variability and decadal ENSO amplitude modulation. Geophys. Res. Lett., **32**, L05703.

Yin, J.H., 2005: A consistent poleward shift of the storm tracks in simulations of 21st century climate. Geophys. Res. Lett., submitted.

Yokohata, S., S. Emori, T. Nozawa, T. Ogura, Y. Tsushima, and M. Kimoto, 2005: Testing the likelihood of different climate sensitivites by hindcasting the response to the Pinatubo eruption. in preparation.

Yonetani, T., and H.B. Gordon, 2001: Simulated changes in the frequency of extremes and regional features of seasonal/annual temperature and precipitation when atmospheric CO_2 is doubled. J. Clim., **14**, 1765-1779.

Yoshimori, M., M.C. Reader, A.J. Weaver, and N.A. McFarlane, 2002: On the causes of glacial inception at 116 kaBP. Clim. Dyn., **18**, 383-402.
Yoshimura, J., and M. Sugi, 2005: Tropical cyclone climatology in a high-resolution AGCM: Impacts of SST warming and CO_2 increase. SOLA, submitted.
Yoshimura, J., M. Sugi, and A. Noda, 2005: Influence of greenhouse warming on tropical cyclone frequency. J. Met. Soc. Japan, submitted.
Yu, B., and G.J. Boer, 2002: The roles of radiation and dynamical processes in the El Niño-like response to global warming. Clim. Dyn., **19**, 539-553.
Yukimoto, S., A. Noda, T. Uchiyama, and S. Kuzunoki, 2005: Climate Change of the twentieth through twenty-first centuries simulated by the MRI-CGCM2.3. Pap. Meteorol. Geophys., submitted.
Yukimoto, S., and K. Kodera, 2005: Interdecadal Arctic Oscillation in twentieth century climate simulations viewed as internal variability and response to external forcing. Geophys. Res. Lett., **32**, L03707, doi:10.1029/2004GL021870.
Zelle, H., G.J. van Oldenborgh, G. Burgers, and H.A. Dijkstra, 2005: El Niño and greenhouse warming: Results from ensemble simulations with the NCAR CCSM. J. Clim., submitted.
Zeng, G., and J.A. Pyle, 2003: Changes in tropospheric ozone between 2000 and 2100 modeled in a chemistry-climate model. Geophys. Res. Lett., **30**, doi:10.1029/2002GL016708.
Zhang, X.Q., and J.E. Walsh, 2005: Toward a seasonally ice-covered Arctic Ocean: Scenarios from the IPCC AR4 model simulations. J. Clim., submitted.
Zuo, Z., and J. Oerlemans, 1997: Contribution of glaciel melt to sea level rise since AD 1865: A regionally differentiated calculation. Clim. Dyn., **13**, 835-845.
Zwally, H.J., W. Abdalati, T. Herring, K. Larson, J. Saba, and K. Steffen, 2002: Surface melt-induced acceleration of Greenland ice-sheet flow. Science, **297**, 218-222.
Zwiers, F.W., 2002: The 20-year forecast. Nature, **416**, 690-691.

Tables

Table 10.3.1. a) summary of climate change model experiments performed with AOGCMs b) number of ensemble members performed, summarized from the PCMDI webpage (http://www-pcmdi.llnl.gov/ipcc/data_status_tables.htm).

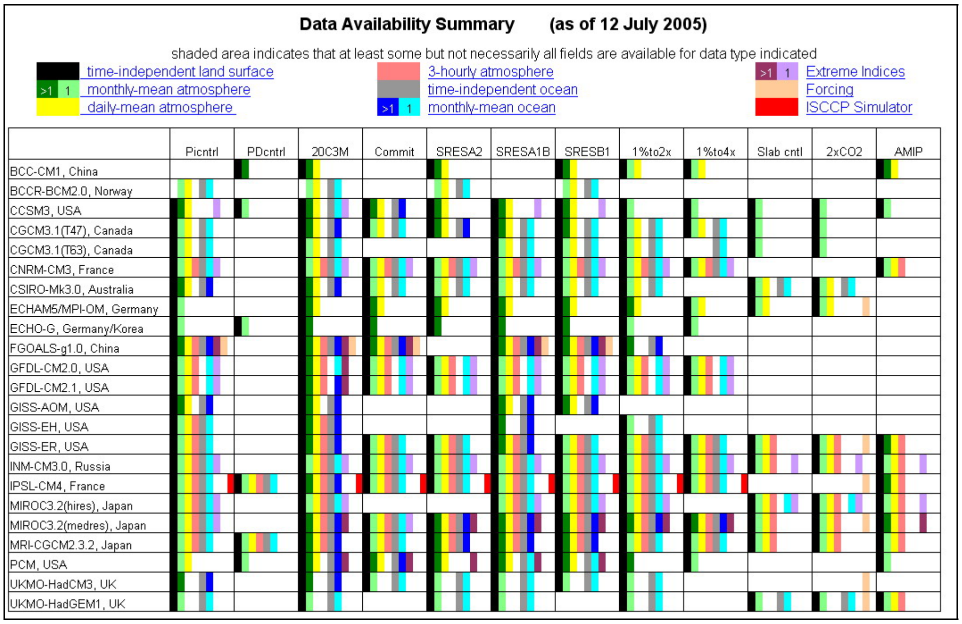

Monthly Mean Atmosphere Data Availability **(as of 12 July 2005)**

1 realization — multiple realizations

	Plcntrl	PDcntrl	20C3M	Commit	SRESA2	SRESA1B	SRESB1	1%to2x	1%to4x	Slabcntl	2xCO2	AMIP
BCC-CM1, China		2	4		2		2	1	1			4
BCCR-BCM2.0, Norway	1		1		1		1					
CCSM3, USA	2	1	9	5	5	7	8	1	1	1	1	1
CGCM3.1(T47), Canada	1		5	1	2	4	4	1	1	1	1	
CGCM3.1(T63), Canada	1		1			1	1	1		1	1	
CNRM-CM3, France	1		1	1	1	1	1	1	1			1
CSIRO-Mk3.0, Australia	2		3	1	1	1	1	1		1	1	
ECHAM5/MPI-OM, Germany	1		3	3	3	3	3	3	1	1	1	
ECHO-G, Germany/Korea	1	1	5	4	3	2	3	1	1			
FGOALS-g1.0, China	3		3	3		3	3	3				
GFDL-CM2.0, USA	1		3	1	1	1	1	1	1			
GFDL-CM2.1, USA	1		3	1	1	1	1	1	1			
GISS-AOM, USA	2		2			2	2					
GISS-EH, USA	1		5			4		1				
GISS-ER, USA	1		9	1	1	5	1	1	1	1	1	4
INM-CM3.0, Russia	1		1	1	1	1	1	1	1	1	1	1
IPSL-CM4, France	1	1	2	1	1	1	1	1	1			6
MIROC3.2(hires), Japan	1		1			1	1	1		1	1	1
MIROC3.2(medres), Japan	1		3	1	3	3	3	3	3	1	1	3
MRI-CGCM2.3.2, Japan	1	1	5	1	5	5	5	1	1	1	1	1
PCM, USA	1	1	4	3	4	4	4	5	1			1
UKMO-HadCM3, UK	2		2	1	1	1	1	1				
UKMO-HadGEM1, UK	1		1		1	1		1		1	1	1

a shaded box indicates that at least some, but not necessarily all, fields of this type are available